2019

INVESTIGATION OF TRANSITION-METAL IONS IN THE NICKEL-RICH LAYERED POSITIVE ELECTRODE MATERIALS FOR LITHIUM-ION BATTERIES

Shuang Gao
University of Kentucky, shuang.gao.cn@gmail.com
Author ORCID Identifier:
https://orcid.org/0000-0002-5919-2532
Digital Object Identifier: https://doi.org/10.13023/etd.2019.134

STUDENT AGREEMENT:

I represent that my thesis or dissertation and abstract are my original work. Proper attribution has been given to all outside sources. I understand that I am solely responsible for obtaining any needed copyright permissions. I have obtained needed written permission statement(s) from the owner(s) of each third-party copyrighted matter to be included in my work, allowing electronic distribution (if such use is not permitted by the fair use doctrine) which will be submitted to UKnowledge as Additional File.

I hereby grant to The University of Kentucky and its agents the irrevocable, non-exclusive, and royalty-free license to archive and make accessible my work in whole or in part in all forms of media, now or hereafter known. I agree that the document mentioned above may be made available immediately for worldwide access unless an embargo applies.

I retain all other ownership rights to the copyright of my work. I also retain the right to use in future works (such as articles or books) all or part of my work. I understand that I am free to register the copyright to my work.

REVIEW, APPROVAL AND ACCEPTANCE

The document mentioned above has been reviewed and accepted by the student's advisor, on behalf of the advisory committee, and by the Director of Graduate Studies (DGS), on behalf of the program; we verify that this is the final, approved version of the student's thesis including all changes required by the advisory committee. The undersigned agree to abide by the statements above.

Shuang Gao, Student

Dr. Yang-Tse Cheng, Major Professor

Dr. Matthew J. Beck, Director of Graduate Studies

INVESTIGATION OF TRANSITION-METAL IONS IN THE NICKEL-RICH LAYERED POSITIVE ELECTRODE MATERIALS FOR LITHIUM-ION BATTERIES

DISSERTATION

A dissertation submitted in partial fulfillment of the
requirements for the degree of Doctor of Philosophy in the
College of Engineering
at the University of Kentucky

By
Shuang Gao
Lexington, Kentucky
Director: Dr. Yang-Tse Cheng, Frank J. Derbyshire Professor of Materials Science
Lexington, Kentucky
2019

https://orcid.org/0000-0002-5919-2532

ABSTRACT OF DISSERTATION

INVESTIGATION OF TRANSITION-METAL IONS IN THE NICKEL-RICH LAYERED POSITIVE ELECTRODE MATERIALS FOR LITHIUM-ION BATTERIES

Layered lithium transition-metal oxides (LMOs) are used as the positive electrode material in rechargeable lithium-ion batteries. Because transition metals undergo redox reactions when lithium ions intercalate in and disintercalate from the lattice, the selection and composition of transition metals largely influence the electrochemical performance of LMOs. Recently, a Ni-rich compound, $LiNi_{0.8}Co_{0.1}Mn_{0.1}O_2$ (NCM811), has drawn much attention. It is expected to replace its state-of-the-art cousins, $LiCoO_2$ (LCO) and $LiNi_{1/3}Co_{1/3}Mn_{1/3}O_2$ (NCM111), because of its higher capacity, lower cost, and reduced toxicity. However, the excess Ni, as a transition-metal element in NCM811, can cause structural and cycling instability.

Starting from NCM811, I modified the composition of transition metals by two approaches: 1) introducing cobalt deficiency and 2) substituting Ni, Co, and Mn with Zr. Their influences on the phase, structure, cycling performance, rate capability, and ionic transport were investigated by a variety of characterization techniques. I found that cobalt non-stoichiometry can suppress Ni^{2+}/Li^{+} cation mixing, but simultaneously promotes the formation of oxygen vacancies, leading to rapid capacity fade and inferior rate capability compared to pristine NCM811. On the other hand, Zr can reside on and expand the lattice of NCM811, and form Li-rich lithium zirconates on their surfaces. In particular, 1% Zr substitution can increase the stability of NCM811 and facilitate Li-ion transport, resulting in enhanced cycling durability and high-rate performance. My studies help improve the understanding of the effects of transition metals on the degradation of the Ni-rich layered positive electrode material and provide modification strategies to enhance its performance and durability for Li-ion battery applications.

KEYWORDS: Li-ion Batteries, Positive Electrode, Layered Lithium Transition-Metal Oxides, Cobalt Deficiency, Zirconium Modification

Shuang Gao

Name of Student

04/26/2019

Date

INVESTIGATION OF TRANSITION-METAL IONS IN THE NICKEL-RICH LAYERED POSITIVE ELECTRODE MATERIALS FOR LITHIUM-ION BATTERIES

By
Shuang Gao

Yang-Tse Cheng
Director of Dissertation

Matthew J. Beck
Director of Graduate Studies

04/26/2019
Date

DEDICATION

To my family and loved ones.

ACKNOWLEDGMENTS

I would like to express my deepest gratitude to Dr. Yang-Tse Cheng, my Ph. D. advisor, for his consistent support and guidance on research and career development. I would also like to thank Dr. Mona Shirpour, my previous advisor, for introducing me to my research field and helping me gain many skills and capabilities.

I would like to extend my sincere thanks to Dr. Fuqian Yang, Dr. Stephen Rankin, Dr. Beth Guiton, and Dr. Jian Shi for serving as my dissertation committees.

I greatly appreciate my former and current lab mates, Dr. Xiaowen Zhan, Dr. Yan Jin, Dr. Baleegh Alobaid, Long Zhang, Jiazhi Hu, Yikai Wang, Dingying Dang, Ming Wang, Andrew Meyer, and Yan Sun. The valuable discussion and assistance benefit my research substantially.

I would also like to acknowledge Dr. Dali Qian and Dr. Nicolas Briot for assisting with SEM and TEM measurements. I very much appreciate Nancy Miller and Nick Cprek for solving various technical issues in the lab throughout my project.

Many thanks to the US National Science Foundation Award 1355438 (Powering the Kentucky Bioeconomy for a Sustainable Future) for partially supporting my work.

Lastly, my appreciation goes to the most important people in my life. The unconditional love and support from my parents should never be forgotten, and the companionship from my dear love is precious, especially during my hard time the past year.

TABLE OF CONTENTS

LIST OF TABLES

LIST OF FIGURES

CHAPTER 1. INTRODUCTION

1.1 Background and Rationale

As the predominant energy resource since the first industrial revolution, fossil fuels have powered our industry, agriculture, household, and transportation for centuries. However, people in the 21st century have learned more about their drawbacks including limited storage, poor recyclability, and polluting byproducts. Researchers have dedicated to developing sustainable energy systems, producing electricity from hydro, solar, wind, tidal, and nuclear instead of fossil fuels. These renewable energy supplies usually fluctuate in both space and time; thus, the produced electricity should be firstly stored and then distributed to consumers stably over time. Therefore, batteries, as the energy storage units, are critical to the new-generation energy system. In addition, governments and the automobile industry are seeking to replace the internal combustion engine by the battery in vehicles, in the hope of reducing the air pollutant, especially for cities that suffer from the automobile exhaust for decades.

Rechargeable lithium-ion batteries (LIBs) are becoming the power sources for both grid energy storage and electric vehicles (EVs) because of their combined high energy and power densities.[1-2] However, the industries and consumers expect LIBs to possess higher energy density, better durability, and fast charging capability; but to be lighter, smaller, safer, and cheaper. In the annual report of 2017, the U.S. Department of Energy (DOE) set the target for battery chemistry and cell technologies that can reduce the cost of EV batteries to less than $100/kWh, ultimately $80/kWh, increase the range to 300 miles, and decrease charge time to 15 minutes or less.[3] These requirements largely depend on the electrode materials of LIBs. For the positive electrodes, $LiCoO_2$ (LCO) and $LiNi_{1/3}Co_{1/3}Mn_{1/3}$ (NCM111) have achieved great success in powering portable devices, such as mobile phones, laptop computers, and tablets.[4-5] However, their relatively low capacity and high price impede their applications in large-scale and high-energy areas.[1-2, 6]

LCO and NCM111 belong to the family of layered lithium metal oxides. The electrochemical performance of such compounds varies with changing the metal-element composition. Researchers found that the layered transition-metal oxides with high nickel concentration had enhanced capacities.[7-9] In addition, replacing Co by Ni can reduce the

cost and toxicity. $LiNi_{0.8}Co_{0.1}Mn_{0.1}O_2$ (NCM811), a typical Ni-rich layered electrode, can deliver 200 mAh/g approximately of the discharge capacity, which is around 30% higher than that of NCM111. Nonetheless, high Ni content can damage the structural stability and cycling durability of NCM811.[10-13] To enable NCM811's high capacity in the commercial applications, researchers have been studying the degradation mechanism and developing practical modification strategies.

Inspired by the previous studies, this dissertation further investigates the influence of transition-metal composition on the Ni-rich layered NCM811. I introduce Co deficiency and Zr substitution to NCM811, discuss their effects on NCM811's structure, surface chemistry, and electrochemical performance in detail, and provide new understandings towards the promising positive electrode for LIBs.

1.2 Rechargeable Lithium-Ion Batteries

Rechargeable LIBs store chemical energy in positive and negative electrodes,[1-2, 4, 6, 14-15] between which the chemical potential difference determines the voltage of a cell. The amount of Li-ion (de)intercalating in each electrode conveys the cell capacity. A porous separator filled with electrolyte, usually a Li-salt organic solution, enables Li^+ transfer but blocks electrons. As illustrated in Figure 1.1, Li ions are reduced to be Li atoms in the negative electrode during charging. Driven by the applied potential, Li ions move from the positive electrode to the negative through the electrolyte. Meanwhile, electrons are transferred in the same direction via the external circuit, and the cations in the positive electrode are oxidized. By this way, a LIB converts and stores energy from the external power source. A reverse process occurs during discharging converting the chemical energy stored to electrical energy and heat.

The energy density of a battery system is the product of voltage and capacity, which depends on electrode materials largely. Figure 1.2 comprehensively demonstrates the average electrode potential against experimental (for negative electrodes and intercalation positive electrodes) or theoretical (for conversion positive electrodes) capacity.[2] Though conversion positive electrodes, such as sulfur, possess an extremely high theoretical capacity, the safety and fabrication issues limit their applications.[2, 16-17] By comparison, intercalation positive electrode materials have been commercialized successfully since

1990s, and been widely studied over the past three decades.[4-5, 18-36] However, their capacities are lower than that of the negative electrodes, such as graphite, metal oxides, and silicon. Clearly, the capacity of positive electrode is a bottleneck towards higher energy density. Developing new positive electrode materials and understanding the degradation mechanisms are critical to realizing high-energy LIBs.

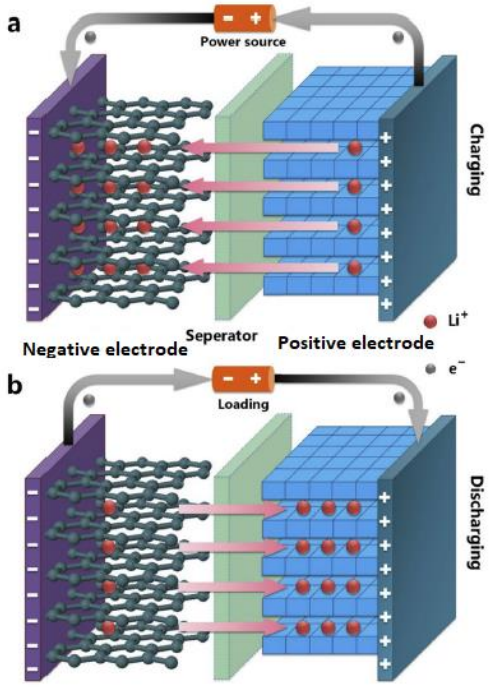

Figure 1.1 Schematic illustration of the basic structure of a LIB along with the charge transport mechanism during (a) charging and (b) discharging.[37]

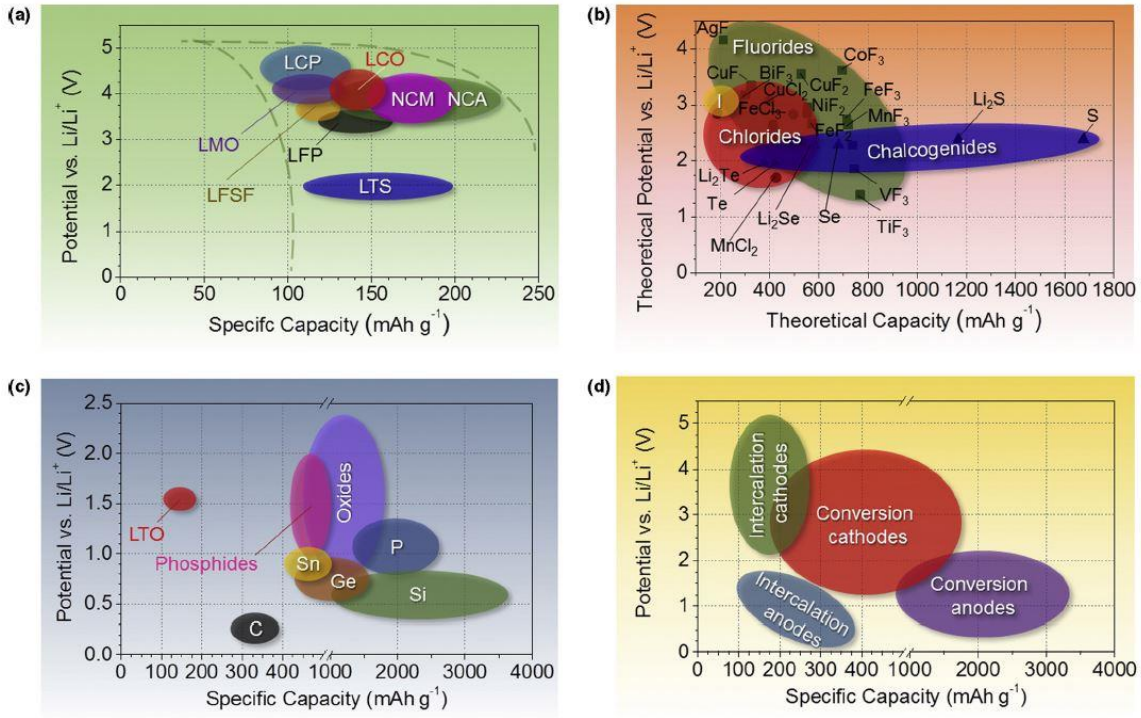

Figure 1.2 Approximate range of average discharge potentials and specific capacity of the common (a) intercalation-type positive electrodes (experimental), (b) conversion-type positive electrodes (theoretical), (c) conversion type anodes (experimental), and (d) an overview of the average discharge potentials and specific capacities for all types of electrodes.[2]

1.3 Positive Electrode Materials of Lithium-Ion Batteries

The dawn of intercalation cathode materials appeared in the 1970s when a variety of layered dichalcogenides were found as the host materials undergoing ionic intercalation reactions electrochemically.[38-39] TiS_2 developed by Whittingham *et al.* is capable to deliver 480 Wh/kg of specific energy density with an operation voltage < 2.5 V versus Li/Li^+. Although it was briefly commercialized by Exxon,[4, 39-40] the dichalcogenides electrodes were soon replaced by transition-metal (TM) oxides and polyanion compounds because of the higher electrochemical potentials of the successors.

The typical crystal structures of intercalation positive electrode materials are layered, spinel, and olivine, as shown in Figure 1.3 schematically.[2, 41] The corresponding specific capacities are summarized in Table 1.1. [2, 42]

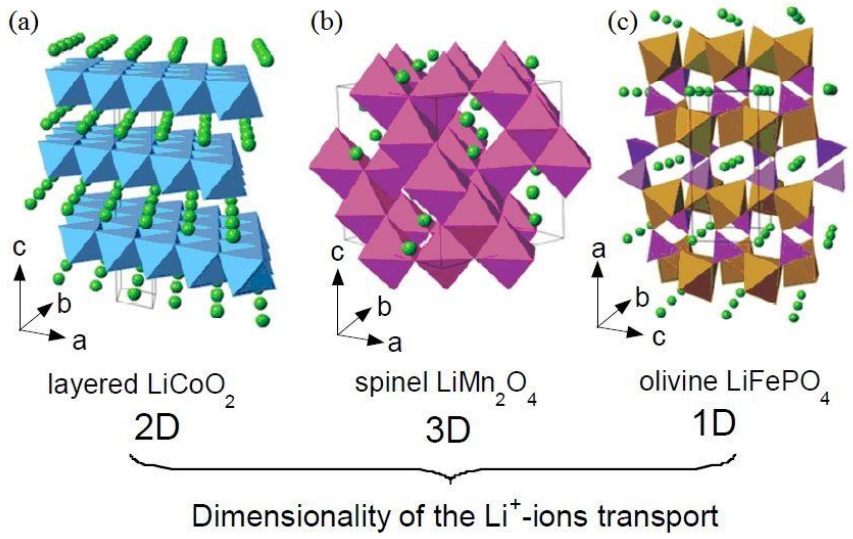

Figure 1.3 Crystal structure of the three Li-insertion compounds in which the Li ions are mobile through the 2-D (layered), 3-D (spinel) and 1-D (olivine) frameworks.[41]

Table 1.1 Characteristics of representative intercalation positive electrode compounds.[2, 42]

Crystal structure	Compound	Specific capacity/mAh·g^{-1} (Theoretical/experimental)	Average voltage/V
Layered	$LiTiS_2$	225/210	1.9
	$LiCoO_2$	274/148	3.8
	$LiNi_{1/3}Co_{1/3}Mn_{1/3}O_2$	280/160	3.7
	$Li_{0.8}Co_{0.15}Al_{0.05}O_2$	279/199	3.7
Spinel	$LiMn_2O_4$	148/120	4.1
	$LiNi_{0.5}Mn_{1.5}O_4$	147/128	4.3
Olivine	$LiFePO_4$	170/165	3.4

$LiCoO_2$ (LCO) is the first layered transition-metal oxide achieving commercial success.[4, 22, 24] It was introduced by Goodenough *et al.* in the 1980s and soon commercialized by Sony Co. The LCO crystal is in the α-$NaFeO_2$ structure (Space group: $R\bar{3}m$) with close-packed O^{2-} ions in a cubic arrangement, where TM and Li ions occupy the octahedral sites. The layers of TM and Li ions stack alternately along [111] direction with the sequence of ABCABC… (Figure 1.4a) forming a hexagonal symmetry.[9, 43] It provides a specific capacity as high as 145 mAh/g with a high average voltage and good cycling durability, however, LCO is expensive, thermally unstable, and fast fading at high-rate current and deep charging.[24, 44-45] The expensiveness of LCO results from the low

availability of Co. Thermal runaway and oxygen release may happen when LCO works at high temperature, causing safety issues such as flame and explosion.[24, 43, 46-48] When the depth of delithiation reaches 50%, $Li_{1-x}CoO_2$ ($x \geq 0.5$) will form a monoclinic symmetry irreversibly,[49] leading to a loss of active Li^+ sites, and, consequently, a capacity degradation.

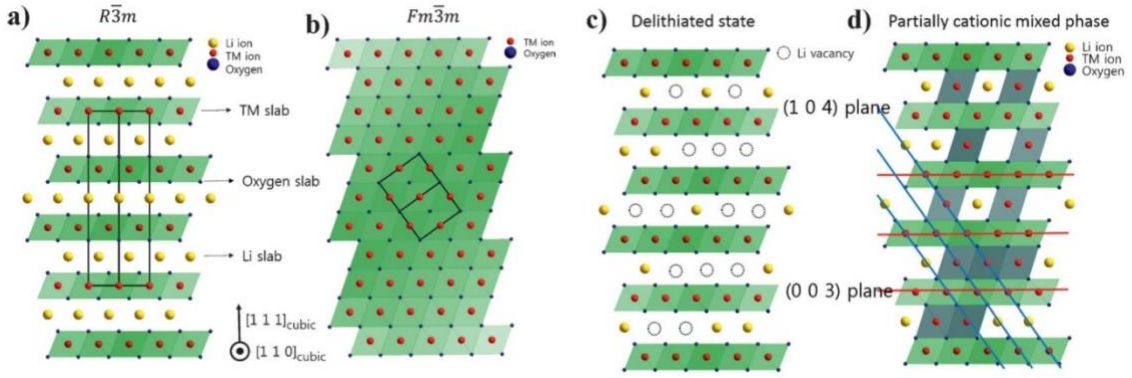

Figure 1.4 Illustration of the ordered and disordered phase in layered lithium metal oxides and their structural transformation. (a) Well-ordered $R\bar{3}m$ structure; (b) Cation mixing phase with Fm-3m structure; (c) $R\bar{3}m$ structure with Li vacancies in highly charged state; and (d) Partially cation mixed phase with TM ions in Li slab.[9]

$LiNiO_2$ (LNO) is isostructural with LCO. Although it has a high theoretical capacity of 275 mAh/g and Ni is much cheaper than Co, it is far from a practical positive electrode material. The pure phase LNO is difficult to synthesize and is unstable during cycling,[23-24, 50-52] because Ni^{2+} ions prefer to occupy the Li-ion sites during synthesis and delithiation, blocking the Li-ion diffusion path.[52-54] The migration of Ni^{2+} to Li^+ sites is known as cation disordering or cation mixing. In addition, the Jahn-Teller distortion (tetragonal distortion) associated with Ni^{3+} is thermodynamically favorable. It can trigger irreversible phase transformation during lithiation and delithiation.[51, 55] Lastly, the exothermic release of oxygen of LNO is worse than that of LCO, therefore, giving rise to a major safety concern.[4, 24]

The layered $LiMnO_2$ (layered-LMO) has a higher theoretical capacity (285 mAh/g) than LCO and LNO,[56] and is more cost-effective and environmentally friendly. However, the hexagonal crystal structure of layered $LiMnO_2$ (layered LMO), more complex than that of LCO and LNO,[25, 57] is thermodynamically unstable. It is prone to form an orthorhombic or monoclinic symmetrical phase and change into a spinel-like structure during Li

extraction, resulting in a capacity fade. Moreover, Mn dissolution occurs when the disproportionation reaction undergoes $2Mn^{3+} \rightarrow Mn^{4+} + Mn^{2+}$. Such dissolution is observed in all Mn-contained positive electrode materials. It will damage the stability of solid-electrolyte interphase (SEI) on the negative electrode.[33, 58-59]

$LiMn_2O_4$ was originally reported by Thackeray *et al.* as a spinel-type positive electrode material in the *Fd3m* space group.[60-61] As shown in Figure 1.3b, O^{2-} ions form a cubic closed-packed sub-lattice, where Li ions and Mn ions occupy tetrahedral (8a) and octahedral (16d) sites, respectively. The lattice offers a three-dimensional network for Li^+ diffusion, in contrast to the two-dimensional planes in the α-$NaFeO_2$ layered structure. The spinel LMOs were the center of interests for the hybrid EVs in the early 2000s,[4, 62-63] due to the high operating voltage ($\geq$ 4.3 V) and that, Mn is abundant and environmentally benign. However, the low capacity (theoretically 148 mAh/g) and poor cyclability limit their applications. The side reaction accompanying oxygen loss and Mn dissolution occurs during electrochemical cycling, irreversibly forming a tetragonal $Li_2Mn_2O_4$ phase, especially at high voltage and high discharging-rate, being responsible for the capacity loss.[4, 25, 63] To address this problem, partial Ni substitution has been applied. $LiMn_{1.5}Ni_{0.5}O_4$ (LMNO) is the most common composition. LMNO deliveries a higher capacity and a better cyclability than spinel LMO.[42, 64-65] In addition, partially doping Ni with Co can suppress the formation of $Li_xNi_{1-x}O_2$, further increasing the capacity retention.

Olivine-type $LiFePO_4$ (LFP) is a state-of-the-art polyanion positive electrode materials with 170 mAh/g in theoretical capacity.[5, 35] The crystal structure of LFP has an orthorhombic symmetry in the *Pnma* space group. O^{2-} ions form a hexagonal close-packed framework, in which P ions occupy one-eighth of the tetrahedral sites. With Li^+ and Fe^{2+} occupying the octahedral sites, the Li^+ composes a one-dimensional chain along the [010] direction. The crystal structure is stabilized by large $PO4^{3-}$ polyanion, resulting in an excellent thermal and cycling stability.[41] The rich availability, low toxicity, and lightweight of Fe and P make LFP attractive and promising. Its major drawbacks are the relatively low potential and inadequate electrical and ionic conductivity.[2, 66] The primary modification methods are 1) partially substituting Fe with other TM elements, such as Ni, Mn, Co, and V, and 2) doping O with F.[67-73]

1.4 Layered Mixed-Transition-Metal Oxides

Among the positive electrode materials aforementioned, layered compounds with mono-transition-metal cations, including LCO, LNO, and layered-LMO, possess the highest theoretical specific capacity, but they are limited by the respective shortcomings. Researchers soon found that two or more TM elements could co-exist in the TM layer of the layered structure. The so-called layered lithium mixed-transition-metal oxides can improve the structure stability, thermal stability, electronic/ionic conductivity, and accessible capacity, compared with their mono-TM counterparts.[2, 4, 8, 41, 64] Many lithium mixed-transition-metal oxides can be derived from a mono-TM compound by substituting with other TM elements; Ni, Co, and Mn are the most commonly used candidates. In addition, the mixed-TM compound can be treated as a solid solution consisting of multiple lithium mono-TM oxides. A triangle compositional phase diagram is shown in Figure 1.5 in which the vertexes are LCO, LNO, and LMO; the three sides of the triangle depict the solid solutions of LNO-LCO, LMO-LCO, and LNO-LMO, respectively.[8]

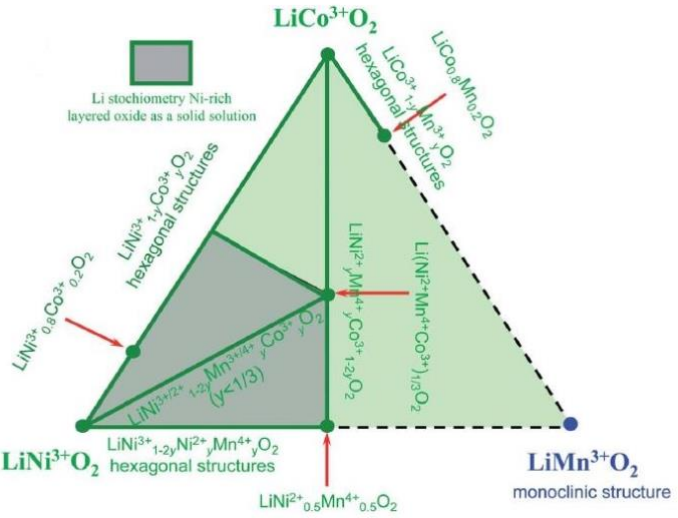

Figure 1.5 Triangle compositional phase diagram of lithium-stoichiometric layered transition metal oxides.[8]

1.4.1 Binary-Transition-Metal Compounds

$LiNi_{1-y}Co_yO_2$ (LNO-LCO) was originally studied by the Delmas group[74-76] and Zhecheva *et al.*[77] In these compounds, the Co substitution improves the ordering of the layered structure by suppressing the migration of Ni^{2+} to Li^+ sites. It also offers more

thermal stability and less oxygen release than the original LNO.[78-81] The O3-type layered structure of $LiNi_{1-y}Co_yO_2$ can be maintained through deep Li extraction, for example, $x < 0.7$ for $Li_{1-x}Ni_{0.85}Co_{0.15}O_2$, which enables 180 mAh/g of the reversible capacity against 140 mAh/g of $LiCoO_2$ with 50% Li extraction.[82-83] While the LNO-LCO system is miscible, Caurant *et al.* demonstrates that $LiNi_{0.8}Co_{0.2}O_2$ can achieve the best electrochemical performance among the family of $LiNi_{1-y}Co_yO_2$.[80] Adding the redox-inactive elements, such as Al and Mg, can stabilize the positive electrode materials structurally and thermally. $LiNi_{0.8}Co_{0.15}Al_{0.05}O_2$, known as NCA, is commercially successful as a positive electrode material in LIBs. It is widely applied in hybrid (HEV), plug-in hybrid (PHEV) and fully electric (EV) vehicles.[84-86]

$LiCo_{1-y}Mn_yO_2$ (LCO-LMO) is attractive due to the cost effectiveness and environmental friendliness arisen from Mn substitution in LCO. Based on the studies conducted by Armstrong *et al.* and Stoyanova *et al.*, a stable α-$NaFeO_2$-type layered structure in the hexagonal symmetry can only occur when $y \leq 0.2$.[87-90] Cubic and tetragonal lattices will take place when $0.2 < y \leq 0.7$ and $y > 0.7$, respectively. $LiCo_{0.8}Mn_{0.2}O_2$ can reach the specific capacity of 134 mAh/g, where the Mn^{3+}/Mn^{4+} is the primary redox pair offering a quasi-flat plateau at above 3.85 V, and the oxidation of Co^{3+} will be involved at a voltage higher than 4.0 V.[91] However, the Jahn-Teller distortion associated with Mn^{3+} facilitates the local tetragonal distortion and leads to the poor cycling performance.[88] The low practical capacity and intrinsic phase instability preclude $LiCo_{1-y}Mn_yO_2$ from a candidate for commercial LIBs.

Investigated by Dahn *et al.* and Ohzuku *et al.*, the maximum solubility of LMO in LNO is 0.5 while maintaining the stable layered structure.[92-94] Therefore, $LiNi_{1-y}Mn_yO_2$ ($y \leq 0.5$) can be treated as a solid solution of $LiNiO_2$ and $LiNi_{0.5}Mn_{0.5}O_2$. $LiNi_{0.5}Mn_{0.5}O_2$ is the best-performing composition, which can deliver 200 mAh/g reversibly referring to low-current-density cycling between 2.5 and 4.5 V.[93, 95] It is more thermally stable than the mono-TM competitors such as LCO and LNO. Ni is the predominant ion involving in the redox reaction, while Mn remains in tetravalent state. Without Mn^{3+}, Jahn-Teller distortion is avoided. In contrast, rock-salt distorted domains occur during electrochemical cycling, due to the cation mixing of Ni^{2+}/Li^+, which blocks the diffusion path and reduces the

number of active sites for Li ions. Therefore, cation mixing is a major problem that causes poor rate capability and low capacity retention of $LiNi_{0.5}Mn_{0.5}O_2$.[96-102]

1.4.2 Ternary-Transition-Metal Compounds

Since the binary-TM compounds possess the superior structural and thermal stability, and thereafter better cycling performance, it is natural to anticipate that the ternary system containing Ni, Co, and Mn, could be more promising. Every stoichiometric $LiNi_{1-x-y}Co_xMn_yO_2$ (as called NCM or NMC) may be represented by a point in the ternary phase diagram shown in Figure 1.5. The layered NCM is isostructural with LCO having the α-$NaFeO_2$-type structure in $R\bar{3}m$ symmetry. The TM ions can randomly occupy the octahedral sites in alternating layers through the close-packed cubic of O^{2-} ions. The NMC electrode materials combine the advantages of the high capacity of LNO, good rate performance of LCO, and stabilizing effect of Mn^{4+}.[2, 4, 8, 41, 103] The main electrochemical active element in NCMs is Ni; Co takes part in the redox reaction only at high potential region; Mn is inactive during the electrochemical process, but it stabilizes the layered structure.

The layered lithium ternary-transition-metal oxides were firstly reported by Liu *et al*. in 1999 and Yoshio *et al*.[27-28] in 2000. They studied $LiNi_{1-x-y}Co_xMn_yO_2$ and found that substituting Ni partially with Co and Mn could stabilize the layered structure, maintain the Li stoichiometry, and suppress the cation mixing between TM and Li ions. According to their results, high-temperature (850 °C and 900 °C) synthesized samples have better electrochemical performance than the low temperature (750 °C) ones, though high temperature and long calcining duration will cause Li loss in these compounds. $LiCo_yMn_{0.2}Ni_{0.8-y}O_2$ can deliver discharge capacities greater than 155 mAh/g operated at 3.0–4.3 V versus Li/Li^+. The symmetric compound $LiNi_{1/3}Co_{1/3}Mn_{1/3}O_2$, well known as NCM111 or NCM333, was initially introduced by Ohzuku *et al*. in 2001.[93] The NCM111 synthesized at 1000 °C was found a capacity of around 150 mAh/g cycled at 30°C between 2.5 and 4.2 V versus Li/Li^+. Shaju *et al*. studied the redox reactions of NCM111 in 2002 and found that the valence states of transition metals were Ni^{2+}, Co^{3+}, and Mn^{4+}, respectively.[29] Ni^{2+}/Ni^{4+} was the major redox pair under 4.0 V and Co^{3+}/Co^{4+} would be electrochemically activated around 4.5 V. Experimental and computational studies from

other groups confirmed these findings.[104-108] A variety of synthesis routes have been studied, such as sol-gel, solid-state, spray drying, spray pyrolysis, combustion, and co-precipitation.[109-114] NCM111 performs better than LCO on specific capacity and energy density, and, more importantly, NCM111 is more cost-efficient and environmentally friendly than LCO by reducing the usage of Co. Therefore, NCM111 replaced LCO successfully as the positive electrode material in commercial LIBs.[115] However, NCM111, like many other positive electrode materials, suffers an irreversible capacity loss at the first cycle and during long-term cycling.

The success of NCM111 enlightens the studies on Co substituting $LiNi_{0.5}Mn_{0.5}O_2$. Adding Co can significantly suppress the cation mixing of Ni^{2+}/Li^+ and increase the electronic conductivity of $LiNi_{0.5}Mn_{0.5}O_2$.[105, 116-118] Among the compounds of $LiNi_{0.5-x}Co_{2x}Mn_{0.5-x}O_2$ ($x < 0.5$), $LiNi_{0.4}Co_{0.2}Mn_{0.4}O_2$ (NCM424) exhibits the best electrochemical performance. Reported by Ngala *et al*., it can achieve an average reversible capacity of 180 mAh/g operating at 1.0 mA/cm^2 between 2.5 and 4.3 V versus Li/Li^+, which drops to 150 mAh/g if doubling the current density.[119] By studying the rate capabilities of $LiNi_{0.5-x}Co_{2x}Mn_{0.5-x}O_2$ ($x < 1/6$) with different Co contents, Oh *et al*. suggested that NCM424 was the optimal composition that delivered at least 160 mAh/g at 160 mA/g (1 C) between 2.8 and 4.4 V when Li metal served as the negative electrode.[118] The other family of cobalt-substituted $LiNi_{0.5}Mn_{0.5}O_2$ is $LiNi_{0.5}Co_xMn_{0.5-x}O_2$ ($x < 0.5$). In the systematic studies conducted by Li *et al*., $LiNi_{0.5}Co_{0.2}Mn_{0.3}O_2$ (NCM523) and $LiNi_{0.5}Co_{0.3}Mn_{0.2}O_2$ performed better than the other compositions, exhibiting around 160 mAh/g of the discharge capacity at the current loading of 40 mA/g between 3.0 and 4.6 V after 20 cycles.[120-121] Yang *et al*. applied co-precipitation method to synthesize spherical NCM523 and achieve 173 mAh/g after 50 cycles operating at 32 mA/g between 3.0 and 4.3 V.[122] Owing to the high electronic conductivity, Li-ion diffusivity, and energy density, NCM523 is also widely implanted as a commercial positive electrode material besides NCM111.

The growing market of EVs demands a high-energy-storage battery system with at least 300 Wh/kg as the energy density.[18, 123] However, the positive electrode made from NCM111 and NCM523 can only deliver 200 Wh/kg at the battery level, corresponding 600 Wh/kg at the materials level.[18, 124-125] To increase the energy density, one must find high-capacity electrode materials. In the family of layered NCMs, high Ni concentration implies

elevated capacity, since Ni is the predominant element undergoing the redox reactions. In the past two decades, extensive studies have focused on the composition of $LiNi_{1-2x}Co_xMn_xO_2$ ($x \leq 0.2$).[9, 18, 125-128] These Ni-rich NCMs are capable to provide 180-240 mAh/g of discharge capacity at 2.7–4.5 V as the voltage window, corresponding 650–800 Wh/kg of energy density.[9, 18] Despite the elevated capacity, implanting electrodes with high Ni concentration brings a variety of challenges to the compounds, such as fast capacity fade and heat/gas release during electrochemical cycling.[9, 11-12, 125, 129] The poor structural and thermal stability preclude the application of Ni-rich NCMs in the commercial LIBs.

1.5 The Role of Transition Metals in Ni-Rich Layered NCM

As discussed in section 1.4, the selection and composition of transition metals largely influence the structure stability and electrochemical performance of layered positive electrode materials. The following paragraphs will discuss the degradation and modification correlating with transition metals, particularly for the Ni-rich layered NCM.

1.5.1 Ni-rich Correlated Degradation

Ni-rich NCM positive electrode materials are in the α-$NaFeO_2$-type layered structure with $R\bar{3}m$ space group. A repeating O3 structure shows a sequence of O-TM-O-Li-O-TM-O-Li-O along [111] direction, where TM and Li ions occupy 3a and 3b octahedral sites, respectively. In the mixed-TM compounds containing Ni, Ni^{2+} is likely to appear from the reduction of Ni^{3+}, because the crystal-field theory that Ni^{3+} has an unstable unpaired electron spin of the orbitals.[41, 130-132] Owing to the similar ionic radius of Ni^{2+} (0.69 Å) and Li^+ (0.76 Å), Ni^{2+} inclines to migrate to Li^+ site, initiating cation mixing.[13, 50, 131, 133-134] The Ni^{2+}/Li^+ disordering can occur during both materials synthesis and electrochemical cycling. The Ni^{2+} occupying in Li-slab will hinder Li-ion diffusion by narrowing the Li slab and repulsing Li^+ by the coulombic force. Therefore, cation mixing can cause a poor rate capability. In addition, it can initiate a local structure transformation from $R\bar{3}m$ to $Fd\bar{3}m/Fm\bar{3}m$ (shown in Figure 1.4c–d), especially in the highly delithiated situation. A capacity loss will occur when such transformation is usually irreversible. Many methods have been developed to detect cation mixing, among which X-ray diffraction (XRD) analysis is simple but effective. The Ni^{2+}/Li^+ disordering can weaken the

constructive interference of (003) planes, but enhance that of (104) planes, as illustrated in Figure 1.4d.[9] Reflecting on the XRD pattern, the lower intensity ratio of (003)/(104) suggests a more severe cation mixing. The (003)/(104) intensity ratio greater than 1.2 is usually considered as a good cation ordering. Furthermore, the Rietveld refinements on X-ray and other high-energy diffraction patterns can interpret the ratio of Ni^{2+}/Li^{+} antisite quantitatively.[29, 103, 131, 135]

Because of the high concentration of Ni^{2+}, Ni-rich NCMs subject more severe cation-mixing condition than their low-Ni counterparts do. Noh *et al*. studied the composition of $LiNi_xCo_yMn_zO_2$ with x ranging from 0.33 to 0.85.[11] They found that the Ni-rich composition could achieve high initial capacity, however, show high-degree cation mixing, poor thermal stability, and fast capacity degradation. Cation mixing directly corresponds to the structural instability of Ni-rich NCM, and it is a major reason for capacity fading.[9, 136]

High capacity of Ni-rich NCM is expectable if more Li can be utilized in the host structure. Nonetheless, it is a trade-off between capacity and the surface stability of the electrode. At highly delithiated state, namely high voltage (> 4.4 V), the reactive Ni^{4+} most likely exists.[12-13, 24, 125, 137-138] Ni^{4+} has a tendency to reduce to Ni^{3+} and/or Ni^{2+}, which will be intensified at elevated temperature. The reduction of Ni^{4+} triggers oxygen release when Li intercalation is absence under delithiated state, giving rise to serious safety issues such as packing leakage, ignition, and explosion. When the non-aqueous electrolyte is used, the situation will be even worse.[41, 139-140] Furthermore, a layered/spinel/rock-salt phase transformation will take place with the reduction of Ni^{4+}, causing an irreversible capacity loss. Such structural degradation was studied by Bak *et al*. for the moderate Ni concentration (NCM433 and NCM523) and Ni-rich (NCM622 and NCM811) compounds.[12] Cation mixing plays a critical part in the structural degradation. With the increasing Ni content, the activation temperature of phase decomposition/transformation decreases, resulting in more oxygen release.

Even if the NCM positive electrode materials are carefully operated at a safe temperature, the reactive Ni^{4+} still causes problems to the charged electrodes, especially at the interface between the active material and electrolyte.[141-143] According to the studies of Choi *et al*. and Watanabe *et al*., the highly oxidizing Ni^{4+} accelerates the organic electrolyte

decomposing, leading to an electrolyte depletion, Ni^{2+} dissolution, and SEI formation.[144-146] At the first cycle of delithiation/lithiation, SEI consisting of polycarbonates, LiF, Li_xPF_y, and $Li_xPF_yO_z$ forms on the surface of positive electrode facing the electrolyte of $LiPF_6$-EC (ethylene carbonate)/DEC (diethyl carbonate).[9, 125, 128, 147] The electronic insulating and electrochemical inactive SEI will result in low coulombic efficiency and irreversible capacity loss for the first charging/discharging cycle. SEI is not a static layer, but dynamically decomposes and reforms during the continuous electrochemical operation.[58, 148] The ongoing Ni^{4+} reduction, Ni^{2+} dissolution, and gas evolution can lead to an accumulative capacity degradation of NCM positive electrode materials during long-term cycling.

1.5.2 Effects of Transition-Metal Non-Stoichiometry

From the viewpoint of defect chemistry, various types of point defects can form in a Ni-rich NCM compound, including Li-ion vacancy, TM-ion vacancy, O vacancy, and cation antisite. Ni^{2+}/Li^{+} antisite and surface O vacancies correspond to cation mixing and oxygen release, respectively. They have been discussed in the earlier sections. However, the studies of TM vacancies in Ni-rich NCMs are limited. Intuitively, the formation of negatively charged TM vacancies can either increase the valence state of the remaining cations or introduce positively charged O vacancies, in order to satisfy the charge neutrality in the compounds. Such phenomenon has been reported at highly delithiated states.[9, 12, 128, 131, 149] The dissolution of the cations reduced from Ni^{4+} and Co^{4+} will facilitate the surface reactions to form SEI.

According to the degradation mechanism aforementioned, controlling cation mixing of Ni^{2+}/Li^{+} is critical to stabilizing the layered structure during lithiation and delithiation. To address the cation-mixing problem, modifications have been applied to enhance the energy barrier for Ni^{2+} migration. Cationic doping elements, such as Na and Mg, are inserted into Li slabs, showing a "pillar" effect to hinder Ni^{2+} migration.[150-152] Cho *et al*. proposed a pre-forming thin cation-disordering layer that could prevent further cation migration so that improve the cycling performance.[153] These two methods take advantage of the electrostatic repulsion between the cations occupying Li layer and the Ni^{2+} in TM layer. I suggest that forming TM vacancies, such as introducing Co deficiency during

synthesis, could have a similar effect to prevent cation mixing, because of the electrostatic attraction between negatively charged Co vacancies and Ni^{2+}. However, it is also possible to generate O vacancies when removing TM cations because of charge balance. The O vacancies can introduce surface instability and cause more degradation problems.[125, 130, 154-156] The effects of TM vacancies on Ni-rich layered NCM materials could be complex, thus, an experimental study is necessary.

1.5.3 Modification by Transition-Metal Doping

In order to improve the structural and cycling stability of Ni-rich NCM, many modification approaches are investigated, such as coatings, core-shell structures, full-concentration-gradient (FCG) particles, and elemental doping. Among these techniques, doping is facile and cost-efficient,[7, 32, 34, 123, 157-160] which optimizes the composition of the layered NCM materials. For instance, Ni-rich NCM is developed from doping high-capacity LNO with Co and Mn to ameliorate the conductivity and structural stability. For Ni-rich NCMs, the most common dopant elements are Na,[161-163] Mg,[164-169] Al,[164-166, 170-173] Zr,[174-178] Cr,[166, 179] and Mo.[180-181] The benefits of these elements are usually attributed to 1) replacing highly active elements such as Li and Ni by elements that are electrochemically inactive and structurally stable; 2) preventing cation mixing by increasing the energy barrier for Ni^{2+} migration; 3) reducing oxygen release during electrochemical cycling by strengthening oxygen-metal bonds.

Many studies of Zr-doped/modified Ni-rich NCMs have been proposed in recent years. Although improvements in cycling stability and high-rate performance have been reported, there are disagreements on the mechanisms. Schipper *et al.* observed the fast electrochemical kinetics in their Zr-substituted $LiNi_{0.6}Co_{0.2}Mn_{0.2}O_2$ samples. They ascribed the improved structural stability to the destabilization of Ni tetrahedral sites and the reduced concentration of Jahn-Teller active Ni^{3+} ions.[175, 182] On the contrary, Li *et al.* found that Ni^{3+} increased in their Zr-doped $LiNi_{0.8}Co_{0.1}Mn_{0.1}O_2$ samples, but significant enhancements in cycling stability and rate capability were still achieved.[178] A Li_2ZrO_3 coating layer formed on the particle surface as a side effect of Zr doping, which was reported by both groups including Li *et al.*'s previous study on Zr-doped $LiNi_{1/3}Co_{1/3}Mn_{1/3}O_2$.[183] They proposed that the enhanced electrochemical performance

partially results from the protection and surface stabilization offered by the Li_2ZrO_3 layer, as originally reported in Li_2ZrO_3-coating studies.[184-185] However, such coating layer was absent in $LiNi_{0.4}Co_{0.2}Mn_{0.4}O_2$ and $LiNi_{0.5}Co_{0.2}Mn_{0.3}O_2$ studies.[174, 177] While low surface-film resistance and high Li-ion diffusivity were stated in the aforementioned studies, the measurements were conducted in the coin cell configuration where the effects of Zr modification on Li diffusion in the bulk of NCMs may be obscured. In this dissertation, I report a comprehensive experimental study to help understand the structure, electrochemistry, and Li-ion transport behavior of the Zr-modified Ni-rich NCM electrode materials.

CHAPTER 2. EXPRIMENTAL METHODS

This chapter introduces the general concepts of the experiments I have conducted in this dissertation, including materials synthesis, characterization of structure, morphology, composition, and surface condition, and electrochemical measurements. The detailed operation and parameters will be discussed in the experimental sections in the following two chapters.

2.1 Materials Synthesis

Solid-state calcination and sol-gel method are applied to synthesize cobalt-deficient and zirconium-modified NCM811, respectively.

In terms of solid-state calcination, the powder precursors are uniformly mixed and then calcined at a specific temperature to achieve the target phase and composition. Usually, precursor mixture will be pressed into pellets for calcining. To ensure phase homogeneity, multi-step mixing-pelletizing-calcining may be necessary, especially for the precursors that undergo decomposition, such as carbonates, nitrates, and acetates.

The sol-gel method describes a procedure consisting of precursor solution formation, gel conversion, and calcination. The pH value of the solution and calcination temperature are critical to the phase and morphology of the final products.

In my work, solid-state calcination is favorable to synthesizing cobalt-deficient NCM811, because it more easily retains the cationic non-stoichiometry being introduced intentionally. Comparatively, the sol-gel method, as a wet-chemistry route, can prevent non-uniformity in the yields. Therefore, it is used for synthesizing NCM811 samples with different amounts of Zr substitution.

2.2 Characterization Techniques

Several complementary characterization techniques are utilized in this dissertation to investigate the structure, composition, and surface chemical state of samples.

The crystallinity is measured by X-ray powder diffraction (XRD). The phase of samples can be identified by comparing the diffraction pattern to the database of Powder Diffraction Files (PDF). By using General Structure Analysis System (GSAS) software

created by Argonne National Laboratory, I can refine the diffraction pattern to extract the lattice parameters. Siemens D500 and D5000 diffractors are used in Chapter 3 and 4 to perform XRD on the as-synthesized materials and electrochemically cycled electrodes, where the Cu *a* X-ray has a wavelength of 1.5406 Å. High-resolution X-ray diffraction (HRXRD) is applied in Chapter 4. The X-ray's wavelength is 0.4127 Å, provided by the Advanced Photon Source, Argonne National Laboratory. HRXRD can provide more detailed structural information than the conventional XRD by reducing fluorescence problem and sample absorption. In Chapter 4, it reveals a secondary phase in the Zr-modified samples, which is too minute to be discovered by the conventional XRD.

In Chapter 3, inductively coupled plasma optical emission spectroscopy (ICP-OES) is applied to analyze the composition of the cobalt-deficient NCM811s. About 10 mg of each sample is dissolved in around 5 ml aqua regia at 95 °C, then diluted to 50 ml with deionized water. The standards of Li, Ni, Co, and Mn are prepared in 0.01, 0.1, 1, 10, and 100 μg/ml, respectively.

NCM811 particles are observed through a scanning electron microscope (SEM). The secondary electron signal, which gives a good contrast of surface roughness, is utilized to image the morphology of the samples. In both cobalt-deficient and Zr-modified NCM811, coating and phase deviation may occur on or near the surface of particles. Since nano-size features are difficult to be revealed by SEM, a high-resolution transmission electron microscope (HRTEM) is applied. HRTEM uses both transmitted and scattered electron beams to create an interference image with phase contrast. In both SEM and HRTEM, energy-dispersive X-ray spectroscopy (EDS) can quantify elemental distribution (except Li) at specific locations on the samples.

X-ray photoelectron spectroscopy (XPS) is a powerful tool investigating the surface chemistry of solid samples. A monochromic X-ray impinges on the sample surface that emits photoelectrons with particular characteristic energy. The detection depth is normally less than 10 nm. The spectrum is obtained by counting the number of the ejected electrons (y-axis) over a range of kinetic energy (x-axis). The location and height of the spectra reflect the chemical state of a specific element. In this dissertation, XPS is used to ascertain the valence states of TM ions in the NCM811 samples.

2.3 Electrochemical Measurements

This dissertation studies the NCM811s as the positive electrode materials in LIBs. Thus, the electrochemical properties are essential to these materials, which are investigated by the following techniques.

To fabricate the positive electrode, the synthesized NCM811s are cast on a carbon-coated Al foil with carbon black (CB) and polyvinylidene fluoride (PVDF). The NCM811 electrodes are assembled in 2032-type coin cells with Li metal as the counter electrode. Various electrochemical measurements are performed to these cells.

Galvanostatic cycling with potential limitation technique (GCPL) cyclically charges and discharges a cell at a specific current density between the high and low cut-off voltages. It examines the cycling durability and rate capability of the NCM811 cells. In this dissertation, a constant current/constant voltage (CC-CV) mode is applied to each charging step. It means that the positive electrode will be delithiated at a constant current, and then be held at the cut-off voltage until the current drops to a specific value. The CC-CV mode ensures that the positive electrode reaches the same delithiation state before discharging. Constant current (CC) mode is applied to the discharging steps. Combining CC-CV and CC mode aims to simulate the battery cycling in the real world, generating the capacity more accurately, especially for high current loading cycles.

Cyclic voltammetry (CV) proceeds a constant-rate voltage scanning to an electrochemical cell, repeatedly ramping forward and backward in a potential range. The current is recorded at each step of voltage. In the current versus potential plot, positive and negative peaks may occur, regarding to cathodic and anodic currents, respectively. The location and shape of the peak pairs can indicate the kinetics of the redox reactions in the working electrode. In addition, the variation of these peaks during the cyclic voltage scanning infers the reversibility of the redox reactions, and, herein, the stability of the active material.

Electrochemical impedance spectroscopy (EIS) is powerful to investigate the factors limiting the performance of LIBs. Applying to NCM811 cells, the spectra can reveal the properties of SEI, as well as the rate of charge transfer and Li-ion conduction.

Galvanostatic intermittent titration technique (GITT) is applied in this dissertation to study the Li-ion diffusion in the coin cell environment. On the other hand, direct current

(DC) polarization method evaluates the Li-ion diffusivity in terms of the NCM811 bulk materials. These two techniques together convey the influence of Zr modification on the Li-ion diffusion of NCM811, which is discussed in detail in Chapter 5.

CHAPTER 3. Effects of Cobalt Deficiency on Nickel-rich Layered $LiNi_{0.8}Co_{0.1}Mn_{0.1}O_2$ Positive Electrode Materials for Li-Ion Batteries

I synthesized pristine and cobalt-deficient NCM811 samples via solid-state reaction. Using a variety of characterization techniques and electrochemical measurements, I show that Co non-stoichiometry can suppress Ni^{2+}/Li^{+} cation mixing, but simultaneously promote the formation of O vacancies, leading to a rapid capacity fade and inferior rate capability compared to pristine NCM811. The effects of Co deficiency on the crystal structure, surface chemistry, and electrochemical performance of Ni-rich layered NCM811 positive electrode materials were experimentally studied possibly for the first time.

3.1 Introduction

One of the strategies to increase the energy density and specific energy of LIBs is to extend the rechargeable capacity of the positive electrode material. Among the layered lithium metal oxides ($LiMO_2$), $LiCoO_2$ was the first commercialized positive electrode material in LIBs.[22] However, Co is scarce, expensive, and toxic. In addition, the relatively low capacity (145 mAh/g in practice) and thermal instability of $LiCoO_2$ preclude its use in large-scale applications such as EVs.[2, 8, 24, 45, 48, 66] The isostructural $LiNiO_2$ and $LiMnO_2$ phases contain less expensive and more abundant elements but are unsuitable substitutes because $LiNiO_2$ can release oxygen upon Li removal, raising major safety issues, and $LiMnO_2$ converts to the spinel ($LiMn_2O_4$) with an unacceptable irreversible capacity loss.[8, 23, 25, 56-57] Therefore, mixed-transition-metal oxides, such as $LiNi_{1-2x}Co_xMn_xO_2$ (NCM), have been extensively studied to overcome the shortcomings of $LiCoO_2$. Each TM element plays a role in the layered NCM positive electrode material. Ni is the predominant electrochemically active cation at low potential (< 4.0 V) and provides high storage capacities. Co can only participate in the redox reaction at high voltage region (> 4.0 V), but it provides electronic conductivity and improves layered characteristics when considered as a substitution in $LiNi_{1-x}Mn_xO_2$. The electrochemically inactive Mn^{4+} provides, when $x \leq 0.2$ in $LiNi_{1-2x}Co_xMn_xO_2$, structural stability by avoiding Jahn-Teller distortion associated with Mn^{3+}.[4, 8] Among the mixed-transition-metal positive electrode

materials, the symmetric compound $LiNi_{1/3}Co_{1/3}Mn_{1/3}O_2$ (NCM111) has attracted much attention due to its high specific capacity (150 mAh/g cycled between 2.5 and 4.2 V versus Li/Li^+), structural stability, and excellent cycle life. This compound can deliver a specific capacity close to 200 mAh/g when charged to 4.6 V. However, the main drawback of this compound is its poor cycle life when undergoing charge/discharge between 3 and 4.6 V, hindering its application in high-energy batteries.[8, 28, 93, 106, 146, 186]

Because Ni is the main active redox species in the ternary-TM oxides, the electrochemical capacity of $LiNi_{1-x-y}Co_xMn_yO_2$ strongly depends on the Ni content. Thus, Ni-rich lithium mixed-transition-metal oxides have recently been studied as candidates to reach higher capacities.[9, 133-134, 187-189] These compounds are capable of delivering 200 mAh/g capacity and 800 Wh/kg energy density.[9, 133-134, 188-190] They are also more environmentally benign and less expensive than $LiCoO_2$. Because of the similar ionic radii of Li^+ (7.6 Å) and Ni^{2+} (6.9 Å), Ni ions can migrate from the TM layer to the Li layer and form antisite defects. This cation migration, also known as cation mixing or cation disordering, can occur during synthesis and electrochemical cycling, especially when the Ni content is high.[131, 191-195] Ni migration reduces the active Li sites, resulting in gradual capacity decline during electrochemical cycling or poor initial capacity if formed during synthesis.[9] By impeding Li-ion diffusion, cation mixing also lowers the rate capability of the material during electrochemical cycling. Additionally, side reactions strongly depend on the defects at or near the surface, such as Li and O vacancies, which may be affected by the presence of cations, particularly highly oxidizing and unstable Ni^{4+} at high voltages.[9, 189, 196-199] The reaction layers (spinel-like and/or rock-salt phases) on the surfaces are often electronically and ionically insulating, causing capacity loss and reduced rate capability.[55, 200]

Various types of point defects in a Ni-rich NCM compound, including Li-ion vacancy, TM vacancy, O vacancy, and cation antisite, are shown in Figure 3.1. The effects of Ni^{2+}/Li^+ antisite and surface O vacancies have been extensively studied;[10, 130-131, 133-134, 154-156, 192, 199, 201] however, the studies of TM vacancies in Ni-rich NCM are limited. Though the computational studies by Hoang and Johannes showed that the formation of TM vacancies are likely energetically unfavorable,[202-203] such defects may form because synthesis and electrochemical cycling are kinetic processes where the system may deviate

from thermodynamic equilibrium. The formation of negatively charged TM vacancies will cause an increase in either the valence state of the remaining cations or positively charged O vacancies in order to satisfy charge neutrality. In this study, I synthesized NCM811 with different amounts of Co deficiency and investigated their microstructure, morphology, surface chemistry, and electrochemical performance.

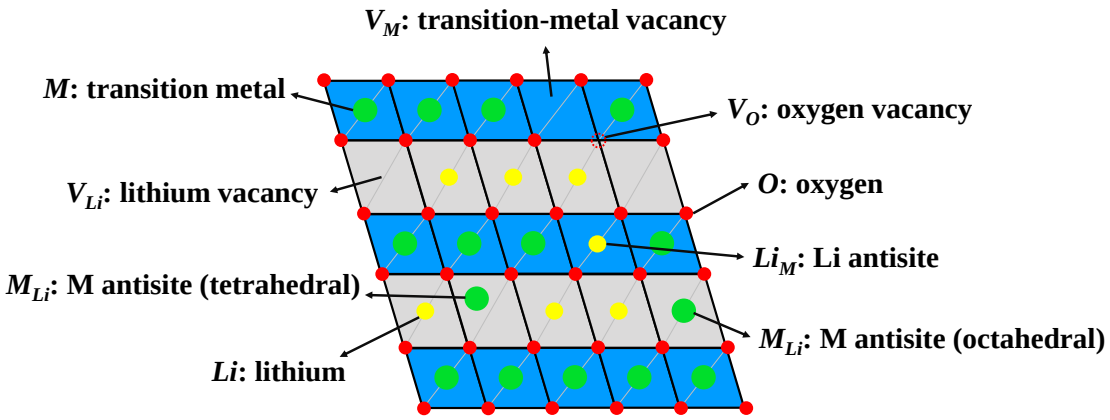

Figure 3.1 Defects in the lattice of layered lithium metal oxide.

3.2 Experimental

Cobalt-deficient NCM811 samples were synthesized by a solid-state-reaction method. Li_2CO_3 (Sigma-Aldrich, ≥99%), NiO (Alfa Aesar 99%), Co_3O_4 (Alfa Aesar, ≥99%), and MnO_2 (Alfa Aesar, 98%) in molar ratios of Li:Ni:Co:Mn = 1.05:0.8:(0.10, 0.09, and 0.08):0.10 were uniformly mixed in a mortar. The samples were named as Co0.10, Co0.09, and Co0.08 for the pristine NCM811, 10%, and 20% cobalt-deficient samples, respectively. The mixtures were calcined at 800 °C for 12 h to discompose the carbonates. The calcined powders were milled in isopropanol at 300 rpm for 12 h and dried overnight at 80 °C, and then uniaxially pressed. The pressed pellets were fired at 900 °C for 12 h in air, crushed into powder, and again milled and pelletlized for a final firing at 900 °C for 12 h in air. Before characterization and electrochemical testing, the milled powders were annealed at 800 °C in pure oxygen for 1 hour to compensate for the surface oxygen loss during synthesis and then stored in an Ar-filled glovebox.

Phase identification for the synthesized powder and cycled electrodes was performed using XRD (Siemens D500, Cu Kα radiation). The diffraction patterns were

analyzed by Rietveld refinements using the GSAS developed by Argonne National Laboratory with the EXPGUI interface developed by Los Alamos National Laboratory.[204-205] The chemical composition of each sample was determined by ICP-OES (Varian Vista-Pro CCD simultaneous). Using SEM (Hitachi S4300) and TEM (JOEL 2010F), the morphology of NCM811 particles and surface layers were examined, respectively. The surface composition was studied using XPS (Thermo Scientific K-Alpha).

To make the electrode slurries, 80 wt.% NCM811 powder, 10 wt.% CB (Super P C65, Sigma Aldridge), and 10 wt.% PVDF (MW ≈ 1100 g/mol, Kureha Corporation) were uniformly dispersed in NMP (VWR, Biotechnology Grade) in a planetary mixer (Kurabo Mazerustar KK250S) for 30 mins. The slurries were cast onto carbon-coated aluminum foil (MTI Corporation, 20 μm in thickness) and baked at 120 °C in a vacuum oven overnight. Then the electrode film was punched into circular disks (1/2 inch in diameter) in an Ar-filled glovebox. The mass loading of NCM was 2.5±0.1 mg/cm^2.

Each coin cell was assembled using a piece of the as-made positive electrode disk, Li foil (Alfa Aeser, 0.75 mm in thickness), Celgard 2400 separator, 1 M $LiPF_6$ in EC:DEC (1:1 in vol., BASF), and the 2032-type casing (MTI corporation). The electrochemical cycling between 2.75 and 4.3 V versus Li/Li$^+$ was performed on an electrochemistry workstation (Biologic VSP). For each charging cycle, the voltage was held at 4.3 V until current loading drops to 0.1C. In this chapter, 1C was set as 200 mAh/g. Long-term cycling was performed at 0.2C, and rate capabilities were checked via varying current loading from 0.1C to 2C. Electrochemical impedance spectroscopy (EIS) was carried out over the frequency range from 1 MHz to 10 mHz. The EIS spectra were recorded during 1C cycling after the 1st, 5th, 20th, and 100th charging cycles.

3.3 Results and Discussion

The XRD patterns of Co0.10, Co0.09, and Co0.08, representing pristine NCM811, 10, and 20% cobalt-deficient samples, respectively. The Rietveld refinement results are shown in Figure 3.2. The patterns match well with the α-$NaFeO_2$-type phase of the $R\bar{3}m$ space group. Impurity phases are not detected. The clear splitting of the (006)/(102) and (108)/(110) diffraction peaks indicates a well-ordered layered structure.[29, 156] Table 3.1 summarizes the structural parameters obtained from Rietveld refinement, as well as the

intensity ratio of (003)/(104). The composition of each TM cation acquired from ICP-OES measurement is listed in Table 3.2, illustrating the Co non-stoichiometry in the cobalt-deficient NCM811s. The phase and chemical analysis show a decreasing trend for Ni^{2+}/Li^{+} disordering with increasing Co deficiency; 11.37% disordering for Co0.10, 8.69% for Co0.09, and 8.59% for Co0.08. In the cobalt-deficient compounds, cation mixing cannot be unambiguously identified by the intensity ratio of (003)/(104)[156] because the intensity of the (003) plane is not only affected by the disordering of Ni^{2+} and Li^{+}, but also by the atomic occupancy on the transition metal layer. Co non-stoichiometry leaves unoccupied sites on the transition metal layer, that is, Co vacancies (V_{Co}'' or V_{Co}'''). According to the refinement result in Table 3.1, cation defects will result in a lattice expansion. I suppose that the electrostatic attraction between the V_{Co}'' or V_{Co}''' and the Ni^{2+} cations is responsible for the descending trend of cation mixing. The attractive force will increase the energy barrier for Ni migrating to the Li site, and therefore impede the disordering of Ni^{2+}/Li^{+}, which is the principal degradation mechanism in the layered Ni-rich NCMs. A similar coulombic interaction between negatively charged Li-TM antisite and positively charged Li-ion has been reported.[202] Using Rietveld refinement analysis, I also find that O occupancy dropped gradually with decreasing Co concentration, an evidence of the formation of O vacancies ($V_O^{\cdot\cdot}$) in the cobalt-deficient compounds. Thus, the NCM811 compound with higher Co deficiency shows less cation mixing and lower O occupancy.

Similar morphologies were observed for Co0.10, Co0.09, and Co0.08 (SEM images, shown in Figure 3.3a–c. However, high-resolution TEM (HRTEM) shows that the cobalt deficiency strongly affects the surface morphology. For all the samples, there is an amorphous surface layer with varying thickness (Figure 3.3d–f) of 1.5, 2.5, and 4.6 nm for Co0.10, Co0.09, and Co0.08, respectively. Apparently, the amorphous surface layer becomes thicker when Co concentration decreases. As suggested by Bi *et al.*,[154] the amorphous layer on the surface of Ni-rich NCM particles can be linked to the O defects caused by surface decomposition. Other studies pointed out that the absence of O^{2-} ions in the layered lattice could lower the energy barrier for Ni^{2+}/Li^{+} exchanging positions, facilitating the formation of the spinel-like and rock-salt domains.[55, 142, 206-208] These electrochemically inactive and ionic/electronic blocking domains will lead to a rapid

capacity fade and inferior rate capability. Beneath the surface layer, all the three samples show lattice fringes in their HRTEM images, indicating well-crystalized structures.

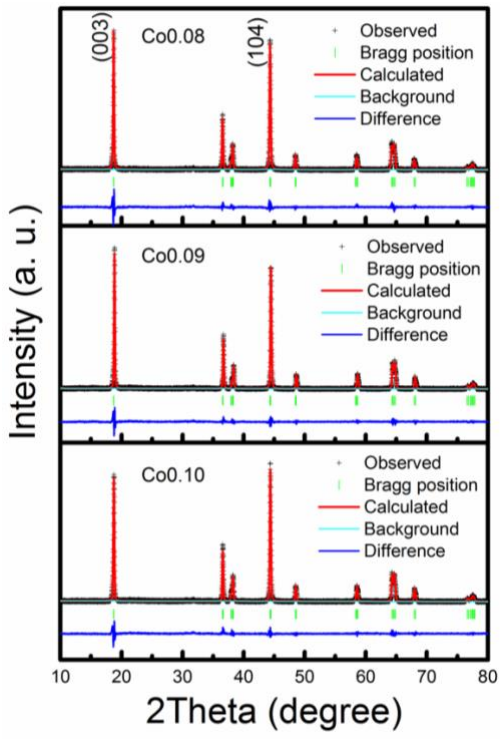

Figure 3.2 XRD and Rietveld refinement patterns of the as-synthesized particles.

Table 3.1 Structure parameters obtained from XRD patterns and Rietveld refinement.

	Co0.10	Co0.09	Co0.08
a/Å	2.8805	2.8815	2.8828
c/Å	14.2222	14.2257	14.2318
c/3a	1.646	1.646	1.646
V/Å^3	102.195	102.291	102.428
Ni_{Li}	11.37%	8.69%	8.59%
O occ. (6c)	0.8711	0.8686	0.8578
CHI^2	1.509	1.528	1.868
$I_{(003)}/I_{(104)}$	0.92	1.17	1.08

Table 3.2 Composition of transition-metal elements characterized by ICP-OES.

	Co0.10	Co0.09	Co0.08
Ni	0.7999	0.8001	0.8003
Co	0.0995	0.0850	0.0754
Mn	0.1005	0.0995	0.0995

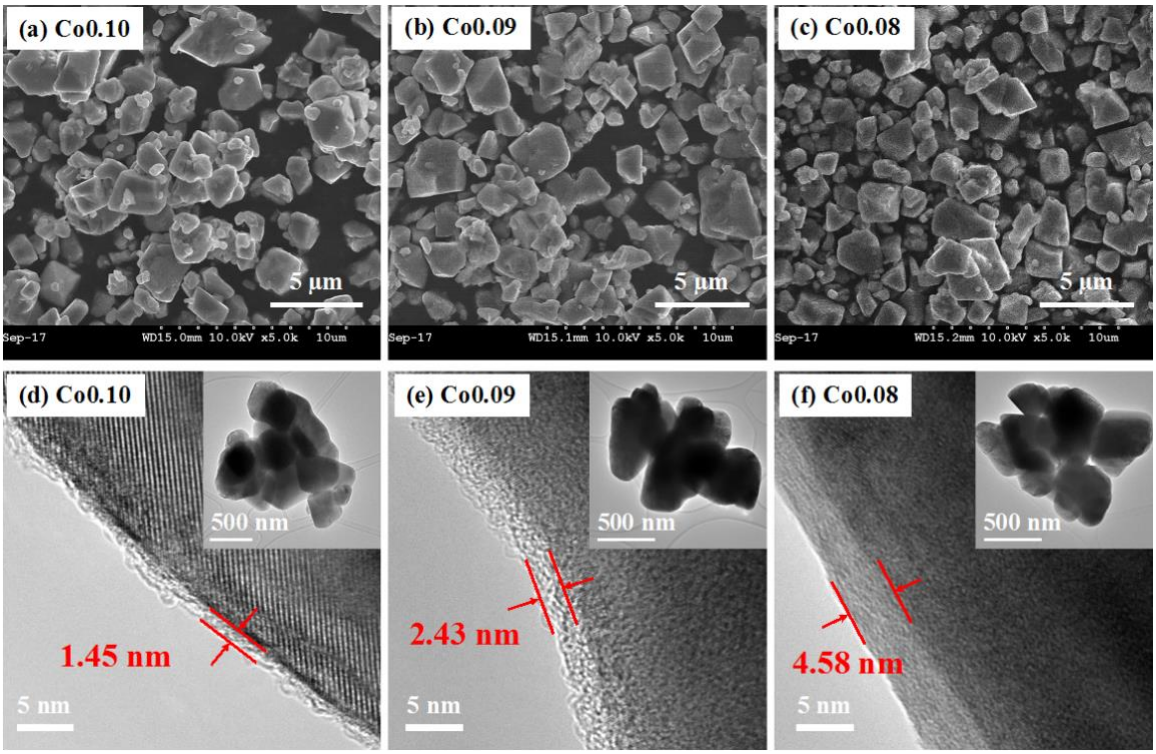

Figure 3.3 SEM (a–c) and TEM (d–f) images of the as-synthesized particles. The inserts show low-magnitude TEM images.

To further investigate the surface chemistry of the NCM particles, I conducted XPS. For each sample, photoelectron signals have been collected for C 1s, O 1s, Ni 2p, Mn 2p and Co 2p electron orbitals. All peaks were calibrated using –C–C– of 284.8 eV in C 1s.[209] For Ni-rich compounds, Co $2p_{2/3}$ and Mn $2p_{2/3}$ orbitals overlap with strong Auger signals of Ni;[133, 210] therefore, I only analyzed the Co $2p_{1/2}$ and Mn $2p_{1/2}$ orbitals. Figure 3.4 plots the raw data and fitting curves. An individual peak represents a specific charge state for each element.

By comparing the integrated area under the peaks, I estimate the proportion of ions in various chemical states. As shown in Table 3.3, each TM ion has two valences for all the three samples. The valence states of cations may differ from that reported in the literature because of the different calcining atmospheres. The peaks located at 854.8 eV and 860.9 eV represent Ni^{2+}, while the peaks belong to Ni^{3+} are 856.3 eV and 864.2 eV. The peak at 796.1 eV belongs to Co^{2+} whereas the peak at 794.9 eV can be attributed to Co^{3+}. When the Co concentration declines, the ratios of Ni^{2+}/Ni^{3+} and Co^{2+}/Co^{3+} are unchanged. All the samples consist of 59% Ni^{2+}, 41% Ni^{3+}, 34% Co^{2+} and 66% Co^{3+}. However, Mn^{3+}/Mn^{4+} varies noticeably,[55, 134, 201, 211] indicated by the peak of Mn^{3+} at 654.3 eV and Mn^{4+} at 653.2 eV. The proportion of Mn^{3+} increases from 25% in Co0.10 to 32% in Co0.09, and finally to 35% in Co0.08. To maintain charge neutrality when negatively charged Co defects (V_{Co}'' or V_{Co}''') exist, either the formation of O vacancy ($V_O^{\cdot\cdot}$) or oxidizing the remaining metal cations to the higher states of charge (i.e., oxidizing Ni^{2+} to Ni^{3+}, Co^{2+} to Co^{3+}, and Mn^{3+} to Mn^{4+}) must occur. However, based on XPS data, the concentration of Mn^{4+} decreases in the cobalt-deficient samples, which agrees with the formation of $V_O^{\cdot\cdot}$. Since the ratio of $Co^{2+}/Co^{3+} \approx 1{:}2$ for all the pristine and cobalt-deficient NCM811 samples, I believe that both V_{Co}'' and V_{Co}''' are generated when Co ions are removed from the lattice. Figure 3.4a shows the XPS results acquired from O 1s spectra. The ratio of the peak located at 528.9 eV, attributed to lattice O, decreases with the decreasing Co concentration.[55, 155] Meanwhile, surface O, that is, impurity oxides other than layered NCM with a peak at around 531.4 eV, increases with the decreasing Co concentration. The variation of O 1s peaks results from the formation of surface O defects. $V_O^{\cdot\cdot}$, initially introduced by Co deficiencies, will produce a highly reactive surface.[154] The succeeding surface reaction forming oxide impurities will enrich $V_O^{\cdot\cdot}$ on the surface, which agrees with the observed surface layer by TEM (Figure 3.3d–f). Consistent with the XPS analysis, I propose formula 3.1 to explain O vacancies and Mn reduction when Co is deficient.

$$Co_{Co}^{X} + 2O_O^X + Mn^{4+} \rightarrow 1/3\, V_{Co}'' + 2/3\, V_{Co}''' + 11/6\, V_O^{\cdot\cdot} + Mn^{3+} \qquad (3.1)$$

Together with HRTEM results, I believe that non-stoichiometry is more favorable at the surface of NCM particles.

Table 3.3 Proportions of O, Ni, Co and Mn ions in Co0.10, Co0.09, and Co0.08.

	O Lattice	O surface	Ni^{2+}	Ni^{3+}	Co^{2+}	Co^{3+}	Mn^{3+}	Mn^{4+}
Co0.08	0.21	0.79	0.58	0.42	0.34	0.66	0.35	0.65
Co0.09	0.20	0.80	0.60	0.40	0.33	0.67	0.32	0.68
Co0.10	0.30	0.70	0.58	0.42	0.35	0.65	0.25	0.75

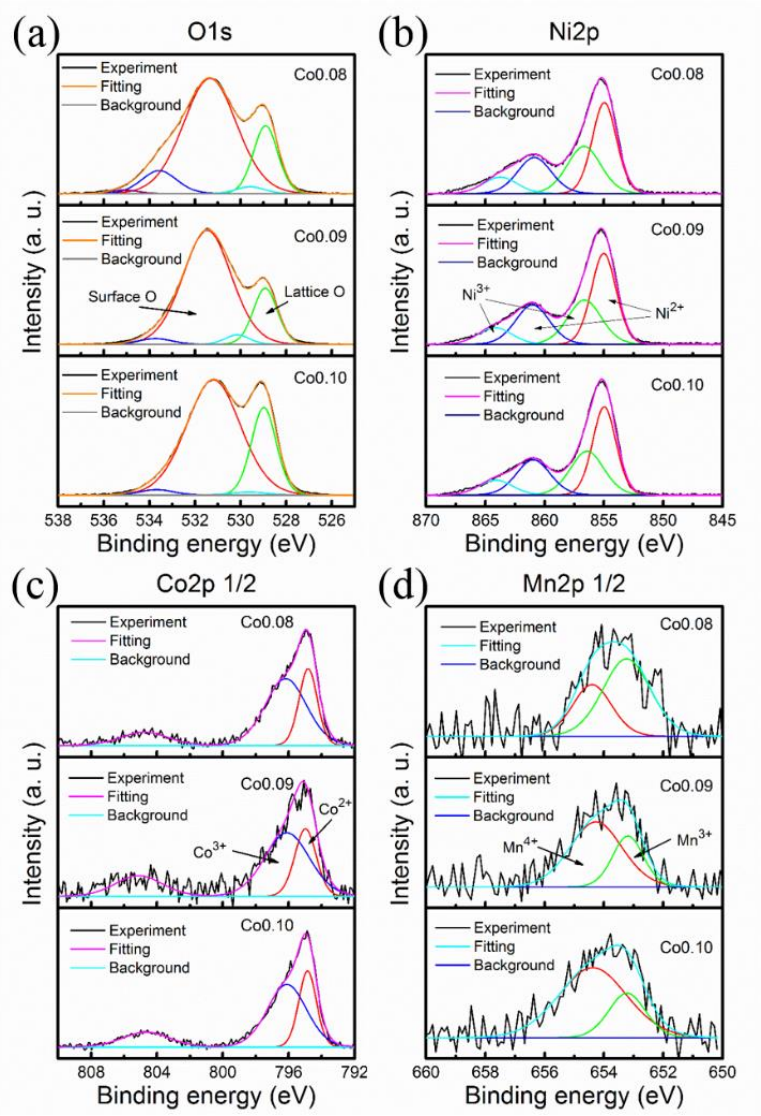

Figure 3.4 XPS data and fitting results of (a) O 1s, (b) Ni 2p, (c) Co 2p, and (d) Mn 2p for Co0.10, Co0.09, and Co0.08.

Figure 3.5 compares the electrochemical performance of the pristine and cobalt-deficient NCM811 samples. As shown in Figure 3.5a, Co0.10, Co0.09, and Co0.08 deliver

the discharge capacities of 147.5, 144.2, and 141.0 mAh/g during the first cycle at 0.2C, while the coulombic efficiencies are 58.4%, 59.6%, and 67.6%, respectively. Overall, the pristine NCM811, that is, Co0.10, performs better than the cobalt-deficient samples for both long-term cycling and rate capability (Figure 3.5b). The initial poor performance of cobalt-deficient sample results from the O defects and the thick amorphous surface layer revealed by XPS and HRTEM. During 0.2C cycling, the cobalt-deficient NCM811 exhibits rapid fading of discharge capacity as well as cutoff voltage, displayed in Fig 3.5c–e. After 60 cycles of 0.2C charging/discharging, the discharge capacity of Co0.10 is 26 mAh/g higher than Co0.08, and 42 mAh/g higher than Co0.09. The capacity difference between pristine and cobalt-deficient NCM811 becomes larger at high C-rate. At the first cycle of 1C, Co0.10 achieves 40 mAh/g more capacity versus the cobalt-deficient samples. Although the performance of Co0.09 is in between that of Co0.10 and Co0.08 during the first 20 cycles at 0.2C, its capacity unexpectedly falls below that of Co0.08 after the 20th cycle, becoming the worst among the three samples. I observe a similar tendency in the rate performance measurement: Co0.09 performs better than Co0.08 at the low C-rate of 0.1, 0.2, and 0.5C, but becomes the worst when current loading increases to 1 and 2C. After returning to 0.1C after 30 cycles, the capacity of Co0.09 and Co0.08 is similar to that for the 0.2C cycling.

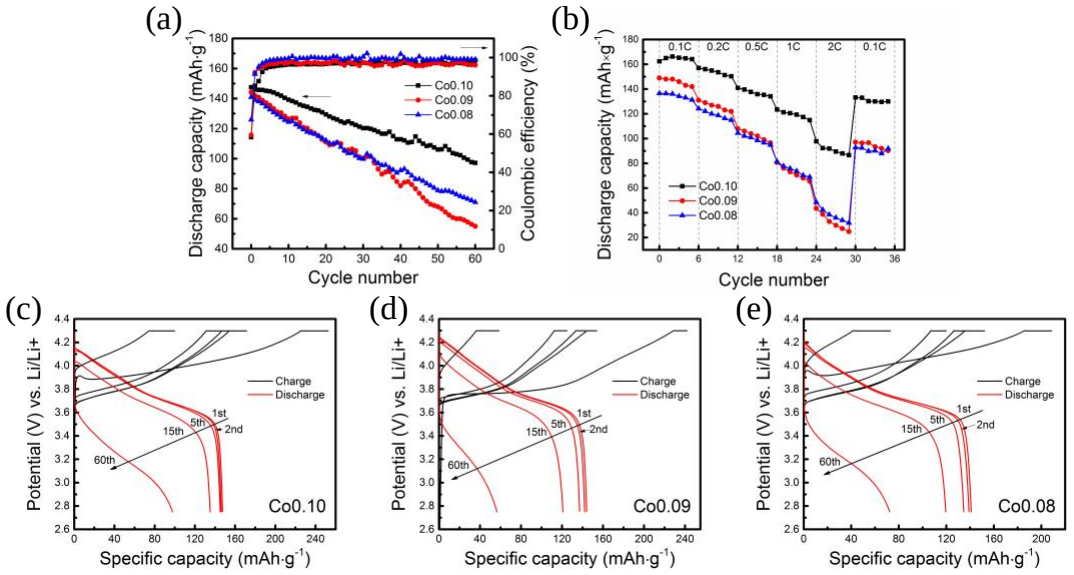

Figure 3.5 Electrochemical performance: (a) 0.2C cycling performance; (b) rate capabilities; (c–e) charging/discharging curves at different cycles in 0.2C cycling of Co0.10, Co0.09, and Co0.08.

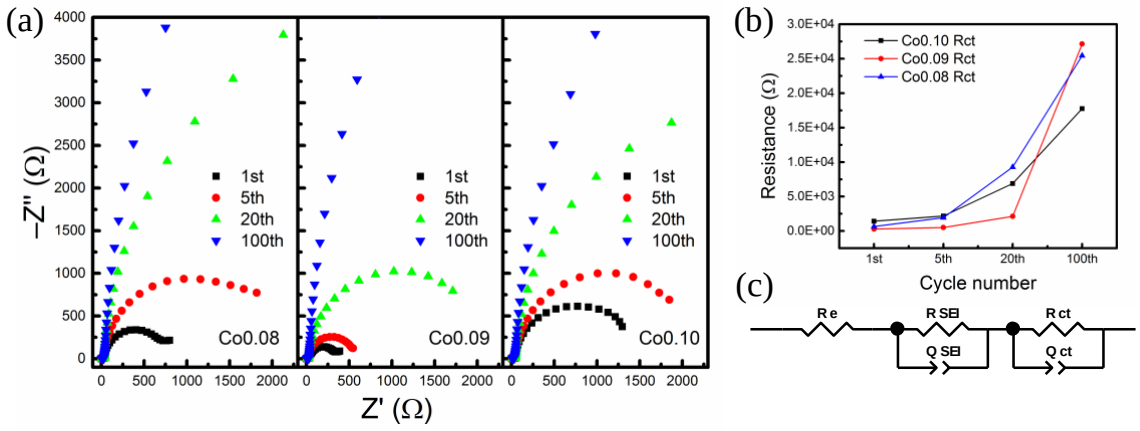

Figure 3.6 (a) EIS results and (b) charge-transfer resistances of Co0.10, Co0.09 and Co0.08 at 1st, 5th, 20th, and 100th cycles of 1C cycling. (c) The equivalent circuit.

To elucidate the factors causing the fastest fading of Co0.09, I analyzed the EIS data (Figure 3.6) during 1C cycling for each sample at 1st, 5th, 20th, and 100th cycles while fully charged. Figure 3.6a plots the Nyquist curves, where the semicircles in low-frequency range change significantly during cycling. I assign these semicircles to the charge-transfer resistance (R_{ct}).[155, 212-213] By fitting the curves to the equivalent circuit shown in Figure 3.6c, I acquire the values of R_{ct} as a function of the cycle number shown

in Figure 3.6b. The initial R_{ct} values of the three samples are similar, and then they increase gradually with increasing cycles. After 20 cycles, the R_{ct} of the cobalt-deficient samples climbs more rapidly than that of the pristine NCM811. More interestingly, Co0.09 shows the sharpest increase in R_{ct} from 20th to 100th cycle, which accords with the fastest capacity fading in the cycling test. The value of R_{ct} is related to the surface quality of active materials.[18, 130] The enhancement of R_{ct} corresponds to the structure collapse and side reactions occurring at the surface of the electrode materials. The EIS results suggest that more surface damage takes place for the cobalt-deficient samples, and the situation is more severe for Co0.09 than Co0.08.

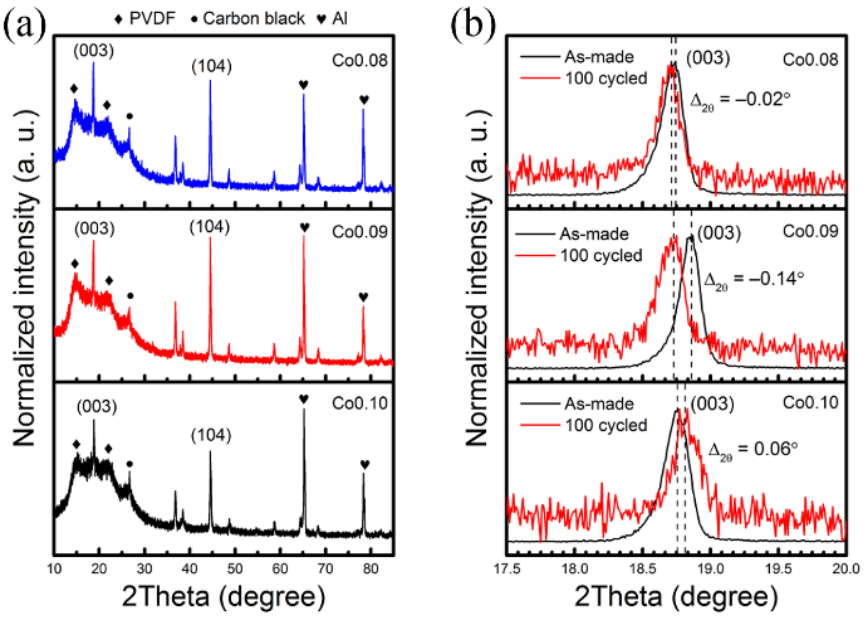

Figure 3.7 (a) XRD patterns of postcycle electrode disks and (b) the shift of (003) peak compared to the positive electrode particles.

After the 100th 1C cycling, XRD measurements were carried out on the cycled positive electrode disks. Before being opened, the coin cells were rested for 12 h after the last discharging step to make sure that the electrodes were at the same state of charge. The electrode disks were washed with DMC (BASF) and sealed in Kapton tape. The XRD measurement was completed in 2 h after taking each electrode disk out of the glovebox. Figure 3.7 shows the XRD patterns of the post-cycle electrodes, where Figure 3.7b illustrates the comparison between positive electrode particles and post-cycle electrodes. Indicated by the largest (003) peak shift, Co0.09 suffers the most severe phase damage

among the three samples.[10, 155, 214] The left shift of the (003) peak witnesses the expansion in the *c*-axis in the layered NCM, which correlates with the unoccupancy of the Li-site. When the three samples are equally charged or discharged, the largest left peak shift of Co0.09 implies the lowest reversibility of the Li-site during cycling. The loss of active Li site can result in forming inactive domains with spinel-like or rock-salt structure, which is consistent with the EIS results. The EIS and post-cycling XRD results indicate that Co0.09 is more vulnerable during charge-discharge cycles. More side reactions and phase damage on the surface will happen to Co0.09, which causes the loss of active sites of Li ions and impedes charge carrier transport, causing poor electrochemical performance.

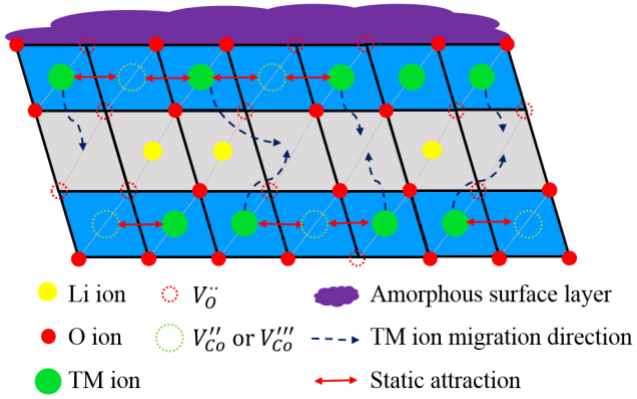

Figure 3.8 Effects of Co deficiency on NCM811.

Several publications on Ni-rich NCM positive electrode materials suggest that suppressing cation mixing and reducing O defects can lead to good electrochemical performance.[131, 134, 155-156, 201, 210] However, as illustrated in Figure 3.8, Co deficiencies in NCM811 simultaneously reduce cation mixing and introduce O defects, making the effects of Co non-stoichiometry convoluted. According to our experiments, Co deficiencies do not behave monotonically upon decreasing Co concentration, for example, Co0.09 performs worse than the less cobalt-containing Co0.08. Co vacancies can stabilize the layered structure of NCM811 by preventing the Ni-ion migration during electrochemical delithiation/lithiation because of the electrostatic attraction between the negatively charged V_{Co}''/V_{Co}''' and the positively charged Ni^{2+}. When Co non-stoichiometry reaches a specific level, for example, in Co0.08, the lattice stabilizing effect can overcome the negative effect of introducing O defects, causing the positive electrode to degrade slower than Co0.09 during long-term cycling. In general, Co deficiency should be avoided in the Ni-rich

layered positive electrode materials because of its impairment to electrochemical performance. However, it may still be possible to take advantage of the effect of Co deficiency to control cation mixing, when O vacancies can be diminished by other methods.

3.4 Summary

I have synthesized raw NCM811 (Co0.10), 10% (Co0.09), and 20% (Co0.08) cobalt-deficient NCM811 via a solid-state-reaction method, and systematically examined their crystal structure, morphology, surface chemistry, and electrochemical performance. The Co deficiency can reduce cation mixing in NCM811, probably because of the strong electrostatic attraction between V_{Co}''/V_{Co}''' and Ni^{2+}. However, the cobalt-deficient samples show worse cycling stability and rate capability than the raw NCM811. The worse performance can be linked to the O vacancies ($V_O^{\cdot\cdot}$) induced by Co deficiency, which can impair the surface stability of the Ni-rich positive electrode material, increase charge-transfer resistance during electrochemical charging/discharging, and finally cause fast capacity fading. Interestingly, Co0.09 shows the lowest capacity retention after long-term cycling among the three samples, albeit it has less cobalt deficiency than Co0.08. The reason is probably that, when Co deficiencies reach 20% in Co0.08, the benefit of suppressing cation disordering becomes more significant than the surface damage caused by O vacancies for long-term electrochemical cycling.

According to these findings, Co deficiency needs to be avoided in Ni-rich layered NCM positive electrode materials, when the formation of O defects, especially at the surface area, cannot be effectively mitigated.

CHAPTER 4. Structural, Electrochemical and Li-Ion Transport Properties of Zr-Modified $LiNi_{0.8}Co_{0.1}Mn_{0.1}O_2$ Positive Electrode Materials for Li-Ion Batteries

I modified a Ni-rich layered NCM811 positive electrode material by substituting the transition metals with Zr to mitigate its structural instability and capacity degradation. I show that Zr, over a concentration range of 0.5–5.0 at.%, can simultaneously reside on the lattice of NCM811 and form Li-rich lithium zirconates on the surfaces NCM811 particles. In particular, $Li(Ni_{0.8}Co_{0.1}Mn_{0.1})_{0.99}Zr_{0.01}O_2$ (1% Zr-NCM811) exhibits the best rate capability among all the compositions in this study. It shows higher cycling durability than the raw NCM811 at both low and high current density cycling. According to XPS and CV measurements, 1% Zr-NCM811 sample is more chemically/electrochemically stable than the raw. In addition to comparing the diffusivities in the coin-cell measurements, I demonstrate that Zr modification can facilitate Li-ion diffusion in the NCM811 balk material by DC polarization measurements. The elevated Li-ion diffusivity of Zr-NCM811 results from the lattice expansion induced by Zr doping and the presence of ion-conducting lithium zirconates partially coating on the surface of Zr-NCM811 particles.

4.1 Introduction

As the growth of the global EV market accelerates, it is vital to develop positive electrode materials for LIBs with high energy density and fast charging durability.[2, 115, 215]

The symmetric layered mixed-transition-metal compound, $LiNi_{1/3}Co_{1/3}Mn_{1/3}O_2$, can deliver about 155 mAh/g of capacity when operating between 3.0 and 4.3 V versus Li/Li^+.[93, 104, 107-108] By substituting Co in $LiCoO_2$ with Ni and Mn, $LiNi_{1/3}Co_{1/3}Mn_{1/3}O_2$ improved capacity, stability, and cost efficiency. However, its capacity is still insufficient for EVs application.[216-217] Since the redox pair of Ni^{2+}/Ni^{3+} contributes the majority of the capacity when the voltage is below 4.3 V versus Li/Li^+,[9, 127] a high Ni concentration usually implies elevated capacity in the family of the layered NCMs.

In the past two decades, extensive studies have focused on the composition of $LiNi_{1-2x}Co_xMn_xO_2$ ($x \leq 0.2$). These Ni-rich NCMs are capable of delivering 180–240 mAh/g of discharge capacity with 2.7–4.3 V as the voltage window, corresponding to 650–800 Wh/kg of energy density at the material level.[9, 18] Despite their promising high

capacity, Ni-rich NCMs face several challenges, for example, fast capacity fade and significant heat/gas release during electrochemical cycling.[125-126, 128, 139, 149] Ni^{2+} can migrate to the Li slab during synthesis and cycling, due to their similar ionic radii, leading to a disordered structure and eventually irreversible phase transformation. At the high state of charge (> 4.5 V), Ni^{2+} will be oxidized to highly reactive Ni^{4+}, which reacts with the organic electrolyte, releasing O_2 and forming SEI. The cation disorder and side reactions will cause capacity loss and hinder the transport of Li ions. Furthermore, the Li-ion diffusion in Ni-rich compounds is not fast enough to meet the demands for fast charging, which results in significant capacity drop during high rate cycling. Therefore, stabilizing the layered structure and facilitating Li-ion transport are important topics of research worldwide.

Zr modification has been proposed as an effective method addressing the abovementioned issues of Ni-rich NCM. However, controversies exist among researchers regarding the mechanism of the Zr modification, as discussed in Chapter 1. In the present chapter, I look forward to offering a better understanding by experimentally studying the structure, electrochemistry, and Li-ion transport behavior of Zr-modified Ni-rich NCM811 positive electrode materials in LIBs.

4.2 Experimental

To synthesize pristine and Zr-modified $LiNi_{0.8}Co_{0.1}Mn_{0.1}O_2$ (Zr-NCM811) by sol-gel method, I dissolved $LiNO_3$ (Reagent plus@, Sigma-Aldrich), $Ni(NO_3)_2 \cdot 6H_2O$ (98%, Alfa Aesar), $Co(NO_3)_2 \cdot 6H_2O$ (ACS, 98.0-102.0%, Alfa Aesar) and $Mn(NO_3)_2 \cdot 4H_2O$ (98%, Alfa Aesar) in D.I. water. In another beaker, $Zr(C_5H_7O_2)_4$ (Alfa Aesar) was dissolved in a 1:1 (by volume) mixture of D.I. water and ethanol. Then the two solutions were mixed together, where the cation ratio followed the formula of $Li_{1.05}(Ni_{0.8}Co_{0.1}Mn_{0.1})_{1-x}Zr_xO_2$, x = 0, 0.005, 0.01, 0.02, 0.05, representing the pristine, 0.5, 1.0, 2.0, and 5.0% Zr-NCM811, respectively. Citric acid (99%+, Alfa Aesar) was added to the precursor solution based on a 1:1 molar ratio to total cations. After stirring shortly, I slowly added $NH_3 \cdot H_2O$ (50% v/v aqueous solution, Alfa Aesar) to the light green transparent solution to keep the pH value within 7.0 to 7.2. I then set the temperature of the hot plate to 90 °C and kept stirring for around 15 h until an aqua blue gel was formed. The gel was baked at 150 °C for 24 h in an

ambient oven and was then transferred to a box oven. After a calcination at 480 °C for 8 h in air, organic components were removed and intermediate products were obtained as fine powders in dark brown. The powders were then collected and calcined at 900 °C for 15 h in oxygen. The as-prepared electrode powders were stored in argon-filled glovebox for further characterizations and measurements.

Phase identification for synthesized powders was performed by HRXRD on beamline 11-BM at the Advanced Photon Source of Argonne National Laboratory. The samples were loaded into Kapton capillaries and rotated during the measurement. The measurement conditions were 22 °C, a wavelength of 0.41272 Å, and a 2θ step-size of 0.001° from -6.0° to 28.0°. Rietveld refinements were carried out using GSAS software and EXPGUI interface (Los Alamos National Laboratory, USA).[204-205] Morphology of the particles was observed using SEM (Hitachi S4300) and TEM (JOEL 2010F), while the element distribution was examined by EDS (FEI Quanta 250). The surface chemical condition was studied using XPS (Thermo Scientific K-Alpha).

The electrode slurry was made by dispersing the NCM811 powders, CB (Super P C65, Sigma Aldridge), and PVDF (MW ≈ 1100 g/mol, Kureha Corporation) in NMP (VWR, Biotechnology Grade). The slurry was cast uniformly onto carbon-coated aluminum foil (MTI Corporation, 18 μm in thickness), and was dried at 120 °C overnight under vacuum. Then the electrode films were transferred into glovebox and punched into circular disks in 1/2 inch diameter. The electrode contained 80 wt.% NCM, 10 wt.% CB, and 10 wt.% PVDF. The typical mass loading of active material was 3.8 $mg \cdot cm^{-2}$.

Half cells using Li (Alfa Aesar, 0.75 mm in thickness), Celgard 2400 separator, and 1 M $LiPF_6$ in EC:DEC (1:1 in vol., BASF) were assembled in 2032 coin cells (MTI Corporation) inside an Ar-filled glovebox. All electrochemistry measurements were conducted on the electrochemistry workstation (Biologic VSP). The cells were cycled with the voltage window between 2.8 and 4.3 V versus Li/Li^+. For each cycle of charging, the voltage was held at 4.3 V until current loading drops to 0.1C (1C = 200 mAh/g). CV was performed under the scanning rate of 0.1 mV/s between 2.8 and 4.3 V. EIS was performed at fully discharging state after specific cycle numbers during 1C charging/discharging, over the frequency range from 1 MHz to 10 mHz. All the electrochemistry measurements were performed at room temperature.

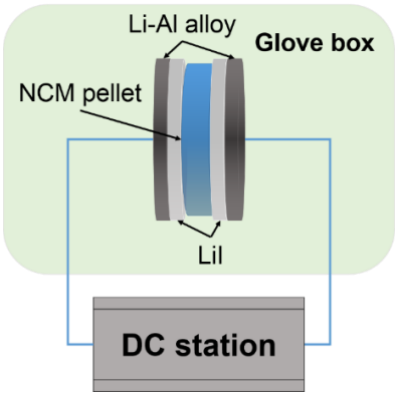

Figure 4.1 Configuration for the DC polarization measurement.

DC polarization was carried out on the pellet sample to determine the bulk Li-ion diffusion coefficient of Zr-NCM811, of which the measurement setup is shown in Figure 4.1. LiI pellets served as the electron blocking electrodes while Li–Al alloy pellets act as the Li-ion sink as well as current collectors. The contact resistances at the LiI/NCM and LiI/Li–Al alloy interfaces were minimized by heating the assembled cell under vacuum at 200 °C for 20 h. The sample pellet was sintered following the same procedures for the NCM811 particles. The testing cell, Li–Al/LiI/NCM/LiI/Li–Al, is clamped by copper blocks and connected to a DC station (Keithley 2400 Multimeter).

4.3 Results and Discussion

Figure 4.2a shows the HRXRD patterns (synchrotron X-ray) for Zr-NCM811 samples with different Zr concentrations. The peaks labeled with Miller index represent the α-$NaFeO_2$-type layered structure belonging to NCM811. The clear splitting of (006)/(102) and (108)/(110) pairs observed in all the samples confirms the expected hexagonal arrangements of O^{2-} ions.[131, 195] The intensity ratios of (003)/(104) are 2.20, 2.18, 2.14, 1.92, and 1.92 for the raw NCM811, 0.5%, 1%, 2%, and 5% Zr, respectively, indicating a well-ordered layered structure for each composition. As presented in Figure 4.2b–c, the (003) and (104) peaks shift to the left with increasing Zr content. The lattice expansion is most likely caused by Zr residing in the layered lattice. The down arrows in Figure 4.2a mark the impurity phases present in the 5% Zr-NCM811. When plotting the intensity in log scale, as shown in Figure 4.3, the impurities become visible in the 0.5% Zr-NCM811, the least Zr-containing sample in the present study. According to the reference

patterns shown in Figure 4.3, the impurities can be assigned to multiple lithium zirconates, including Li_2ZrO_3, Li_4ZrO_4, and $Li_6Zr_2O_7$. It is important to point out that Li_2ZrO_3 only appears in the 5% Zr-NCM811 sample while Li-rich zirconates start to form at lower Zr concentrations. Based on HRXRD results, Zr can simultaneously reside on the crystal lattice of NCM811 and form lithium zirconates. I suggest that these two effects are both thermodynamically favorable, consistent with DFT calculations.[175, 182, 218]

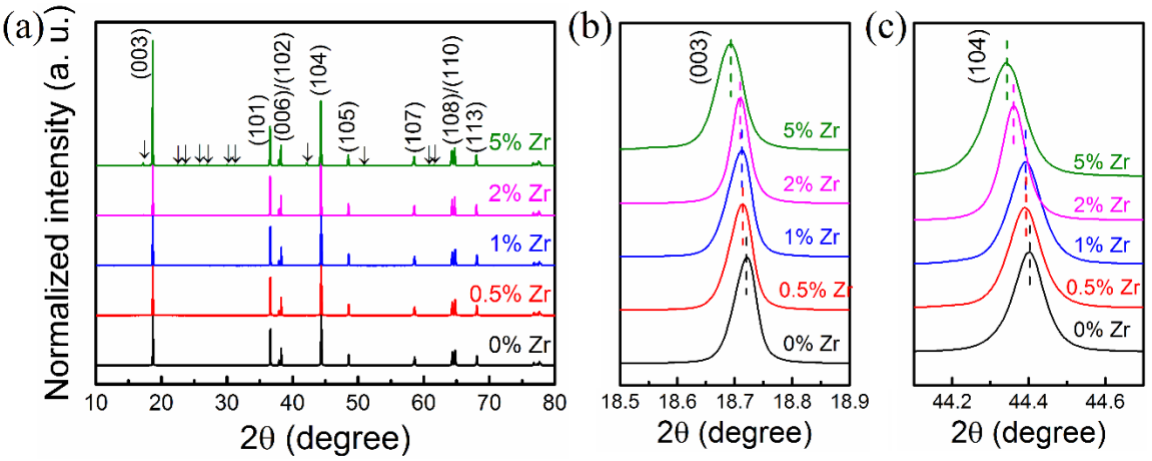

Figure 4.2 (a) Synchrotron HRXRD patterns of NCM811s with different Zr concentrations, and enlarged display of (b) (003) and (c) (104) peaks.

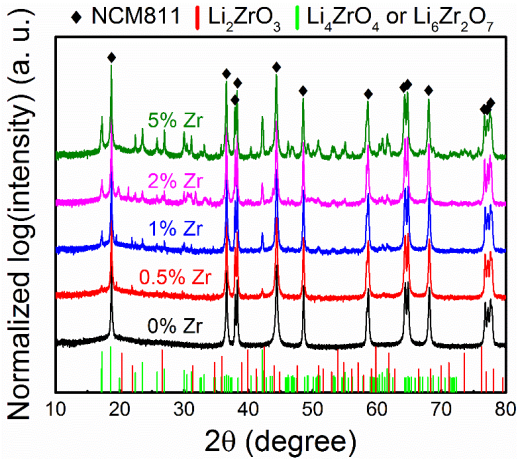

Figure 4.3 HRXRD patterns showing intensity (in log-scale) versus diffraction angle and reference peaks of several lithium zirconates.

SEM images in Figure 4.4 exhibit no apparent differences among the as-synthesized electrode particles with different Zr concentrations. The primary cobblestone-like particles are 1–5 μm in diameter. EDS mappings (Figure 4.5) reveal uniform distributions of Ni, Co, and Mn in all the samples, labeled by purple, green, and yellow,

respectively. Meanwhile, the red regions representing Zr enlarge gradually with increasing Zr as expected, indicating that lithium zirconates form on the surfaces of electrode particles. By measuring the proportion of Zr-aggregated areas in the EDS maps, I estimated that lithium zirconates cover approximately 4.9, 7.6, 11.4, and 18.4% of the surface area of the particles for the 0.5, 1, 2, and 5% Zr-NCM811, respectively.

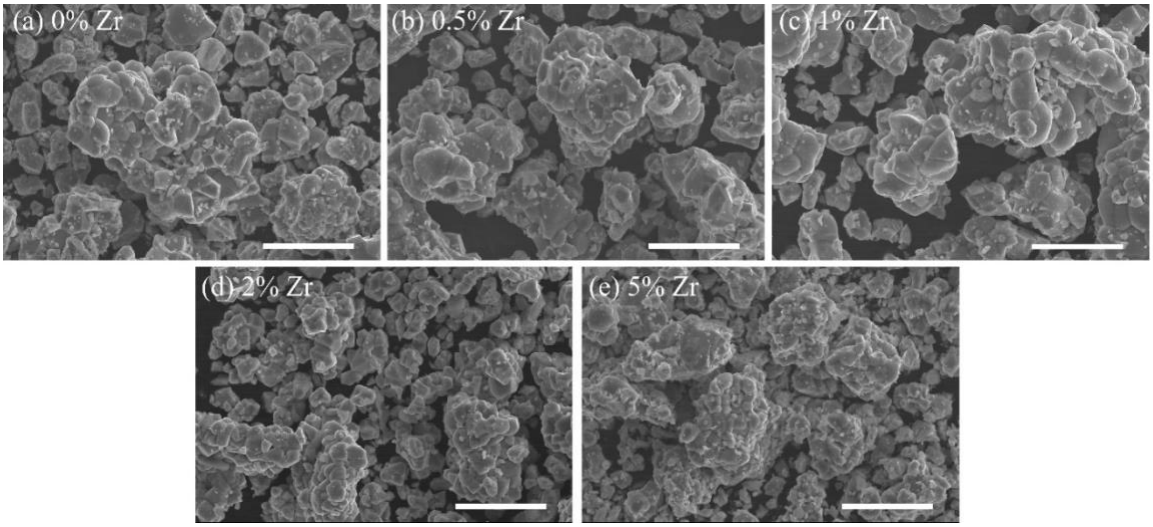

Figure 4.4 SEM images of NCM811s with different Zr concentrations. Scale bars represent 10 μm.

Rate capability measurements were carried out upon the raw, 0.5, 1, and 2% Zr-modified NCM811 samples. As shown in Figure 4.6a, 1% Zr-NCM811 performs the best among all the samples, delivering discharging capacities of 192, 185, 173, 162, 149, 125, and 100 mAh/g, respectively, at the current rate of 0.1, 0.2, 0.5, 1, 2, 5, and 10C. The performance of the raw NCM811 agrees with the published results on co-precipitation and sol-gel synthesis.[176, 178, 219-220] As can be seen in Figure 4.6b, the lead of 1% Zr-NCM811 against the pristine sample is smaller than 10 mAh/g at 0.1C but reaches over 20 mAh/g at the high rate of 5C. 0.5% Zr-NCM811 possesses the second-best performance, slightly worse than the 1% Zr one through all C-rates. For 2% Zr-NCM811, 180 mAh/g is achieved at 0.1C, which is similar to that of NCM811. However, its capacity quickly degrades to 130 mAh/g during 1C cycles, approximately 20 mAh/g lower than that of the raw NCM811. The poor performance of 2% Zr-NCM811 may be linked to the excessive inactive lithium zirconates identified by XRD and EDS. Similar adverse effects of impurities have been widely reported in doping and coating studies.[163, 171, 221]

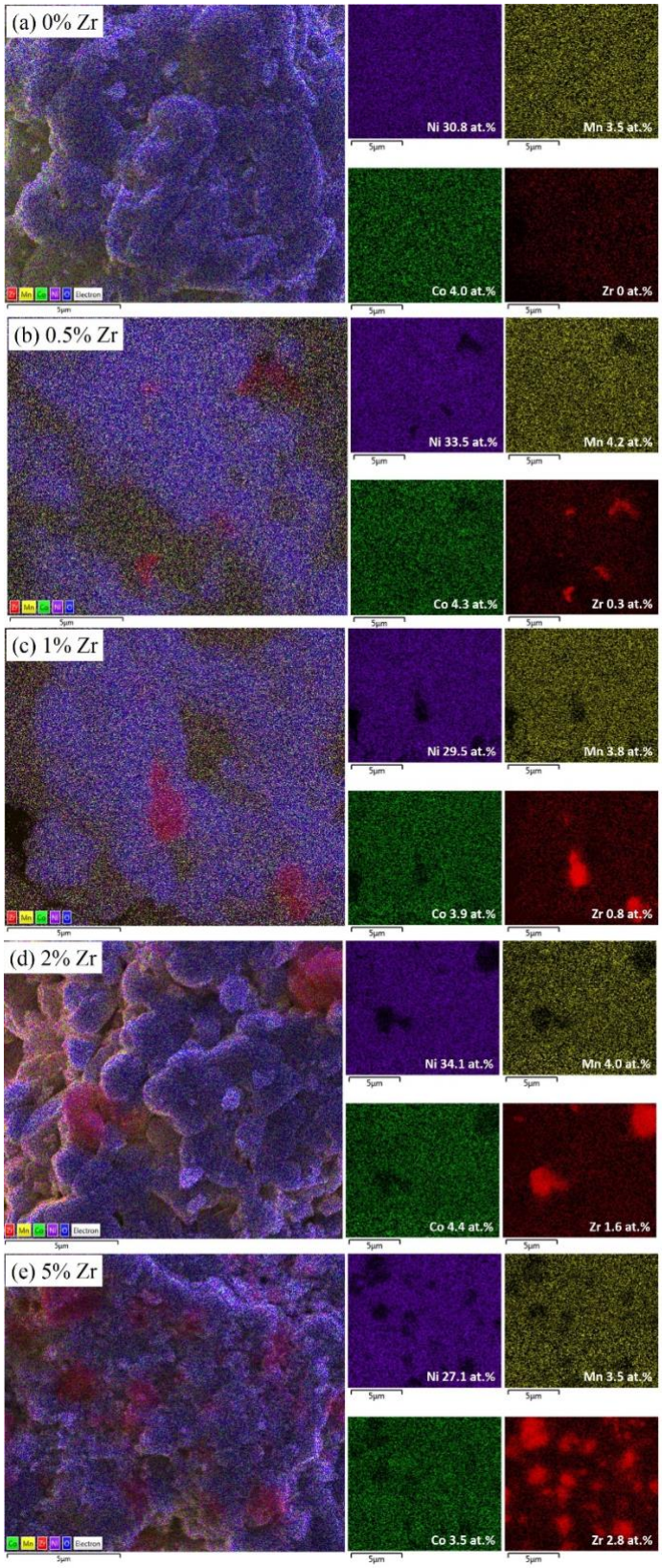

Figure 4.5 EDS mappings of NCM811s of different Zr concentrations.

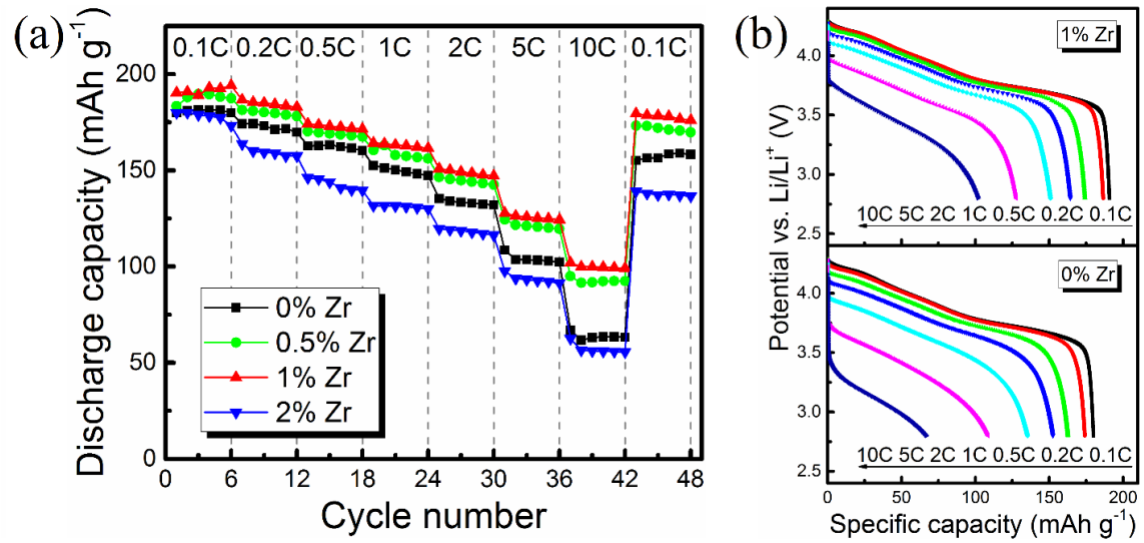

Figure 4.6 (a) Rate performance of NCM811s with different Zr concentrations. (b) Discharging curves at different C-rates of raw NCM811 and 1% Zr-NCM811.

Following the rate capability results, 1% Zr-NCM811 is further investigated along with the raw NCM811. Figure 4.7 shows their cycling performance at 0.2 and 2C. At the first cycle of 0.2C, the pristine and 1% Zr-modified NCM811 have comparable performance, delivering discharging capacities of 184.0 and 183.8 mAh/g with the coulombic efficiencies (CE) of 78.5 and 78.7%, respectively. The capacity of 1% Zr-NCM811 then increases to 184.7 mAh/g due to an activation process. Such activation phenomenon has been reported in the doping and coating studies regarding to the layered NCM positive electrode materials.[180, 222-223] After about 10 cycles, the CE increases to approximate 100% for each sample. After 60 cycles, 1% Zr-NCM811 retains 84.2% of its initial capacity in contrast to 80.0% of the raw NCM811. Evidently, the CE of the raw NCM811 is higher than the 1% Zr sample, which is over 100% after 5 cycles. It suggests that more side reactions take place for the raw NCM811 than that with 1% Zr.[224-225] 2C cycling starts after two activation cycles at 0.2C. The discharge capacities of the first cycle for 2C discharging are 163.0, 159.0 mAh/g for the raw, and 1% Zr-modified NCM811, respectively. Each sample deliveries an approximate 99% coulombic efficiency. The capacity retention of 1% Zr-NCM811 is 84.3% after 60 cycles, which is 15.1% higher than that of the raw sample. Interestingly, the capacity retention of 1% Zr-NCM811 at 2C is as good as that at 0.2C. In contrast, the raw NCM811 fades faster at high rates. Furthermore, the average voltage plotted in Figure 4.8 follows a similar trend, where Zr modification

effectively slows down the voltage decay, especially during high-rate cycling. The EIS results shown in Figure 4.9 illustrate that 1% Zr-NCM811 cell maintains a lower R_{SEI} than raw NCM811 after 30 and 60 cycles at 1C, which matches well with the better cycling performance of 1% Zr-NCM811.

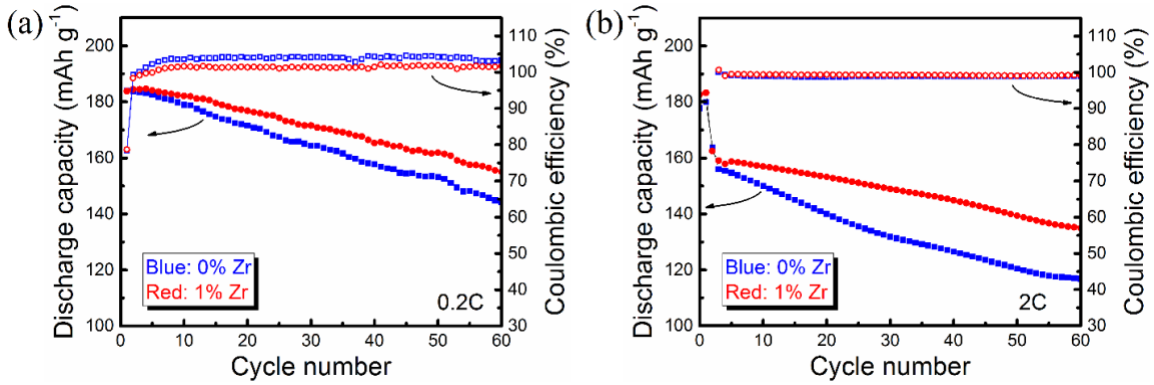

Figure 4.7 Discharge capacity and Coulombic efficiency versus cycle number of raw NCM811 and 1% Zr-NCM811 at (a) 0.2 and (b) 2C.

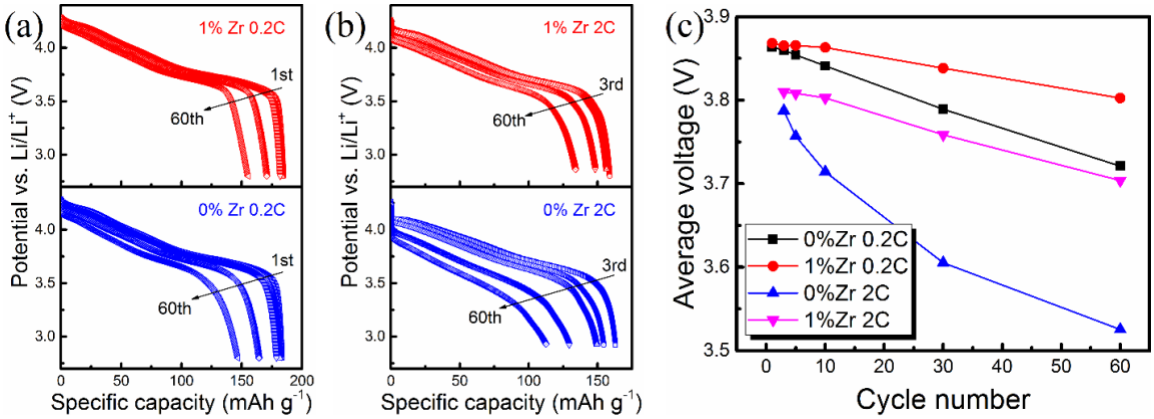

Figure 4.8 Discharging curves of raw NCM811 and 1% Zr-NCM811 at (a) 0.2C and (b) 2C; (c) the corresponding voltage degradation.

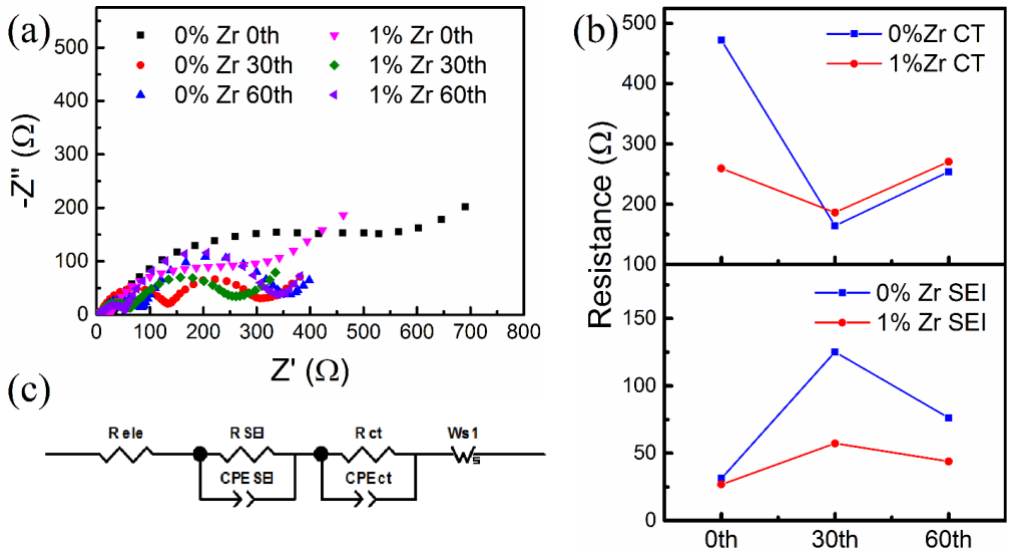

Figure 4.9 (a) EIS results of raw and 1% Zr-modified NCM811 cells at different stage of 1C cycling, (b) the interpreted R_{SEI} (lower plot) and R_{ct} (upper plot) by (c) the equivalent circuit: R_{ele} is mainly related to the electrolyte solution resistance. Two semicircles can be associated, from high frequency to low frequency, with the resistance of solid-electrolyte interphase (R_{SEI}) and the charge-transfer resistance (R_{ct}), respectively.

The mechanisms responsible for the better capacity retention and high-rate capability of 1% Zr-NCM811 relative to the raw sample were explored in detail by several characterization techniques. Figure 4.10 shows the refinement results of the HRXRD patterns for both samples, and Table 4.1 lists the lattice parameters. 1% Zr-NCM811 shows a volume expansion, which agrees with the peak shift shown in Figure 4.2b–c, most likely due to the elongation along *c*-axis induced by Zr incorporation,[174-175, 178] while the lattice parameters show little change in the *a*- and *b*-axis. The increment along the *c*-axis enlarges the space between cation and oxygen slabs, herein reduces the energy barrier for Li-ion migration within the Li layer, and benefits Li-ion diffusion.[9, 180] The refinement result also indicates that Zr ions occupy 0.57% TM sites in the lattice of 1% Zr-NCM811. Thus, 57% of Zr ions reside in the layered structure and the rest form Li-rich zirconates on the surface of particles.

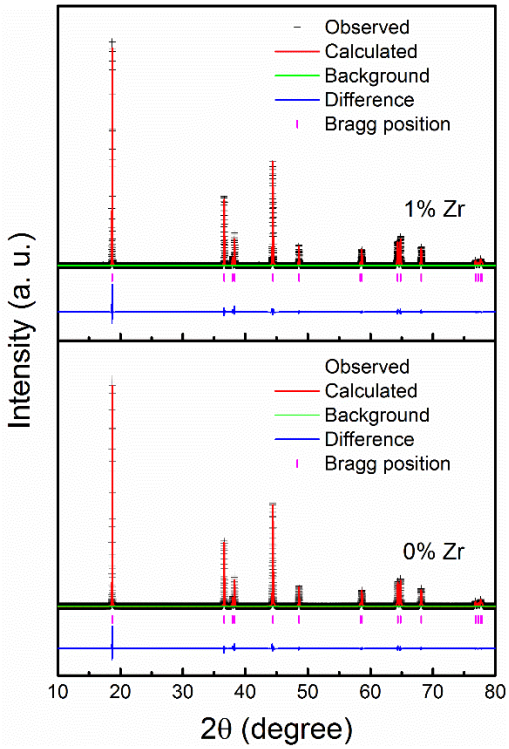

Figure 4.10 HRXRD patterns of raw NCM811 and 1% Zr-NCM811 with refinement.

Table 4.1 Lattice parameters of raw NCM811 and 1% Zr-NCM811.

	a/Å	b/Å	c/Å	Vol./Å^3	c/3a	Ni/Li (3c)	Zr Occ.	Rp	Chi^2
0% Zr	2.8745	2.8745	14.2106	101.689	1.648	2.1%	0%	9.7%	6.070
1% Zr	2.8744	2.8744	14.2167	101.723	1.649	1.8%	0.57%	9.6%	7.178

Under TEM, I studied elemental distribution using EDS in the central and marginal regions of the electrode particles, as shown in Figure 4.11. The atomic ratio of transition metals is shown in the table inserted in Figure 4.11c. For the raw NCM811, the atomic ratio of three TM elements does not change for the four detected areas. It suggests that Ni, Co, and Mn distribute uniformly through the whole particle. For the 1% Zr modified sample, however, region B shows Zr enrichment, while no Zr trace appears in the other three regions. The observation agrees with the EDS mapping results shown in Figure 4.5. I then moved to the edge of the raw NCM811 and the Zr-rich region of the modified sample, where high-magnification images were collected. For the raw NCM811, the fringes of layered lattice are revealed from the center to the edge (Figure 4.11b), suggesting a well-

crystallized NCM811 particle. In contrast, I found a coating layer present on the Zr-rich surface of 1% Zr particle, where crystalline and amorphous lithium zirconates coexist, as shown in Figure 4.11d. Such partial-coating configuration can protect the active material underneath and improve Li-ion diffusion in the vicinity, as reported in Li_2ZrO_3-coating studies.[184-185] Combining the results of XRD refinement and TEM/EDS, I further confirm the dual functions of Zr modification, in that Zr can function as dopants to expand the lattice and form lithium zirconates coating on the electrode particles.

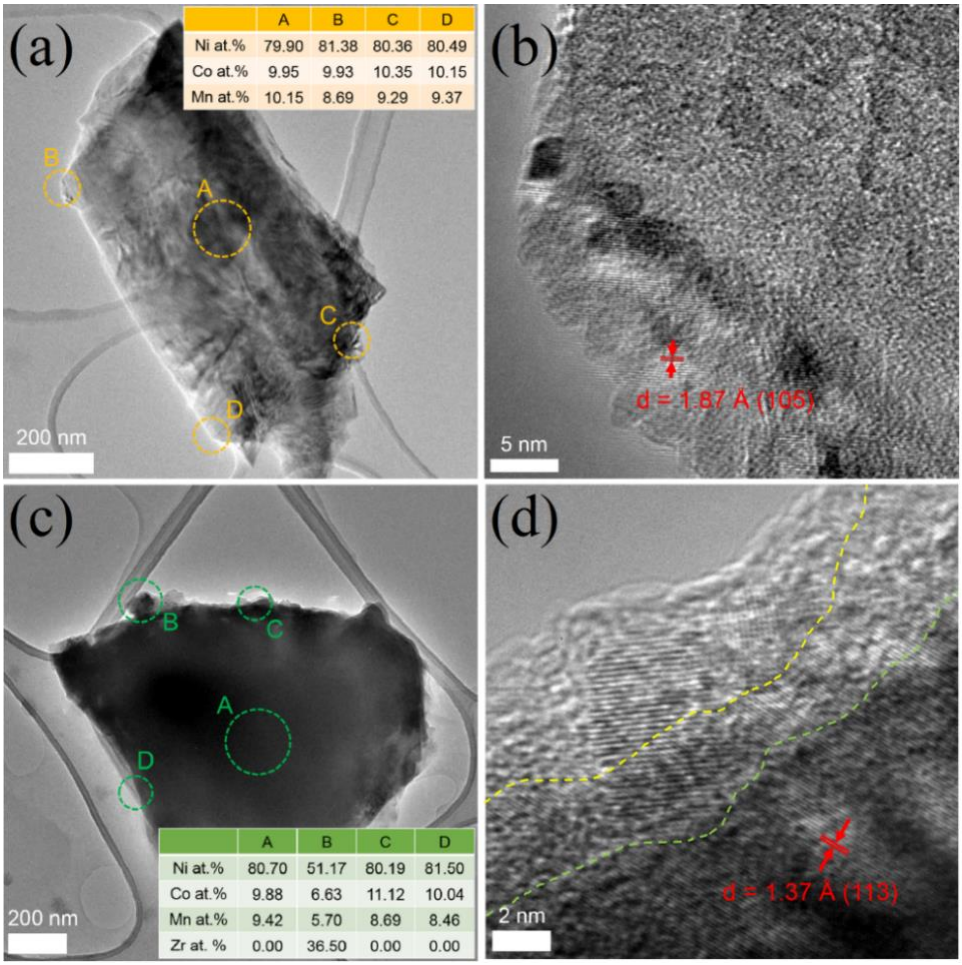

Figure 4.11 TEM images and EDS results of (a, b) raw NCM811 and (c, d) 1% Zr-NCM811.

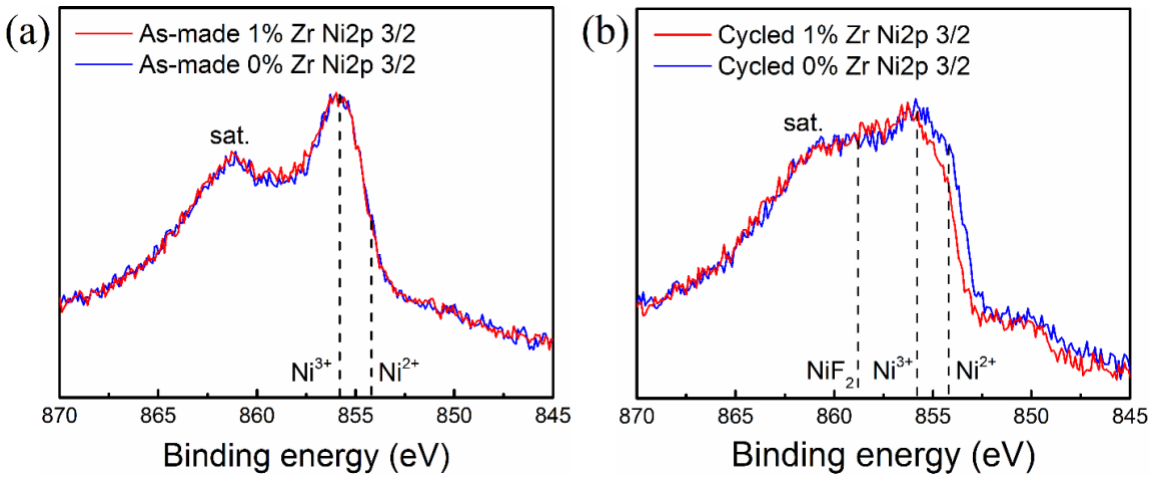

Figure 4.12 XPS spectra (Ni $2p_{3/2}$) of raw NCM811 and 1% Zr-NCM811 for (a) as-made and (b) 0.5C cycled electrode disks.

In order to investigate the chemical variation of electrode particles during cycling, I compared the XPS spectra of the as-made and cycled electrodes for both samples. The major difference lies in Ni 2p signals shown in Figure 4.12. The as-made raw and the Zr-modified samples show almost identical spectra, where the dash lines mark the peaks at 854.2 and 855.8 eV for the respective Ni^{2+} and Ni^{3+}.[133, 210, 226] Clearly, Ni^{3+} is the predominant Ni ions in the as-made electrodes, which is consistent with previous reports,[133, 155] but the chemical states of transition metals do not change with Zr incorporation. After being cycled at 0.5C for 60 cycles (Figure 4.12b), a peak at 858.8 eV rises significantly in each sample and it can be assigned to NiF_2 produced from side reactions during cycling.[170, 227] In addition, the proportion of Ni^{2+} increases in each sample. More interestingly, the raw NCM811 possesses more Ni^{2+} than that in 1% Zr-NCM811. The appearance of Ni^{2+} can be linked to the irreversible phase changes, that is, layered structure converts to spinel and/or rock-salt phase, and concomitant side reactions, which are considered as the main factors for the capacity degradation.[18, 228] Accordingly, the XPS results show that 1% Zr-NCM811 is more stable during electrochemical cycling, and thus has a better capacity retention than the raw sample.

Using CV measurements, I further compare the stability of the raw and the Zr modified NCM811 electrodes. Figure 4.13a plots the CV curves at specific cycle numbers. Three pairs of anodic and cathodic peaks locate at around 3.8, 4.0, and 4.2 V correspond to the phase transition of hexagonal (H1) to monoclinic (M), monoclinic (M) to hexagonal

(H2), and hexagonal (H2) to hexagonal (H3), respectively.[11] According to the CV curves shown in Figure 4.13a, the features of the M-H2 and H2-H3 peaks retain better for 1% Zr-NCM811 than the raw. Additionally, Figure 4.13b demonstrates the evolution of the potential gap between the major anodic and cathodic peaks (H1-M) for the two samples. In an electrochemistry system, the smaller potential gap implies that a redox reaction is more reversible.[175, 178] For these two samples, the values of 1% Zr-NCM811 are higher than the raw in the initial five cycles. This phenomenon is consistent with the activation process discussed in the cycling results. More importantly, the potential gap for 1% Zr-NCM811 sample climbs slower than that for raw NCM811, suggesting that the Zr modified sample shows better retention in redox kinetic and, therefore, superior stability during cycling, in accordance with the XPS analysis. The superior chemical and electrochemical stability of 1% Zr-NCM811 are due to the stabilization of the bulk NCM811 by Zr doping and the formation of lithium zirconates on the surface of the NCM811 particles. As Schipper *et al.* reported, the doped Zr^{4+} can stabilize the layered lattice by hindering the phase transformation from layered to spinel.[175, 182] In addition, the partially coated lithium zirconates will not participate in the redox reaction during lithiation and delithiation, but protect the active material underneath from dissolution and side reactions, which has been reported in several coating studies of NCMs.[123, 184, 223] However, I believe that the Zr^{4+} doping contributes more to improving NCM811's stability than the Li-rich zirconate coating, because more Zr ions reside in the layered lattice and the coating coverage is lower than those reported in literature.[182, 184]

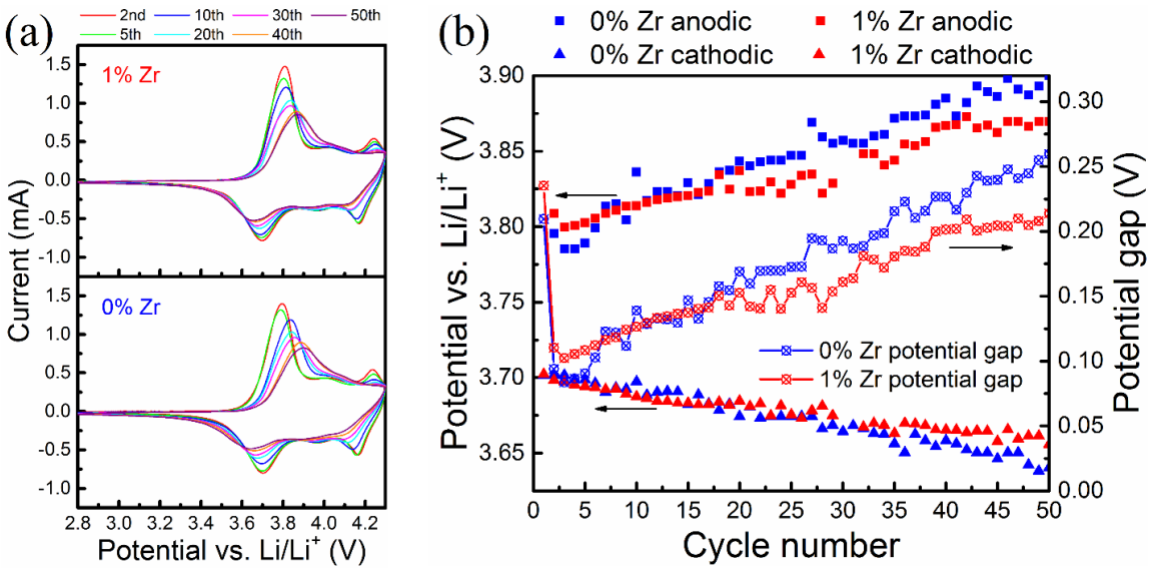

Figure 4.13 (a) CV curves and (b) anodic/cathodic peak position and the potential gap values versus cycle number of raw NCM811 and 1% Zr-NCM811.

I performed DC polarization to investigate the Li-ion diffusion behavior of the balk NCM materials. Driven by a DC current, Li-ions sluggishly pass through the NCM and LiI pellet and insert into Li–Al alloy, meanwhile the polarization voltage is monitored. According to the equilibrium potential and the duration to reach such state, I am able to extract the diffusivity of Li-ion.[229-230] However, in a material such as NCM, where electronic conductivity dominates, and the time for polarization of Li-ion to reach the equilibrium state is usually beyond the instrument's capability. Herein, I apply formula 4.1 to estimate the equilibrium potential (U_{ion}), where i_p is the bias current, L the thickness of sample, σ the total conductivity, $\sigma_{el}$the electronic conductivity, σ_{ion} the ionic conductivity, t the time, and τ^{δ} the relaxation time for the polarization process. Figure 4.14a displays the measured data and fitting results. I replot the data with $ln|U - U_{\infty}|$ versus time, as shown in Figure 4.14b, and calculate Li-ion diffusion coefficient, D_{Li}, using formula 4.2 by fitting the linear parts. D_{Li} of 1% Zr-NCM811 is 4.23×10^{-8} cm^2/s, more than three times higher than 1.26×10^{-8} cm^2/s of raw NCM811. Thus, the improvement in high rate performance of 1% Zr-NCM811 is likely caused by its enhanced Li-ion diffusivity.

$$U_{ion} = \left[(i_p L)/\sigma\right] + \left(\frac{\sigma_{el}}{\sigma}\right)\left[\frac{i_p L}{\sigma_{ion}}\right]\left\{1 - (8/\pi^2)exp\left[-\left(\frac{t}{\tau^{\delta}}\right)\right]\right\} \qquad (4.1)$$

$$\tau^{\delta} = \left(\frac{L^2}{\pi^2}\right)\frac{1}{D_{Li}} \tag{4.2}$$

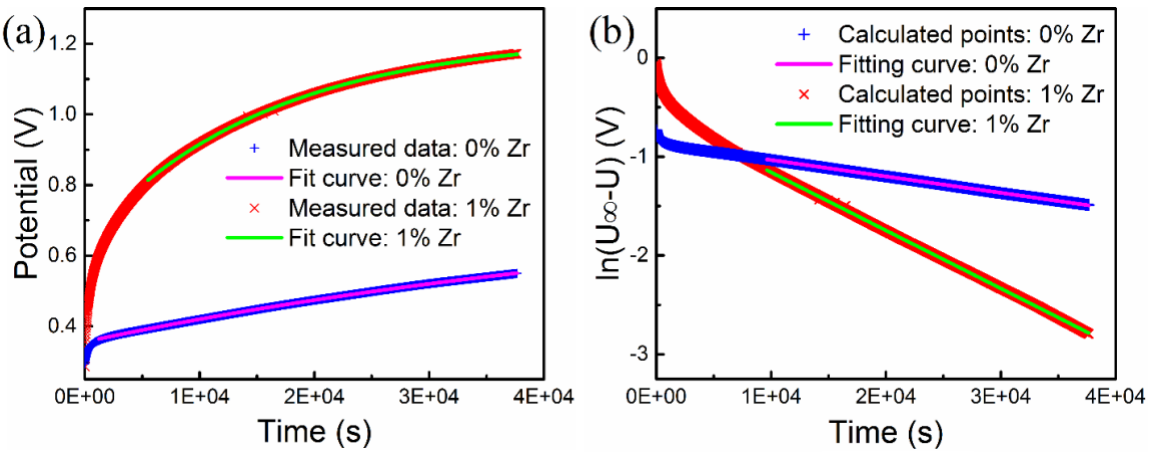

Figure 4.14 (a) Time dependent of DC polarization voltage obtained from the electron-blocking cell fitted by formula 4.1. (b) Polarization results fitted by formula 4.2.

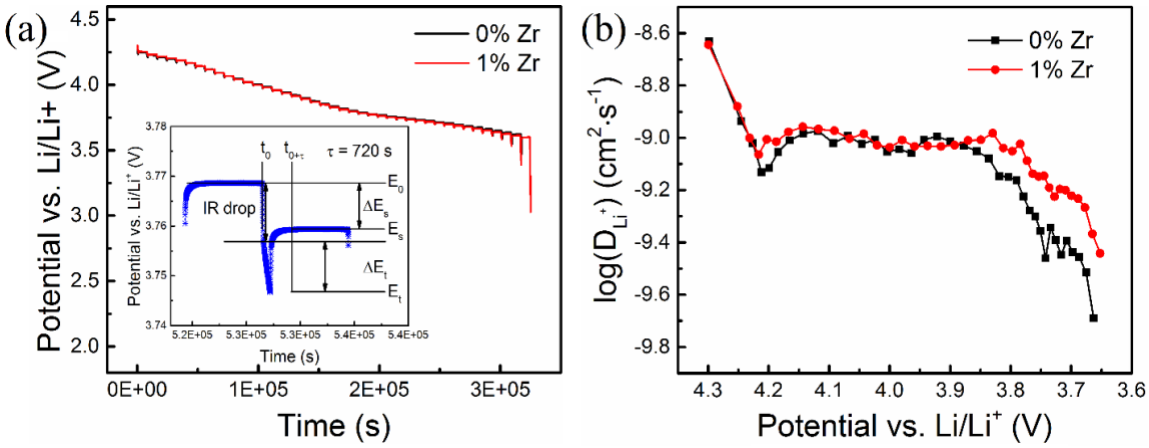

Figure 4.15 (a) GITT curves of a discharging process. (b) Li-ion diffusion coefficient versus state of charge calculated by formula 4.3.

Galvanostatic intermittent titration technique (GITT) was applied on coin cells to study the Li-ion diffusivity. The titration and rest duration was 12 min and 2 h, respectively, while the current loading was 0.1C. After four charging/discharging cycles at 0.1C, I charged the cell and then performed GITT during the following discharging process, as shown in Figure 4.15a, where the inserted image elaborates one typical titration/rest cycle and the parameters one can extract. Based on formula 4.3,[180, 228] where m_B is the mass of

active material, M_B the molar mass of active material, V_m the active material's molar volume, and S the electrode area, I collect the Li-ion diffusion coefficients at the different states of charge for the raw and 1% Zr-NCM811 in Figure 4.15b. Both cells show similar Li-ion diffusivities at the high states of charge. In addition, I notice that D_{Li} generally increases for both cells with deepening delithiation. This is due to the reduced energy barrier for Li-ion diffusion when Li layers are less occupied, as evidenced by computational and experimental studies.[180, 228-230] However, the Zr-modified sample apparently shows higher values of D_{Li} at the low potential region. It agrees with the result acquired from DC polarization measurement on the as-synthesized materials. The improvement on the Li-ion diffusivity of 1% Zr-NCM811 can be attributed to both Zr doping effect and the formation of Li-conductive lithium zirconates.

$$D_{Li} = \frac{4}{\pi\tau}\left(\frac{m_B V_M}{M_B S}\right)^2 \left(\frac{\Delta E_S}{\Delta E_\tau}\right)^2 \tag{4.3}$$

I note that D_{Li} acquired via the DC approach is about one order of magnitude higher than that from GITT. The difference may be linked to the different configurations adopted. GITT measures a coin cell containing the electrode made from the NCM samples, the counter electrode of Li metal, and the organic liquid electrolyte. In such a complex configuration, the data acquired is affected by many transport processes occurring in not only the positive electrode material but also liquid electrolyte in the porous electrode material. In contrast, the DC technique measures the Li diffusivity in the bulk material, and thus represents the material's property more accurately.

4.4 Summary

I examined the effects of Zr modification on the cycling stability and high rate performance of NCM811. I systematically analyzed the phase, crystal structure, and morphology of NCM811s with 0 (raw NCM811), 0.5, 1.0, 2.0, and 5.0 at.% Zr modifications by using multiple characterization tools such as synchrotron HRXRD, TEM, and EDS. With increasing Zr contents, the layered crystal expands along the *c*-axis and, meanwhile, more Zr aggregates on the surface of the electrode particle forming a coating of lithium zirconates. In the samples with low Zr concentrations, Li-rich phases, such as Li_4ZrO_4 and/or $Li_6Zr_2O_7$, are observed, while Li_2ZrO_3 only forms in 5% Zr-NCM811.

Among all the samples, 1% Zr-NCM811 exhibits the best rate capability, delivering 192, 185, 173, 162, 149, 125, and 100 mAh/g at the current rate of 0.1, 0.2, 0.5, 1.0, 2.0, 5.0, and 10C. Furthermore, it is more durable in long-term cycling compared with raw NCM811, especially at high C-rate. It can retain 15.1% more capacity than the raw after 60 cycles at 2C. The better capacity retention of 1% Zr-NCM811 can be linked to the improved chemical/electrochemical stability revealed by XPS and CV techniques; and the enhanced high-rate capability is a consequence of the high Li-ion diffusivity in the bulk material revealed by DC polarization.

The improved stability of 1% Zr-NCM811 may be attributed to the dual effects of Zr modification. (1) Zr^{4+} in the lattice can stabilize the layered structure of NCM811 by suppressing the layered-spinel phase transformation and (2) the coating layer consisting of the Li-rich lithium zirconates can protect the surface of the electrode particle from Li-consuming side reactions during cycling. I believe (1) is more important than (2) because there are more Zr ions reside in the layered lattice than in the coating. In addition, both Zr doping and lithium zirconates can facilitate Li-ion diffusion: (1) The lattice expansion can reduce the energy barrier for Li-ion migration and (2) Li ion-conducting coating can accelerate Li-ion transport into and out of NMC811 particles.

CHAPTER 5. Conclusions and Future Work

In this dissertation, I investigate the effects of transition metals in Ni-rich NCM811 positive electrode material in LIBs from two perspectives: 1) introducing Co non-stoichiometric and 2) substituting Ni, Co, and Mn with Zr. In particular, this dissertation reports, possibly for the first time, the effects of TM non-stoichiometry and the Li-ion diffusion behavior in bulk Ni-rich NCM811. The main conclusions are:

(1) Co deficiency can reduce the cation mixing between Ni^{2+} and Li^{+}, possibly because of the electrostatic attraction between V_{Co}''/V_{Co}''' and Ni^{2+} that increases the energy barrier for Ni^{2+} migration. Simultaneously, Co deficiency will introduce O vacancies to NCM811, especially at and near the surface of the NCM811 particles.

(2) Cobalt-deficient NCM811s show an inferior electrochemical performance compared with the raw NCM811. I attribute it to the effects of the introduced O vacancies, which destabilize the surface of NCM811 particles and impede Li-ion transport, impairing both the cycling durability and rate capability.

(3) Despite the detrimental effect of the Co deficiency on NCM811 positive electrode material, the 20% cobalt-deficient sample (Co0.08) shows better capacity retention than the 10% one (Co0.09). The reason is probably that, when the Co deficiency reaches 20%, the benefit of suppressing cation disordering becomes more significant than the surface damage caused by O vacancies.

(4) When substituting the three transition metals in NCM811, Zr can simultaneously reside in the layered lattice and form Li-rich zirconates partially coating on the surface of NCM811 particles. A single phase Zr-doped NCM811 is unlikely to be synthesized, even for the 0.5% Zr modified sample, which is the least Zr containing sample in this study.

(5) The 1% Zr-NCM811 shows the best rate capability among all raw and Zr-modified NCM811s. Its capacity retention is also higher than the raw sample, especially for the high C-rate cycles.

(6) The dual effects of Zr modification can stabilize the layered structure of NCM811 and protect the surface of electrode particles during cycling. Furthermore, Zr modification can facilitate Li-ion diffusion by 1) expanding the layered lattice

expansion that reduces the energy barrier for Li-ion migration, and 2) forming a Li ion-conducting coating, which facilitates Li-ion transport during Li-ion (de)intercalation.

My work discovers a new way to suppress the cation mixing by introducing Co deficiency in the Ni-rich layered positive electrode materials for LIBs. However, the mechanism stays unclear. More experimental and computational work, such as neutron diffraction and DFT modeling, have to be done to study how Co non-stoichiometry interacts with cation disordering and O defects in the layered structure. In addition to Co, the effects of Ni and Mn deficiencies can also be investigated. Such studies can help improve the understanding of the Ni-rich layered structure and may inspire new modification strategies.

In addition to Zr substitution, several other elemental doping studies have been reported for the Ni-rich layered positive electrode materials. Several research directions, not only for Zr but also for other candidate dopants, are promising:

(1) Systematically evaluating the feasibility of the potential doping elements in positive electrodes for the commercial LIBs, based on the cost of precursors, ease of synthesis, and environmental risks.

(2) Exploring the synthesis route that incorporates elemental doping with other modification methods, such as coatings and core-shell structures.

(3) Understanding the effects of doping modification on structure and electrochemical performance from molecular and atomic levels, which requires *in situ* characterizations and MD/DFT calculations.

BIBLIOGRAPHY

(1) Tarascon, J.-M.; Armand, M. Issues and challenges facing rechargeable lithium batteries. In *Materials for Sustainable Energy: A Collection of Peer-Reviewed Research and Review Articles from Nature Publishing Group*; World Scientific: 2011; pp 171-179.

(2) Nitta, N.; Wu, F.; Lee, J. T.; Yushin, G. Li-ion battery materials: present and future. *Materials today* **2015,** *18* (5), 252-264.

(3) Howell, D. Electrochemical Energy Storage R&D Overview. https://www.energy.gov/sites/prod/files/2017/06/f34/es000_howell_2017_o.pdf.

(4) Whittingham, M. S. Lithium batteries and cathode materials. *Chemical reviews* **2004,** *104* (10), 4271-4302.

(5) Ellis, B. L.; Lee, K. T.; Nazar, L. F. Positive electrode materials for Li-ion and Li-batteries. *Chemistry of Materials* **2010,** *22* (3), 691-714.

(6) Etacheri, V.; Marom, R.; Elazari, R.; Salitra, G.; Aurbach, D. Challenges in the development of advanced Li-ion batteries: a review. *Energy & Environmental Science* **2011,** *4* (9), 3243-3262.

(7) Sun, Y.-K.; Myung, S.-T.; Kim, M.-H.; Prakash, J.; Amine, K. Synthesis and characterization of Li [(Ni0. 8Co0. 1Mn0. 1) 0.8 (Ni0. 5Mn0. 5) 0.2] O2 with the microscale core− shell structure as the positive electrode material for lithium batteries. *Journal of the American Chemical Society* **2005,** *127* (38), 13411-13418.

(8) He, P.; Yu, H.; Zhou, H. Layered lithium transition metal oxide cathodes towards high energy lithium-ion batteries. *Journal of Materials Chemistry* **2012,** *22* (9), 3680-3695.

(9) Liu, W.; Oh, P.; Liu, X.; Lee, M. J.; Cho, W.; Chae, S.; Kim, Y.; Cho, J. Nickel‐Rich Layered Lithium Transition‐Metal Oxide for High‐Energy Lithium‐Ion Batteries. *Angewandte Chemie International Edition* **2015,** *54* (15), 4440-4457.

(10) Kim, H.-R.; Woo, S.-G.; Kim, J.-H.; Cho, W.; Kim, Y.-J. Capacity fading behavior of Ni-rich layered cathode materials in Li-ion full cells. *Journal of Electroanalytical Chemistry* **2016,** *782*, 168-173.

(11) Noh, H.-J.; Youn, S.; Yoon, C. S.; Sun, Y.-K. Comparison of the structural and electrochemical properties of layered Li [Ni x Co y Mn z] O 2 (x= 1/3, 0.5, 0.6, 0.7, 0.8 and 0.85) cathode material for lithium-ion batteries. *Journal of Power Sources* **2013,** *233*, 121-130.

(12) Bak, S.-M.; Hu, E.; Zhou, Y.; Yu, X.; Senanayake, S. D.; Cho, S.-J.; Kim, K.-B.; Chung, K. Y.; Yang, X.-Q.; Nam, K.-W. Structural Changes and Thermal Stability of Charged LiNi x Mn y Co z O2 Cathode Materials Studied by Combined In Situ Time-Resolved XRD and Mass Spectroscopy. *ACS applied materials & interfaces* **2014,** *6* (24), 22594-22601.

(13) Dixit, M.; Markovsky, B.; Schipper, F.; Aurbach, D.; Major, D. T. The Origin of Structural Degradation during Cycling and Low Thermal Stability of Ni-Rich Layered Transition Metal-Based Electrode Materials. *The Journal of Physical Chemistry C* **2017**.

(14) Kang, K.; Meng, Y. S.; Bréger, J.; Grey, C. P.; Ceder, G. Electrodes with high power and high capacity for rechargeable lithium batteries. *Science* **2006,** *311* (5763), 977-980.

(15) Wu, Y.-P.; Rahm, E.; Holze, R. Carbon anode materials for lithium ion batteries. *Journal of Power Sources* **2003,** *114* (2), 228-236.

(16) Takada, K. Progress and prospective of solid-state lithium batteries. *Acta Materialia* **2013,** *61* (3), 759-770.
(17) Zhang, S. S. Liquid electrolyte lithium/sulfur battery: fundamental chemistry, problems, and solutions. *Journal of Power Sources* **2013,** *231*, 153-162.
(18) Myung, S.-T.; Maglia, F.; Park, K.-J.; Yoon, C. S.; Lamp, P.; Kim, S.-J.; Sun, Y.-K. Nickel-rich layered cathode materials for automotive lithium-ion batteries: achievements and perspectives. *ACS Energy Letters* **2016,** *2* (1), 196-223.
(19) Sinha, S.; Murphy, D. Lithium intercalation in cubic TiS2. *Solid State Ionics* **1986,** *20* (1), 81-84.
(20) Tarascon, J.; Wang, E.; Shokoohi, F.; McKinnon, W.; Colson, S. The spinel phase of LiMn2 O 4 as a cathode in secondary lithium cells. *Journal of the Electrochemical Society* **1991,** *138* (10), 2859-2864.
(21) Scrosati, B. Lithium rocking chair batteries: An old concept? *Journal of The Electrochemical Society* **1992,** *139* (10), 2776-2781.
(22) Mizushima, K.; Jones, P.; Wiseman, P.; Goodenough, J. B. LixCoO2 ($0<x\leqslant 1$): A new cathode material for batteries of high energy density. *Materials Research Bulletin* **1980,** *15* (6), 783-789.
(23) Dahn, J.; Von Sacken, U.; Juzkow, M.; Al‐Janaby, H. Rechargeable LiNiO2/carbon cells. *Journal of the Electrochemical Society* **1991,** *138* (8), 2207-2211.
(24) Dahn, J.; Fuller, E.; Obrovac, M.; Von Sacken, U. Thermal stability of LixCoO2, LixNiO2 and λ-MnO2 and consequences for the safety of Li-ion cells. *Solid State Ionics* **1994,** *69* (3-4), 265-270.
(25) Gummow, R. J.; Thackeray, M. An Investigation of Spinel‐Related and Orthorhombic LiMnO2 Cathodes for Rechargeable Lithium Batteries. *Journal of The Electrochemical Society* **1994,** *141* (5), 1178-1182.
(26) Kawai, H.; Nagata, M.; Tukamoto, H.; West, A. R. High-voltage lithium cathode materials. *Journal of power sources* **1999,** *81*, 67-72.
(27) Liu, Z.; Yu, A.; Lee, J. Y. Synthesis and characterization of LiNi1− x− yCoxMnyO2 as the cathode materials of secondary lithium batteries. *Journal of Power Sources* **1999,** *81*, 416-419.
(28) Yoshio, M.; Noguchi, H.; Itoh, J.-i.; Okada, M.; Mouri, T. Preparation and properties of LiCo y Mn x Ni 1− x− y O 2 as a cathode for lithium ion batteries. *Journal of Power Sources* **2000,** *90* (2), 176-181.
(29) Shaju, K.; Rao, G. S.; Chowdari, B. Performance of layered Li (Ni 1/3 Co 1/3 Mn 1/3) O 2 as cathode for Li-ion batteries. *Electrochimica Acta* **2002,** *48* (2), 145-151.
(30) Kannan, A. M.; Manthiram, A. Structural Stability of Li1−xNi0.85Co0.15 O 2 and Li1-x Ni0.85Co0.12Al0.03 O 2 Cathodes at Elevated Temperatures. *Journal of The Electrochemical Society* **2003,** *150* (3), A349-A353, DOI: 10.1149/1.1553766.
(31) Kim, J.-H.; Yoon, C.; Sun, Y.-K. Structural Characterization of Li [Li0. 1Ni0. 35Mn0. 55] O 2 Cathode Material for Lithium Secondary Batteries. *Journal of The Electrochemical Society* **2003,** *150* (4), A538-A542.
(32) Sun, Y.-K.; Myung, S.-T.; Park, B.-C.; Prakash, J.; Belharouak, I.; Amine, K. High-energy cathode material for long-life and safe lithium batteries. *Nature materials* **2009,** *8* (4), 320-324.

(33) Liu, D.; Han, J.; Goodenough, J. B. Structure, morphology, and cathode performance of Li 1− x [Ni 0.5 Mn 1.5] O 4 prepared by coprecipitation with oxalic acid. *Journal of Power Sources* **2010,** *195* (9), 2918-2923.
(34) Mohanty, D.; Dahlberg, K.; King, D. M.; David, L. A.; Sefat, A. S.; Wood, D. L.; Daniel, C.; Dhar, S.; Mahajan, V.; Lee, M. Modification of Ni-Rich FCG NMC and NCA Cathodes by Atomic Layer Deposition: Preventing Surface Phase Transitions for High-Voltage Lithium-Ion Batteries. *Scientific reports* **2016,** *6*, 26532.
(35) Padhi, A. K.; Nanjundaswamy, K. S.; Goodenough, J. B. Phospho ‐ olivines as positive ‐ electrode materials for rechargeable lithium batteries. *Journal of the electrochemical society* **1997,** *144* (4), 1188-1194.
(36) Gaubicher, J.; Wurm, C.; Goward, G.; Masquelier, C.; Nazar, L. Rhombohedral form of Li3V2 (PO4) 3 as a cathode in Li-ion batteries. *Chemistry of materials* **2000,** *12* (11), 3240-3242.
(37) Yue, Y.; Liang, H. Hierarchical micro-architectures of electrodes for energy storage. *Journal of Power Sources* **2015,** *284*, 435-445.
(38) Murphy, D. W.; Trumbore, F. A. The Chemistry of TiS3 and NbSe3 Cathodes. *Journal of The Electrochemical Society* **1976,** *123* (7), 960-964.
(39) Whittingham, M. S. The role of ternary phases in cathode reactions. *Journal of The Electrochemical Society* **1976,** *123* (3), 315-320.
(40) Whittingham, M. S. Electrical energy storage and intercalation chemistry. *Science* **1976,** *192* (4244), 1126-1127.
(41) Julien, C. M.; Mauger, A.; Zaghib, K.; Groult, H. Comparative issues of cathode materials for Li-ion batteries. *Inorganics* **2014,** *2* (1), 132-154.
(42) Santhanam, R.; Rambabu, B. Research progress in high voltage spinel LiNi0. 5Mn1. 5O4 material. *Journal of Power Sources* **2010,** *195* (17), 5442-5451.
(43) Antolini, E. LiCoO 2: formation, structure, lithium and oxygen nonstoichiometry, electrochemical behaviour and transport properties. *Solid State Ionics* **2004,** *170* (3), 159-171.
(44) Reimers, J. N.; Dahn, J. Electrochemical and in situ X ‐ ray diffraction studies of lithium intercalation in Li x CoO2. *Journal of The Electrochemical Society* **1992,** *139* (8), 2091-2097.
(45) Antolini, E.; Ferretti, M. Synthesis and thermal stability of LiCoO2. *Journal of Solid State Chemistry* **1995,** *117* (1), 1-7.
(46) Wang, H.; Jang, Y. I.; Huang, B.; Sadoway, D. R.; Chiang, Y. M. TEM study of electrochemical cycling ‐ induced damage and disorder in LiCoO2 cathodes for rechargeable lithium batteries. *Journal of The Electrochemical Society* **1999,** *146* (2), 473-480.
(47) Jang, Y.-I.; Dudney, N. J.; Blom, D. A.; Allard, L. F. High-voltage cycling behavior of thin-film LiCoO2 cathodes. *Journal of The Electrochemical Society* **2002,** *149* (11), A1442-A1447.
(48) Baba, Y.; Okada, S.; Yamaki, J.-i. Thermal stability of LixCoO2 cathode for lithium ion battery. *Solid State Ionics* **2002,** *148* (3-4), 311-316.
(49) Imanishi, N.; Fujiyoshi, M.; Takeda, Y.; Yamamoto, O.; Tabuchi, M. Preparation and 7Li-NMR study of chemically delithiated Li1− xCoO2 (0< x< 0.5). *Solid State Ionics* **1999,** *118* (1-2), 121-128.

(50) Li, W.; Reimers, J.; Dahn, J. In situ x-ray diffraction and electrochemical studies of Li1− xNiO2. *Solid State Ionics* **1993,** *67* (1-2), 123-130.
(51) Ohzuku, T.; Ueda, A.; Nagayama, M. Electrochemistry and structural chemistry of LiNiO2 (R3m) for 4 volt secondary lithium cells. *Journal of The Electrochemical Society* **1993,** *140* (7), 1862-1870.
(52) Molenda, J.; Wilk, P.; Marzec, J. Structural, electrical and electrochemical properties of LiNiO 2. *Solid State Ionics* **2002,** *146* (1), 73-79.
(53) Reimers, J.; Rossen, E.; Jones, C.; Dahn, J. Structure and electrochemistry of LixFeyNi1-yO2. *Solid State Ionics* **1993,** *61* (4), 335-344.
(54) Cho, J.; Kim, G.; Lim, H. S. Effect of Preparation Methods of LiNi1− x Co x O 2 Cathode Materials on Their Chemical Structure and Electrode Performance. *Journal of The Electrochemical Society* **1999,** *146* (10), 3571-3576.
(55) Moses, A. W.; Flores, H. G. G.; Kim, J.-G.; Langell, M. A. Surface properties of LiCoO 2, LiNiO 2 and LiNi 1− x Co x O 2. *Applied surface science* **2007,** *253* (10), 4782-4791.
(56) G. Bruce, P.; Robert Armstrong, A.; L. Gitzendanner, R. New intercalation compounds for lithium batteries: layered LiMnO2. *Journal of Materials Chemistry* **1999,** *9* (1), 193-198, DOI: 10.1039/A803938K.
(57) Obrovac, M. N.; Mao, O.; Dahn, J. R. Structure and electrochemistry of LiMO2 (M=Ti, Mn, Fe, Co, Ni) prepared by mechanochemical synthesis. *Solid State Ionics* **1998,** *112* (1–2), 9-19, DOI: http://dx.doi.org/10.1016/S0167-2738(98)00225-2.
(58) Arora, P.; White, R. E.; Doyle, M. Capacity fade mechanisms and side reactions in lithium‐ion batteries. *Journal of the Electrochemical Society* **1998,** *145* (10), 3647-3667.
(59) Wohlfahrt-Mehrens, M.; Vogler, C.; Garche, J. Aging mechanisms of lithium cathode materials. *Journal of power sources* **2004,** *127* (1), 58-64.
(60) Thackeray, M.; Johnson, P.; De Picciotto, L.; Bruce, P.; Goodenough, J. Electrochemical extraction of lithium from LiMn2O4. *Materials Research Bulletin* **1984,** *19* (2), 179-187.
(61) Thackeray, M.; Mansuetto, M.; Bates, J. Structural stability of LiMn2O4 electrodes for lithium batteries. *Journal of power sources* **1997,** *68* (1), 153-158.
(62) Yonemura, M.; Yamada, A.; Kobayashi, H.; Tabuchi, M.; Kamiyama, T.; Kawamoto, Y.; Kanno, R. Synthesis, structure, and phase relationship in lithium manganese oxide spinel. *Journal of Materials Chemistry* **2004,** *14* (13), 1948-1958.
(63) Thackeray, M. M. Spinel electrodes for lithium batteries. *Journal of the American Ceramic Society* **1999,** *82* (12), 3347-3354.
(64) Fergus, J. W. Recent developments in cathode materials for lithium ion batteries. *Journal of Power Sources* **2010,** *195* (4), 939-954.
(65) Amine, K.; Tukamoto, H.; Yasuda, H.; Fujita, Y. A New Three‐Volt Spinel Li1+ x Mn1. 5Ni0. 5 O 4 for Secondary Lithium Batteries. *Journal of The Electrochemical Society* **1996,** *143* (5), 1607-1613.
(66) Xu, B.; Qian, D.; Wang, Z.; Meng, Y. S. Recent progress in cathode materials research for advanced lithium ion batteries. *Materials Science and Engineering: R: Reports* **2012,** *73* (5–6), 51-65, DOI: http://dx.doi.org/10.1016/j.mser.2012.05.003.
(67) Zhong, S.; Letong, L.; Jiang, J.; Yanwei, L.; Jian, W.; Jiequn, L.; Yanhong, L. Preparation and electrochemical properties of Y-doped Li3V2 (PO4) 3 cathode materials for lithium batteries. *Journal of rare earths* **2009,** *27* (1), 134-137.

(68) Barker, J.; Saidi, M.; Swoyer, J. Electrochemical insertion properties of the novel lithium vanadium fluorophosphate, LiVPO4 F. *Journal of the Electrochemical Society* **2003,** *150* (10), A1394-A1398.
(69) Recham, N.; Chotard, J.-N.; Dupont, L.; Delacourt, C.; Walker, W.; Armand, M.; Tarascon, J.-M. A 3.6 V lithium-based fluorosulphate insertion positive electrode for lithium-ion batteries. *Nature materials* **2010,** *9* (1), 68.
(70) Morgan, D.; Ceder, G.; Saıdi, M.; Barker, J.; Swoyer, J.; Huang, H.; Adamson, G. Experimental and computational study of the structure and electrochemical properties of monoclinic LixM2 (PO4) 3 compounds. *Journal of power sources* **2003,** *119*, 755-759.
(71) Wolfenstine, J.; Allen, J. LiNiPO4–LiCoPO4 solid solutions as cathodes. *Journal of Power Sources* **2004,** *136* (1), 150-153.
(72) Shiratsuchi, T.; Okada, S.; Doi, T.; Yamaki, J.-i. Cathodic performance of LiMn1− xMxPO4 (M= Ti, Mg and Zr) annealed in an inert atmosphere. *Electrochimica Acta* **2009,** *54* (11), 3145-3151.
(73) Delacourt, C.; Laffont, L.; Bouchet, R.; Wurm, C.; Leriche, J.-B.; Morcrette, M.; Tarascon, J.-M.; Masquelier, C. Toward understanding of electrical limitations (electronic, ionic) in LiMPO4 (M= Fe, Mn) electrode materials. *Journal of the Electrochemical Society* **2005,** *152* (5), A913-A921.
(74) Rougier, A.; Saadoune, I.; Gravereau, P.; Willmann, P.; Delmasa, C. Effect of cobalt substitution on cationic distribution in LiNi1− y CoyO2 electrode materials. *Solid State Ionics* **1996,** *90* (1-4), 83-90.
(75) Saadoune, I.; Delmas, C. On the LixNi0. 8Co0. 2O2System. *Journal of Solid State Chemistry* **1998,** *136* (1), 8-15.
(76) Saadoune, I.; Delmas, C. LiNi1−yCoyO2 positive electrode materials: relationships between the structure, physical properties and electrochemical behaviour. *Journal of Materials Chemistry* **1996,** *6* (2), 193-199.
(77) Zhecheva, E.; Stoyanova, R. Stabilization of the layered crystal structure of LiNiO2 by Co-substitution. *Solid state ionics* **1993,** *66* (1-2), 143-149.
(78) Julien, C.; Letranchant, C.; Lemal, M.; Ziolkiewicz, S.; Castro-Garcia, S. Layered LiNi 1− y Co y O 2 compounds synthesized by a glycine-assisted combustion method for lithium batteries. *Journal of materials science* **2002,** *37* (11), 2367-2375.
(79) Hwang, B.; Santhanam, R.; Chen, C. Effect of synthesis conditions on electrochemical properties of LiNi1− yCoyO2 cathode for lithium rechargeable batteries. *Journal of power sources* **2003,** *114* (2), 244-252.
(80) Caurant, D.; Baffier, N.; Garcia, B.; Pereira-Ramos, J. Synthesis by a soft chemistry route and characterization of LiNixCo1− xO2 (0⩽ x⩽ 1) cathode materials. *Solid State Ionics* **1996,** *91* (1-2), 45-54.
(81) Lee, K. K.; Kim, K. B. Electrochemical and Structural Characterization of LiNi1− y Co y O 2 (0⩽ y⩽ 0.2) Positive Electrodes during Initial Cycling. *Journal of The Electrochemical Society* **2000,** *147* (5), 1709-1717.
(82) Ohzuku, T.; Ueda, A.; Nagayama, M.; Iwakoshi, Y.; Komori, H. Comparative study of LiCoO2, LiNi12Co12O2 and LiNiO2 for 4 volt secondary lithium cells. *Electrochimica Acta* **1993,** *38* (9), 1159-1167.
(83) Li, W.; Currie, J. Morphology Effects on the Electrochemical Performance of LiNi1− x Co x O 2. *Journal of The Electrochemical Society* **1997,** *144* (8), 2773-2779.

(84) Albrecht, S.; Kümpers, J.; Kruft, M.; Malcus, S.; Vogler, C.; Wahl, M.; Wohlfahrt-Mehrens, M. Electrochemical and thermal behavior of aluminum-and magnesium-doped spherical lithium nickel cobalt mixed oxides Li1− x (Ni1− y− zCoyMz) O2 (M= Al, Mg). *Journal of power sources* **2003,** *119*, 178-183.
(85) Madhavi, S.; Rao, G. S.; Chowdari, B.; Li, S. Effect of aluminium doping on cathodic behaviour of LiNi0. 7Co0. 3O2. *Journal of power sources* **2001,** *93* (1-2), 156-162.
(86) Wang, G.; Zhong, S.; Bradhurst, D.; Dou, S.; Liu, H. LiAlδNi1− δO2 solid solutions as cathodic materials for rechargeable lithium batteries. *Solid State Ionics* **1999,** *116* (3-4), 271-277.
(87) Stoyanova, R.; Zhecheva, E.; Zarkova, L. Effect of Mn-substitution for Co on the crystal structure and acid delithiation of LiMnyCo1−yO2 solid solutions. *Solid State Ionics* **1994,** *73* (3), 233-240, DOI: http://dx.doi.org/10.1016/0167-2738(94)90039-6.
(88) Robertson, A. D.; Armstrong, A. R.; Bruce, P. G. Layered Li x Mn1-y Co y O2 Intercalation Electrodes Influence of Ion Exchange on Capacity and Structure upon Cycling. *Chemistry of materials* **2001,** *13* (7), 2380-2386.
(89) Armstrong, A. R.; Robertson, A. D.; Gitzendanner, R.; Bruce, P. G. The Layered Intercalation Compounds Li (Mn1− yCoy) O2: Positive Electrode Materials for Lithium–Ion Batteries. *Journal of Solid State Chemistry* **1999,** *145* (2), 549-556.
(90) Ammundsen, B.; Paulsen, J. Novel lithium‐ion cathode materials based on layered manganese oxides. *Advanced Materials* **2001,** *13* (12‐13), 943-956.
(91) Abuzeid, H.; Hashem, A.; Abdel-Ghany, A.; Eid, A.; Mauger, A.; Groult, H.; Julien, C. De-intercalation of LixCo0. 8Mn0. 2O2: A magnetic approach. *Journal of Power Sources* **2011,** *196* (15), 6440-6448.
(92) Koyama, Y.; Makimura, Y.; Tanaka, I.; Adachi, H.; Ohzuku, T. Systematic Research on Insertion Materials Based on Superlattice Models in a Phase Triangle of LiCoO2 LiNiO2 LiMnO2 : I. First-Principles Calculation on Electronic and Crystal Structures, Phase Stability and New LiNi1/2 Mn1/2O2 Material. *Journal of The Electrochemical Society* **2004,** *151* (9), A1499-A1506, DOI: 10.1149/1.1783908.
(93) Ohzuku, T.; Makimura, Y. Layered Lithium Insertion Material of LiCo1/3Ni1/3Mn1/3O2 for Lithium-Ion Batteries. *Chemistry Letters* **2001,** *30* (7), 642-643, DOI: 10.1246/cl.2001.642.
(94) Rossen, E.; Jones, C.; Dahn, J. Structure and electrochemistry of LixMnyNi1− yO2. *Solid State Ionics* **1992,** *57* (3-4), 311-318.
(95) Abdel-Ghany, A.; Zaghib, K.; Gendron, F.; Mauger, A.; Julien, C. Structural, magnetic and electrochemical properties of LiNi0. 5Mn0. 5O2 as positive electrode for Li-ion batteries. *Electrochimica Acta* **2007,** *52* (12), 4092-4100.
(96) Arachi, Y.; Kobayashi, H.; Emura, S.; Nakata, Y.; Tanaka, M.; Asai, T.; Sakaebe, H.; Tatsumi, K.; Kageyama, H. Li de-intercalation mechanism in LiNi0. 5Mn0. 5O2 cathode material for Li-ion batteries. *Solid State Ionics* **2005,** *176* (9-10), 895-903.
(97) Bréger, J.; Meng, Y. S.; Hinuma, Y.; Kumar, S.; Kang, K.; Shao-Horn, Y.; Ceder, G.; Grey, C. P. Effect of high voltage on the structure and electrochemistry of LiNi0. 5Mn0. 5O2: A joint experimental and theoretical study. *Chemistry of Materials* **2006,** *18* (20), 4768-4781.
(98) Yabuuchi, N.; Kumar, S.; Li, H. H.; Kim, Y.-T.; Shao-Horn, Y. Changes in the crystal structure and electrochemical properties of Li x Ni0. 5Mn0. 5O2 during electrochemical

cycling to high voltages. *Journal of The Electrochemical Society* **2007,** *154* (6), A566-A578.
(99) Yang, X.-Q.; McBreen, J.; Yoon, W.-S.; Grey, C. P. Crystal structure changes of LiMn0. 5Ni0. 5O2 cathode materials during charge and discharge studied by synchrotron based in situ XRD. *Electrochemistry communications* **2002,** *4* (8), 649-654.
(100) Arachi, Y.; Kobayashi, H.; Emura, S.; Nakata, Y.; Tanaka, M.; Asai, T. Structural Change of Li1− x Ni0. 5Mn0. 5O2 Cathode Materials for Lithium-ion Batteries by Synchrotron Radiation. *Chemistry letters* **2002,** *32* (1), 60-61.
(101) Bréger, J.; Dupré, N.; Chupas, P. J.; Lee, P. L.; Proffen, T.; Parise, J. B.; Grey, C. P. Short-and long-range order in the positive electrode material, Li (NiMn) 0.5 O2: a joint X-ray and neutron diffraction, pair distribution function analysis and NMR study. *Journal of the American Chemical Society* **2005,** *127* (20), 7529-7537.
(102) Yabuuchi, N.; Kim, Y.-T.; Li, H. H.; Shao-Horn, Y. Thermal Instability of Cycled Li x Ni0. 5Mn0. 5O2 Electrodes: An in Situ Synchrotron X-ray Powder Diffraction Study. *Chemistry of Materials* **2008,** *20* (15), 4936-4951.
(103) Kim, J.-M.; Chung, H.-T. Role of transition metals in layered Li [Ni, Co, Mn] O2 under electrochemical operation. *Electrochimica Acta* **2004,** *49* (21), 3573-3580.
(104) Koyama, Y.; Tanaka, I.; Adachi, H.; Makimura, Y.; Ohzuku, T. Crystal and electronic structures of superstructural Li1−x[Co1/3Ni1/3Mn1/3]O2 (0⩽x⩽1). *Journal of Power Sources* **2003,** *119-121*, 644-648, DOI: https://doi.org/10.1016/S0378-7753(03)00194-0.
(105) MacNeil, D.; Lu, Z.; Dahn, J. R. Structure and Electrochemistry of Li [NixCo1−2xMnx]O2. *Journal of The Electrochemical Society* **2002,** *149* (10), A1332-A1336.
(106) Belharouak, I.; Sun, Y. K.; Liu, J.; Amine, K. Li(Ni1/3Co1/3Mn1/3)O2 as a suitable cathode for high power applications. *Journal of Power Sources* **2003,** *123* (2), 247-252, DOI: 10.1016/S0378-7753(03)00529-9.
(107) Yabuuchi, N.; Ohzuku, T. Novel lithium insertion material of LiCo 1/3 Ni 1/3 Mn 1/3 O 2 for advanced lithium-ion batteries. *Journal of Power Sources* **2003,** *119*, 171-174.
(108) Hwang, B. J.; Tsai, Y. W.; Carlier, D.; Ceder, G. A Combined Computational/Experimental Study on LiNi1/3Co1/3Mn1/3O2. *Chemistry of Materials* **2003,** *15* (19), 3676-3682, DOI: 10.1021/cm030299v.
(109) Cho, T.; Park, S.; Yoshio, M.; Hirai, T.; Hideshima, Y. Effect of synthesis condition on the structural and electrochemical properties of Li [Ni1/3Mn1/3Co1/3] O2 prepared by carbonate co-precipitation method. *Journal of power sources* **2005,** *142* (1-2), 306-312.
(110) Lee, M.-H.; Kang, Y.-J.; Myung, S.-T.; Sun, Y.-K. Synthetic optimization of Li [Ni 1/3 Co 1/3 Mn 1/3] O 2 via co-precipitation. *Electrochimica Acta* **2004,** *50* (4), 939-948.
(111) Li, D.-C.; Muta, T.; Zhang, L.-Q.; Yoshio, M.; Noguchi, H. Effect of synthesis method on the electrochemical performance of LiNi 1/3 Mn 1/3 Co 1/3 O 2. *Journal of Power Sources* **2004,** *132* (1), 150-155.
(112) Park, S.; Yoon, C.; Kang, S.; Kim, H.-S.; Moon, S.-I.; Sun, Y.-K. Synthesis and structural characterization of layered Li [Ni 1/3 Co 1/3 Mn 1/3] O 2 cathode materials by ultrasonic spray pyrolysis method. *Electrochimica Acta* **2004,** *49* (4), 557-563.
(113) Patoux, S.; Doeff, M. M. Direct synthesis of LiNi1/3Co1/3Mn1/3O2 from nitrate precursors. *Electrochemistry Communications* **2004,** *6* (8), 767-772.

(114) Myung, S.-T.; Lee, M.-H.; Komaba, S.; Kumagai, N.; Sun, Y.-K. Hydrothermal synthesis of layered Li [Ni 1/3 Co 1/3 Mn 1/3] O 2 as positive electrode material for lithium secondary battery. *Electrochimica Acta* **2005,** *50* (24), 4800-4806.
(115) Olivetti, E. A.; Ceder, G.; Gaustad, G. G.; Fu, X. Lithium-ion battery supply chain considerations: analysis of potential bottlenecks in critical metals. *Joule* **2017,** *1* (2), 229-243.
(116) Myung, S.-T.; Ogata, A.; Lee, K.-S.; Komaba, S.; Sun, Y.-K.; Yashiro, H. Structural, Electrochemical, and Thermal Aspects of Li [(Ni0. 5Mn0. 5) 1− x Co x] O2 (0⩽ x⩽ 0.2) for High-Voltage Application of Lithium-Ion Secondary Batteries. *Journal of the Electrochemical Society* **2008,** *155* (5), A374-A383.
(117) Sun, Y.; Ouyang, C.; Wang, Z.; Huang, X.; Chen, L. Effect of Co Content on Rate Performance of LiMn0. 5− x Co2x Ni0. 5− x O 2 Cathode Materials for Lithium-Ion Batteries. *Journal of The Electrochemical Society* **2004,** *151* (4), A504-A508.
(118) Oh, S. W.; Park, S. H.; Park, C.-W.; Sun, Y.-K. Structural and electrochemical properties of layered Li [Ni0. 5Mn0. 5] 1− xCoxO2positive materials synthesized by ultrasonic spray pyrolysis method. *Solid State Ionics* **2004,** *171* (3-4), 167-172.
(119) Ngala, J. K.; Chernova, N. A.; Ma, M.; Mamak, M.; Zavalij, P. Y.; Whittingham, M. S. The synthesis, characterization and electrochemical behavior of the layered LiNi 0.4 Mn 0.4 Co 0.2 O 2 compound. *Journal of materials chemistry* **2004,** *14* (2), 214-220.
(120) Li, D.; Sasaki, Y.; Kageyama, M.; Kobayakawa, K.; Sato, Y. Structure, morphology and electrochemical properties of LiNi0. 5Mn0. 5− xCoxO2 prepared by solid state reaction. *Journal of Power Sources* **2005,** *148*, 85-89.
(121) Li, D.; Sasaki, Y.; Kobayakawa, K.; Sato, Y. Impact of cobalt substitution for manganese on the structural and electrochemical properties of LiNi0. 5Mn0. 5O2. *Electrochimica acta* **2006,** *51* (18), 3809-3813.
(122) Yang, S.; Wang, X.; Yang, X.; Liu, Z.; Bai, Y.; Wang, Y.; Shu, H. Influence of preparation method on structure, morphology, and electrochemical performance of spherical Li [Ni 0.5 Mn 0.3 Co 0.2] O 2. *Journal of Solid State Electrochemistry* **2012,** *16* (8), 2823-2836.
(123) Kalluri, S.; Yoon, M.; Jo, M.; Liu, H. K.; Dou, S. X.; Cho, J.; Guo, Z. Feasibility of Cathode Surface Coating Technology for High‐Energy Lithium‐ion and Beyond‐Lithium‐ion Batteries. *Advanced Materials* **2017**.
(124) Bloom, I.; Jones, S. A.; Battaglia, V. S.; Henriksen, G. L.; Christophersen, J. P.; Wright, R. B.; Ho, C. D.; Belt, J. R.; Motloch, C. G. Effect of cathode composition on capacity fade, impedance rise and power fade in high-power, lithium-ion cells. *Journal of Power Sources* **2003,** *124* (2), 538-550.
(125) Hou, P.; Yin, J.; Ding, M.; Huang, J.; Xu, X. Surface/Interfacial Structure and Chemistry of High‐Energy Nickel‐Rich Layered Oxide Cathodes: Advances and Perspectives. *Small* **2017**.
(126) Ding, Y.; Mu, D.; Wu, B.; Wang, R.; Zhao, Z.; Wu, F. Recent progresses on nickel-rich layered oxide positive electrode materials used in lithium-ion batteries for electric vehicles. *Applied Energy* **2017,** *195*, 586-599.
(127) Min, K.; Kim, K.; Jung, C.; Seo, S.-W.; Song, Y. Y.; Lee, H. S.; Shin, J.; Cho, E. A comparative study of structural changes in lithium nickel cobalt manganese oxide as a function of Ni content during delithiation process. *Journal of Power Sources* **2016,** *315*, 111-119.

(128) Schipper, F.; Erickson, E. M.; Erk, C.; Shin, J.-Y.; Chesneau, F. F.; Aurbach, D. Recent advances and remaining challenges for lithium ion battery cathodes I. Nickel-Rich, LiNixCoyMnzO2. *Journal of The Electrochemical Society* **2017,** *164* (1), A6220-A6228.
(129) Li, W.; Song, B.; Manthiram, A. High-voltage positive electrode materials for lithium-ion batteries. *Chemical Society Reviews* **2017**.
(130) Radin, M. D.; Hy, S.; Sina, M.; Fang, C.; Liu, H.; Vinckeviciute, J.; Zhang, M.; Whittingham, M. S.; Meng, Y. S.; Van der Ven, A. Narrowing the Gap between Theoretical and Practical Capacities in Li‐Ion Layered Oxide Cathode Materials. *Advanced Energy Materials* **2017**.
(131) Zhang, X.; Jiang, W. J.; Mauger, A.; Qilu; Gendron, F.; Julien, C. M. Minimization of the cation mixing in Li1+x(NMC)1−xO2 as cathode material. *Journal of Power Sources* **2010,** *195* (5), 1292-1301, DOI: http://dx.doi.org/10.1016/j.jpowsour.2009.09.029.
(132) Zhang, J.; Yang, Z.; Gao, R.; Gu, L.; Hu, Z.; Liu, X. Suppressing the Structure Deterioration of Ni-rich LiNi0. 8Co0. 1Mn0. 1O2 through Atom-scale Interfacial Integration of Self-forming Hierarchical Spinel Layer with Ni Gradient Concentration. *ACS Applied Materials & Interfaces* **2017**.
(133) Fu, C.; Li, G.; Luo, D.; Li, Q.; Fan, J.; Li, L. Nickel-rich layered microspheres cathodes: lithium/nickel disordering and electrochemical performance. *ACS applied materials & interfaces* **2014,** *6* (18), 15822-15831.
(134) Wu, F.; Tian, J.; Su, Y.; Wang, J.; Zhang, C.; Bao, L.; He, T.; Li, J.; Chen, S. Effect of Ni2+ content on lithium/nickel disorder for Ni-rich cathode materials. *ACS applied materials & interfaces* **2015,** *7* (14), 7702-7708.
(135) Gopukumar, S.; Chung, K. Y.; Kim, K. B. Novel synthesis of layered LiNi 1/2 Mn 1/2 O 2 as cathode material for lithium rechargeable cells. *Electrochimica Acta* **2004,** *49* (5), 803-810.
(136) Hausbrand, R.; Cherkashinin, G.; Ehrenberg, H.; Gröting, M.; Albe, K.; Hess, C.; Jaegermann, W. Fundamental degradation mechanisms of layered oxide Li-ion battery cathode materials: Methodology, insights and novel approaches. *Materials Science and Engineering: B* **2015,** *192*, 3-25.
(137) Zheng, J.; Liu, T.; Hu, Z.; Wei, Y.; Song, X.; Ren, Y.; Wang, W.; Rao, M.; Lin, Y.; Chen, Z. Tuning of Thermal Stability in Layered Li (Ni x Mn y Co z) O2. *Journal of the American Chemical Society* **2016,** *138* (40), 13326-13334.
(138) Lin, F.; Markus, I. M.; Nordlund, D.; Weng, T.-C.; Asta, M. D.; Xin, H. L.; Doeff, M. M. Surface reconstruction and chemical evolution of stoichiometric layered cathode materials for lithium-ion batteries. *Nature communications* **2014,** *5*.
(139) Kim, J.; Lee, H.; Cha, H.; Yoon, M.; Park, M.; Cho, J. Prospect and Reality of Ni‐Rich Cathode for Commercialization. *Advanced Energy Materials* **2017**.
(140) Hu, E.; Wang, X.; Yu, X.; Yang, X.-Q. Probing the Complexities of Structural Changes in Layered Oxide Cathode Materials for Li-Ion Batteries during Fast Charge–Discharge Cycling and Heating. *Accounts of chemical research* **2018**.
(141) Yu, X.; Manthiram, A. Electrode-Electrolyte Interfaces in Lithium-based Batteries. *Energy & Environmental Science* **2018**.
(142) Cherkashinin, G.; Motzko, M.; Schulz, N.; Späth, T.; Jaegermann, W. Electron spectroscopy study of Li [Ni, Co, Mn] O2/electrolyte interface: electronic structure, interface composition, and device implications. *Chemistry of Materials* **2015,** *27* (8), 2875-2887.

(143) Wang, Y.; Jiang, J.; Dahn, J. R. The reactivity of delithiated Li(Ni1/3Co1/3Mn1/3)O2, Li(Ni0.8Co0.15Al0.05)O2 or LiCoO2 with non-aqueous electrolyte. *Electrochemistry Communications* **2007,** *9* (10), 2534-2540, DOI: http://dx.doi.org/10.1016/j.elecom.2007.07.033.
(144) Watanabe, S.; Kinoshita, M.; Nakura, K. Comparison of the surface changes on cathode during long term storage testing of high energy density cylindrical lithium-ion cells. *Journal of Power Sources* **2011,** *196* (16), 6906-6910.
(145) Watanabe, S.; Kinoshita, M.; Hosokawa, T.; Morigaki, K.; Nakura, K. Capacity fade of LiAl y Ni 1− x− y Co x O 2 cathode for lithium-ion batteries during accelerated calendar and cycle life tests (surface analysis of LiAl y Ni 1− x− y Co x O 2 cathode after cycle tests in restricted depth of discharge ranges). *Journal of Power Sources* **2014,** *258*, 210-217.
(146) Choi, J.; Manthiram, A. Investigation of the Irreversible Capacity Loss in the Layered LiNi1 ∕ 3Mn1 ∕ 3Co1 ∕ 3O2 Cathodes. *Electrochemical and Solid-State Letters* **2005,** *8* (8), C102-C105, DOI: 10.1149/1.1943567.
(147) Manthiram, A.; Song, B.; Li, W. A perspective on nickel-rich layered oxide cathodes for lithium-ion batteries. *Energy Storage Materials* **2017,** *6*, 125-139.
(148) Cho, D.-H.; Jo, C.-H.; Cho, W.; Kim, Y.-J.; Yashiro, H.; Sun, Y.-K.; Myung, S.-T. Effect of residual lithium compounds on layer Ni-rich Li [Ni0. 7Mn0. 3] O2. *Journal of The Electrochemical Society* **2014,** *161* (6), A920-A926.
(149) Xu, J.; Lin, F.; Doeff, M. M.; Tong, W. A review of Ni-based layered oxides for rechargeable Li-ion batteries. *Journal of Materials Chemistry A* **2017,** *5* (3), 874-901.
(150) Pouillerie, C.; Croguennec, L.; Biensan, P.; Willmann, P.; Delmas, C. Synthesis and Characterization of New LiNi1− y Mg y O 2 Positive Electrode Materials for Lithium‐Ion Batteries. *Journal of The Electrochemical Society* **2000,** *147* (6), 2061-2069.
(151) Pouillerie, v. C.; Croguennec, L.; Delmas, C. The LixNi1− yMgyO2 (y= 0.05, 0.10) system: structural modifications observed upon cycling. *Solid State Ionics* **2000,** *132* (1-2), 15-29.
(152) Xie, H.; Du, K.; Hu, G.; Peng, Z.; Cao, Y. The role of sodium in LiNi0. 8Co0. 15Al0. 05O2 cathode material and its electrochemical behaviors. *The Journal of Physical Chemistry C* **2016,** *120* (6), 3235-3241.
(153) Cho, Y.; Oh, P.; Cho, J. A new type of protective surface layer for high-capacity Ni-based cathode materials: nanoscaled surface pillaring layer. *Nano letters* **2013,** *13* (3), 1145-1152.
(154) Bi, Y.; Yang, W.; Du, R.; Zhou, J.; Liu, M.; Liu, Y.; Wang, D. Correlation of oxygen non-stoichiometry to the instabilities and electrochemical performance of LiNi 0.8 Co 0.1 Mn 0.1 O 2 utilized in lithium ion battery. *Journal of Power Sources* **2015,** *283*, 211-218.
(155) Meng, K.; Wang, Z.; Guo, H.; Li, X. Enhanced cycling stability of LiNi 0.8 Co 0.1 Mn 0.1 O 2 by reducing surface oxygen defects. *Electrochimica Acta* **2017,** *234*, 99-107.
(156) Zhao, J.; Zhang, W.; Huq, A.; Misture, S. T.; Zhang, B.; Guo, S.; Wu, L.; Zhu, Y.; Chen, Z.; Amine, K. In Situ Probing and Synthetic Control of Cationic Ordering in Ni‐Rich Layered Oxide Cathodes. *Advanced Energy Materials* **2017,** *7* (3).
(157) Chen, Z.; Chao, D.; Lin, J.; Shen, Z. Recent progress in surface coating of layered LiNi x Co y Mn z O 2 for lithium-ion batteries. *Materials Research Bulletin* **2017**.
(158) Chen, Z.; Qin, Y.; Amine, K.; Sun, Y.-K. Role of surface coating on cathode materials for lithium-ion batteries. *Journal of materials chemistry* **2010,** *20* (36), 7606-7612.

(159) Lim, B.-B.; Myung, S.-T.; Yoon, C. S.; Sun, Y.-K. Comparative study of Ni-rich layered cathodes for rechargeable lithium batteries: Li [Ni0. 85Co0. 11Al0. 04] O2 and Li [Ni0. 84Co0. 06Mn0. 09Al0. 01] O2 with two-step full concentration gradients. *ACS Energy Letters* **2016,** *1* (1), 283-289.
(160) Kim, U.-H.; Myung, S.-T.; Yoon, C. S.; Sun, Y.-K. Extending the Battery Life using Al-doped Li [Ni0. 76Co0. 09Mn0. 15] O2 Cathode with Concentration Gradients for Lithium Ion Batteries. *ACS Energy Letters* **2017**.
(161) Huang, Z.; Wang, Z.; Jing, Q.; Guo, H.; Li, X.; Yang, Z. Investigation on the effect of Na doping on structure and Li-ion kinetics of layered LiNi 0.6 Co 0.2 Mn 0.2 O 2 cathode material. *Electrochimica Acta* **2016,** *192*, 120-126.
(162) Hua, W.; Zhang, J.; Zheng, Z.; Liu, W.; Peng, X.; Guo, X.-D.; Zhong, B.; Wang, Y.-J.; Wang, X. Na-doped Ni-rich LiNi0.5Co0.2Mn0.3O2 cathode material with both high rate capability and high tap density for lithium ion batteries. *Dalton Transactions* **2014,** *43* (39), 14824-14832, DOI: 10.1039/c4dt01611d.
(163) Zhao, R.; Yang, Z.; Liang, J.; Lu, D.; Liang, C.; Guan, X.; Gao, A.; Chen, H. Understanding the role of Na-doping on Ni-rich layered oxide LiNi 0.5 Co 0.2 Mn 0.3 O 2. *Journal of Alloys and Compounds* **2016,** *689*, 318-325.
(164) Min, K.; Seo, S.-W.; Song, Y. Y.; Lee, H. S.; Cho, E. A first-principles study of the preventive effects of Al and Mg doping on the degradation in LiNi 0.8 Co 0.1 Mn 0.1 O 2 cathode materials. *Physical Chemistry Chemical Physics* **2017,** *19* (3), 1762-1769.
(165) Woo, S.-W.; Myung, S.-T.; Bang, H.; Kim, D.-W.; Sun, Y.-K. Improvement of electrochemical and thermal properties of Li [Ni 0.8 Co 0.1 Mn 0.1] O 2 positive electrode materials by multiple metal (Al, Mg) substitution. *Electrochimica Acta* **2009,** *54* (15), 3851-3856.
(166) Liu, L.; Sun, K.; Zhang, N.; Yang, T. Improvement of high-voltage cycling behavior of Li (Ni1/3Co1/3Mn1/3) O2 cathodes by Mg, Cr, and Al substitution. *Journal of Solid State Electrochemistry* **2009,** *13* (9), 1381-1386.
(167) Huang, Z.; Wang, Z.; Guo, H.; Li, X. Influence of Mg 2+ doping on the structure and electrochemical performances of layered LiNi 0.6 Co 0.2-x Mn 0.2 Mg x O 2 cathode materials. *Journal of Alloys and Compounds* **2016,** *671*, 479-485.
(168) Huang, Z.; Wang, Z.; Zheng, X.; Guo, H.; Li, X.; Jing, Q.; Yang, Z. Structural and electrochemical properties of Mg-doped nickel based cathode materials LiNi 0.6 Co 0.2 Mn 0.2− x Mg x O 2 for lithium ion batteries. *RSC Advances* **2015,** *5* (108), 88773-88779.
(169) Liao, P.-Y.; Duh, J.-G.; Sheu, H.-S. Structural and thermal properties of LiNi 0.6− x Mg x Co 0.25 Mn 0.15 O 2 cathode materials. *Journal of Power Sources* **2008,** *183* (2), 766-770.
(170) Aurbach, D.; Srur-Lavi, O.; Ghanty, C.; Dixit, M.; Haik, O.; Talianker, M.; Grinblat, Y.; Leifer, N.; Lavi, R.; Major, D. T. Studies of aluminum-doped LiNi0. 5Co0. 2Mn0. 3O2: electrochemical behavior, aging, structural transformations, and thermal characteristics. *Journal of The Electrochemical Society* **2015,** *162* (6), A1014-A1027.
(171) Eilers-Rethwisch, M.; Winter, M.; Schappacher, F. M. Synthesis, electrochemical investigation and structural analysis of doped Li [Ni 0.6 Mn 0.2 Co 0.2-x M x] O 2 (x= 0, 0.05; M= Al, Fe, Sn) cathode materials. *Journal of Power Sources* **2018,** *387*, 101-107.
(172) Zhou, F.; Zhao, X.; Dahn, J. R. Synthesis, Electrochemical Properties, and Thermal Stability of Al-Doped LiNi1 / 3Mn1 / 3Co (1 / 3−z)AlzO2 Positive Electrode

Materials. *Journal of The Electrochemical Society* **2009,** *156* (4), A343-A347, DOI: 10.1149/1.3079424.
(173) Dixit, M.; Markovsky, B.; Aurbach, D.; Major, D. T. Unraveling the Effects of Al Doping on the Electrochemical Properties of LiNi0. 5Co0. 2Mn0. 3O2 Using First Principles. *Journal of The Electrochemical Society* **2017,** *164* (1), A6359-A6365.
(174) Wang, D.; Li, X.; Wang, Z.; Guo, H.; Xu, Y.; Fan, Y.; Ru, J. Role of zirconium dopant on the structure and high voltage electrochemical performances of LiNi 0.5 Co 0.2 Mn 0.3 O 2 cathode materials for lithium ion batteries. *Electrochimica Acta* **2016,** *188*, 48-56.
(175) Schipper, F.; Dixit, M.; Kovacheva, D.; Talianker, M.; Haik, O.; Grinblat, J.; Erickson, E. M.; Ghanty, C.; Major, D. T.; Markovsky, B. Stabilizing nickel-rich layered cathode materials by a high-charge cation doping strategy: zirconium-doped LiNi 0.6 Co 0.2 Mn 0.2 O 2. *Journal of Materials Chemistry A* **2016,** *4* (41), 16073-16084.
(176) He, T.; Lu, Y.; Su, Y.; Bao, L.; Tan, J.; Chen, L.; Zhang, Q.; Li, W.; Chen, S.; Wu, F. Sufficient utilization of Zr4+ on improving the structure and surface property of the Ni-rich cathode materials for lithium ion batteries. *ChemSusChem* **2018**.
(177) Chen, Q.; Du, C.; Qu, D.; Zhang, X.; Tang, Z. Synthesis and characterization of Zr-doped LiNi 0.4 Co 0.2 Mn 0.4 O 2 cathode materials for lithium ion batteries. *RSC Advances* **2015,** *5* (92), 75248-75253.
(178) Li, X.; Zhang, K.; Wang, M.; Liu, Y.; Qu, M.; Zhao, W.; Zheng, J. Dual functions of zirconium modification on improving the electrochemical performance of Ni-rich LiNi 0.8 Co 0.1 Mn 0.1 O 2. *Sustainable Energy & Fuels* **2018**.
(179) Li, L.-j.; Li, X.-h.; Wang, Z.-x.; Guo, H.-j.; Yue, P.; Chen, W.; Wu, L. Synthesis, structural and electrochemical properties of LiNi 0.79 Co 0.1 Mn 0.1 Cr 0.01 O 2 via fast co-precipitation. *Journal of Alloys and Compounds* **2010,** *507* (1), 172-177.
(180) Zhang, Y.; Wang, Z.-B.; Yu, F.-D.; Que, L.-F.; Wang, M.-J.; Xia, Y.-F.; Xue, Y.; Wu, J. Studies on stability and capacity for long-life cycle performance of Li (Ni 0.5 Co 0.2 Mn 0.3) O 2 by Mo modification for lithium-ion battery. *Journal of Power Sources* **2017,** *358*, 1-12.
(181) Wang, L. Q.; Jiao, L. F.; Yuan, H.; Guo, J.; Zhao, M.; Li, H. X.; Wang, Y. M. Synthesis and electrochemical properties of Mo-doped Li [Ni 1/3 Mn 1/3 Co 1/3] O 2 cathode materials for Li-ion battery. *Journal of power sources* **2006,** *162* (2), 1367-1372.
(182) Schipper, F.; Bouzaglo, H.; Dixit, M.; Erickson, E. M.; Weigel, T.; Talianker, M.; Grinblat, J.; Burstein, L.; Schmidt, M.; Lampert, J. From Surface ZrO2 Coating to Bulk Zr Doping by High Temperature Annealing of Nickel‐Rich Lithiated Oxides and Their Enhanced Electrochemical Performance in Lithium Ion Batteries. *Advanced Energy Materials* **2017**.
(183) Li, X.; Peng, H.; Wang, M. S.; Zhao, X.; Huang, P. X.; Yang, W.; Xu, J.; Wang, Z. Q.; Qu, M. Z.; Yu, Z. L. Enhanced Electrochemical Performance of Zr‐Modified Layered LiNi1/3Co1/3Mn1/3O2 Cathode Material for Lithium‐Ion Batteries. *ChemElectroChem* **2016,** *3* (1), 130-137.
(184) Song, B.; Li, W.; Oh, S.-M.; Manthiram, A. Long-life nickel-rich layered oxide cathodes with a uniform Li2ZrO3 surface coating for lithium-ion batteries. *ACS Applied Materials & Interfaces* **2017,** *9* (11), 9718-9725.

(185) Zhang, J.; Li, Z.; Gao, R.; Hu, Z.; Liu, X. High rate capability and excellent thermal stability of Li+-conductive Li2ZrO3-coated LiNi1/3Co1/3Mn1/3O2 via a synchronous lithiation strategy. *The Journal of Physical Chemistry C* **2015,** *119* (35), 20350-20356.
(186) Yabuuchi, N.; Koyama, Y.; Nakayama, N.; Ohzuku, T. Solid-State Chemistry and Electrochemistry of LiCo1 / 3Ni1 / 3Mn1 / 3O2 for Advanced Lithium-Ion Batteries: II. Preparation and Characterization. *Journal of The Electrochemical Society* **2005,** *152* (7), A1434-A1440, DOI: 10.1149/1.1924227.
(187) Jo, C.-H.; Cho, D.-H.; Noh, H.-J.; Yashiro, H.; Sun, Y.-K.; Myung, S. T. An effective method to reduce residual lithium compounds on Ni-rich LiNi0.6Co0.2Mn0.2O2 active material using a phosphoric acid derived Li3PO4 nanolayer. *Nano Research* **2015,** *8* (5), 1464-1479, DOI: 10.1007/s12274-014-0631-8.
(188) Sun, H.-H.; Choi, W.; Lee, J. K.; Oh, I.-H.; Jung, H.-G. Control of electrochemical properties of nickel-rich layered cathode materials for lithium ion batteries by variation of the manganese to cobalt ratio. *Journal of Power Sources* **2015,** *275*, 877-883.
(189) Zheng, J.; Kan, W. H.; Manthiram, A. Role of Mn Content on the Electrochemical Properties of Nickel-Rich Layered LiNi0. 8 − x Co0. 1Mn0. 1+ x O2 (0.0⩽ x⩽ 0.08) Cathodes for Lithium-Ion Batteries. *ACS applied materials & interfaces* **2015,** *7* (12), 6926-6934.
(190) Kim, K. J.; Jo, Y. N.; Lee, W. J.; Subburaj, T.; Prasanna, K.; Lee, C. W. Effects of inorganic salts on the morphological, structural, and electrochemical properties of prepared nickel-rich Li [Ni 0.6 Co 0.2 Mn 0.2] O 2. *Journal of Power Sources* **2014,** *268*, 349-355.
(191) Zhang, B.; Li, L.; Zheng, J. Characterization of multiple metals (Cr, Mg) substituted LiNi0.8Co0.1Mn0.1O2 cathode materials for lithium ion battery. *Journal of Alloys and Compounds* **2012,** *520*, 190-194, DOI: http://dx.doi.org/10.1016/j.jallcom.2012.01.004.
(192) Cai, L.; Liu, Z.; An, K.; Liang, C. Probing Li-Ni Cation Disorder in Li1− xNi1+ x− yAlyO2 Cathode Materials by Neutron Diffraction. *Journal of The Electrochemical Society* **2012,** *159* (7), A924-A928.
(193) Li, H. H.; Yabuuchi, N.; Meng, Y. S.; Kumar, S.; Breger, J.; Grey, C. P.; Shao-Horn, Y. Changes in the Cation Ordering of Layered O3 LixNi0.5Mn0.5O2 during Electrochemical Cycling to High Voltages: An Electron Diffraction Study. *Chemistry of Materials* **2007,** *19* (10), 2551-2565, DOI: 10.1021/cm070139+.
(194) Hinuma, Y.; Meng, Y. S.; Kang, K.; Ceder, G. Phase Transitions in the LiNi0.5Mn0.5O2 System with Temperature. *Chemistry of Materials* **2007,** *19* (7), 1790-1800, DOI: 10.1021/cm062903i.
(195) Reimers, J. N.; Li, W.; Dahn, J. R. Short-range cation ordering in LixNi2-xO2. *Physical Review B* **1993,** *47* (14), 8486-8493.
(196) Aurbach, D. Electrode–solution interactions in Li-ion batteries: a short summary and new insights. *Journal of Power Sources* **2003,** *119–121*, 497-503, DOI: http://dx.doi.org/10.1016/S0378-7753(03)00273-8.
(197) Edström, K.; Gustafsson, T.; Thomas, J. O. The cathode–electrolyte interface in the Li-ion battery. *Electrochimica Acta* **2004,** *50* (2–3), 397-403, DOI: http://dx.doi.org/10.1016/j.electacta.2004.03.049.
(198) Myung, S.-T.; Amine, K.; Sun, Y.-K. Surface modification of cathode materials from nano- to microscale for rechargeable lithium-ion batteries. *Journal of Materials Chemistry* **2010,** *20* (34), 7074-7095, DOI: 10.1039/C0JM00508H.

(199) Garcia, J. C.; Bareno, J. G.; Yan, J.; Chen, G.; Hauser, A.; Croy, J. R.; Iddir, H. Surface Structure, Morphology and Stability of Li (Ni1/3Mn1/3Co1/3) O2 Cathode Material. *The Journal of Physical Chemistry C* **2017**.
(200) Ge, W.-J.; Li, X.; Wang, H.; Li, W.; Wei, A.-J.; Peng, G.-C.; Qu, M.-Z. Multifunctional modification of Li [Ni 0.5 Co 0.2 Mn 0.3] O 2 with NH 4 VO 3 as a high performance cathode material for lithium ion batteries. *Journal of Alloys and Compounds* **2016,** *684*, 594-603.
(201) Yuan, J.; Wen, J.; Zhang, J.; Chen, D.; Zhang, D. Influence of calcination atmosphere on structure and electrochemical behavior of LiNi 0.6 Co 0.2 Mn 0.2 O 2 cathode material for lithium-ion batteries. *Electrochimica Acta* **2017,** *230*, 116-122.
(202) Hoang, K.; Johannes, M. Defect Physics and Chemistry in Layered Mixed Transition Metal Oxide Cathode Materials:(Ni, Co, Mn) vs (Ni, Co, Al). *Chemistry of Materials* **2016,** *28* (5), 1325-1334.
(203) Hoang, K. Defect physics, delithiation mechanism, and electronic and ionic conduction in layered lithium manganese oxide cathode materials. *Physical Review Applied* **2015,** *3* (2), 024013.
(204) Toby, B. H. EXPGUI, a graphical user interface for GSAS. *Journal of applied crystallography* **2001,** *34* (2), 210-213.
(205) Larson, A. C.; Von Dreele, R. B. Gsas. *General Structure Analysis System. LANSCE, MS-H805, Los Alamos, New Mexico* **1994**.
(206) Wu, Y.; Manthiram, A. Effect of surface modifications on the layered solid solution cathodes (1− z) Li [Li1/3Mn2/3] O2−(z) Li [Mn0. 5− yNi0. 5− yCo2y] O2. *Solid State Ionics* **2009,** *180* (1), 50-56.
(207) Hwang, S.; Chang, W.; Kim, S. M.; Su, D.; Kim, D. H.; Lee, J. Y.; Chung, K. Y.; Stach, E. A. Investigation of Changes in the Surface Structure of Li x Ni0. 8Co0. 15Al0. 05O2 Cathode Materials Induced by the Initial Charge. *Chemistry of Materials* **2014,** *26* (2), 1084-1092.
(208) Song, B.; Liu, Z.; Lai, M. O.; Lu, L. Structural evolution and the capacity fade mechanism upon long-term cycling in Li-rich cathode material. *Physical Chemistry Chemical Physics* **2012,** *14* (37), 12875-12883.
(209) Meng, M.; Wu, S.; Ren, L.; Zhou, W.; Wang, Y.; Wang, G.; Li, S. Enlarged Mn 3s splitting and room-temperature ferromagnetism in epitaxially grown oxygen doped Mn2N0. 86 films. *Journal of Applied Physics* **2014,** *116* (17), 173911.
(210) Kosova, N.; Devyatkina, E.; Kaichev, V. Optimization of Ni 2+/Ni 3+ ratio in layered Li (Ni, Mn, Co) O 2 cathodes for better electrochemistry. *Journal of Power Sources* **2007,** *174* (2), 965-969.
(211) Zhong, S.; Lai, M.; Yao, W.; Li, Z. Synthesis and electrochemical properties of LiNi 0.8 Co x Mn 0.2-x O 2 positive-electrode material for lithium-ion batteries. *Electrochimica Acta* **2016,** *212*, 343-351.
(212) Liang, L.; Du, K.; Lu, W.; Peng, Z.; Cao, Y.; Hu, G. Synthesis and characterization of LiNi 0.6 Co x Mn 0.4-x O 2 (x= 0.05, 0.1, 0.15, 0.2, 0.25 and 0.3) with high-electrochemical performance for lithium-ion batteries. *Electrochimica Acta* **2014,** *146*, 207-217.
(213) Jung, S. K.; Gwon, H.; Hong, J.; Park, K. Y.; Seo, D. H.; Kim, H.; Hyun, J.; Yang, W.; Kang, K. Understanding the degradation mechanisms of LiNi0. 5Co0. 2Mn0. 3O2 cathode material in lithium ion batteries. *Advanced Energy Materials* **2014,** *4* (1).

(214) Yang, J.; Xia, Y. Enhancement on the Cycling Stability of the Layered Ni-Rich Oxide Cathode by In-Situ Fabricating Nano-Thickness Cation-Mixing Layers. *Journal of The Electrochemical Society* **2016,** *163* (13), A2665-A2672.
(215) Li, J.; Du, Z.; Ruther, R. E.; An, S. J.; David, L. A.; Hays, K.; Wood, M.; Phillip, N. D.; Sheng, Y.; Mao, C. Toward Low-Cost, High-Energy Density, and High-Power Density Lithium-Ion Batteries. *JOM* **2017,** *69* (9), 1484-1496.
(216) Manthiram, A.; Knight, J. C.; Myung, S. T.; Oh, S. M.; Sun, Y. K. Nickel‐Rich and Lithium‐Rich Layered Oxide Cathodes: Progress and Perspectives. *Advanced Energy Materials* **2016,** *6* (1).
(217) Zheng, J.; Myeong, S.; Cho, W.; Yan, P.; Xiao, J.; Wang, C.; Cho, J.; Zhang, J. G. Li‐and Mn‐Rich Cathode Materials: Challenges to Commercialization. *Advanced Energy Materials* **2016**.
(218) Duan, Y. Electronic structural and electrochemical properties of lithium zirconates and their capabilities of CO 2 capture: a first-principles density-functional theory and phonon dynamics approach. *Journal of Renewable and Sustainable Energy* **2011,** *3* (1), 013102.
(219) Lu, H.; Zhou, H.; Svensson, A. M.; Fossdal, A.; Sheridan, E.; Lu, S.; Vullum-Bruer, F. High capacity Li [Ni 0.8 Co 0.1 Mn 0.1] O 2 synthesized by sol–gel and co-precipitation methods as cathode materials for lithium-ion batteries. *Solid State Ionics* **2013,** *249*, 105-111.
(220) Zhao, E.; Chen, M.; Hu, Z.; Chen, D.; Yang, L.; Xiao, X. Improved cycle stability of high-capacity Ni-rich LiNi 0.8 Mn 0.1 Co 0.1 O 2 at high cut-off voltage by Li 2 SiO 3 coating. *Journal of Power Sources* **2017,** *343*, 345-353.
(221) Wang, J.; Yu, Y.; Li, B.; Fu, T.; Xie, D.; Cai, J.; Zhao, J. Improving the electrochemical properties of LiNi 0.5 Co 0.2 Mn 0.3 O 2 at 4.6 V cutoff potential by surface coating with Li 2 TiO 3 for lithium-ion batteries. *Physical Chemistry Chemical Physics* **2015,** *17* (47), 32033-32043.
(222) Subramaniyam, C. M.; Celio, H.; Shiva, K.; Gao, H.; Goodneough, J. B.; Liu, H. K.; Dou, S. X. Long stable cycling of fluorine-doped nickel-rich layered cathodes for lithium batteries. *Sustainable Energy & Fuels* **2017**.
(223) Chen, S.; He, T.; Su, Y.; Lu, Y.; Bao, L.; Chen, L.; Zhang, Q.; Wang, J.; Chen, R.; Wu, F. Ni-Rich LiNi0. 8Co0. 1Mn0. 1O2 Oxide Coated by Dual-Conductive Layers as High Performance Cathode Material for Lithium-Ion Batteries. *ACS Applied Materials & Interfaces* **2017,** *9* (35), 29732-29743.
(224) Zhao, C.; Zheng, W.; Wang, X.; Zhang, H.; Cui, X.; Wang, H. Ultrahigh capacitive performance from both Co (OH) 2/graphene electrode and K 3 Fe (CN) 6 electrolyte. *Scientific reports* **2013,** *3*, 2986.
(225) Deshpande, R. D.; Ridgway, P.; Fu, Y.; Zhang, W.; Cai, J.; Battaglia, V. The limited effect of VC in graphite/NMC cells. *Journal of The Electrochemical Society* **2015,** *162* (3), A330-A338.
(226) Andersson, A.; Abraham, D.; Haasch, R.; MacLaren, S.; Liu, J.; Amine, K. Surface characterization of electrodes from high power lithium-ion batteries. *Journal of The Electrochemical Society* **2002,** *149* (10), A1358-A1369.
(227) Lee, Y.-M.; Nam, K.-M.; Hwang, E.-H.; Kwon, Y.-G.; Kang, D.-H.; Kim, S.-S.; Song, S.-W. Interfacial origin of performance improvement and fade for 4.6 V LiNi0.

5Co0. 2Mn0. 3O2 battery cathodes. *The Journal of Physical Chemistry C* **2014,** *118* (20), 10631-10639.
(228) Lee, W.; Muhammad, S.; Kim, T.; Kim, H.; Lee, E.; Jeong, M.; Son, S.; Ryou, J. H.; Yoon, W. S. New Insight into Ni‐Rich Layered Structure for Next‐Generation Li Rechargeable Batteries. *Advanced Energy Materials* **2017**.
(229) Amin, R.; Chiang, Y.-M. Characterization of Electronic and Ionic Transport in Li1-xNi0. 33Mn0. 33Co0. 33O2 (NMC333) and Li1-xNi0. 50Mn0. 20Co0. 30O2 (NMC523) as a Function of Li Content. *Journal of The Electrochemical Society* **2016,** *163* (8), A1512-A1517.
(230) Amin, R.; Ravnsbæk, D. B.; Chiang, Y.-M. Characterization of Electronic and Ionic Transport in Li1-xNi0. 8Co0. 15Al0. 05O2 (NCA). *Journal of The Electrochemical Society* **2015,** *162* (7), A1163-A1169.

VITA

Shuang Gao

Education

2015 – 2019, University of Kentucky, Lexington, Kentucky

Ph.D., Materials Science and Engineering

Dissertation: Investigation of transition-metal ions in the Ni-rich layered positive electrode materials for Li-ion batteries.

2012 – 2015, Northwestern Polytechnical University, Xi'an, China

M.E., Composites Materials Engineering

Dissertation: Thermodynamic and kinetic studies on the chemical vapor co-deposition systems of SiC-ZrC coatings.

2008 – 2012, Northwestern Polytechnical University, Xi'an, China

B.E., Materials Science and Engineering

Dissertation: Structure and dielectric properties of new B site 1:1 ordered complex perovskite for the microwave dielectric system.

Publication

1. S. Gao, X. Zhan, & Y. Cheng (2019). Structural, electrochemical and Li-Ion transport properties of Zr-Modified $LiNi_{0.8}Co_{0.1}Mn_{0.1}O_2$ positive electrode materials for lithium-ion batteries. Journal of Power Sources, 410, 45-52.
2. S. Gao, Y. Cheng, & M. Shirpour (2019). Effects of Cobalt Deficiency on the Performance of Nickel-rich Layered $LiNi_{0.8}Co_{0.1}Mn_{0.1}O_2$ Positive Electrode Materials for Lithium-Ion Batteries. ACS Applied Materials and Interfaces, 11, 1, 982-989.
3. X. Zhan, S. Gao, & Y. Cheng (2019). Influence of Annealing Atmosphere on Li_2ZrO_3-Coated $LiNi_{0.6}Co_{0.2}Mn_{0.2}O_2$ and its High-Voltage Cycling Performance. Electrochimica Acta, 300, 36-44.
4. Y. Sun, X. Zhan, J. Hu, Y. Wang, S. Gao, Y. Shen, & Y. Cheng. Improving Ionic Conductivity with Bimodal-Sized $Li_7La_3Zr_2O_{12}$ Fillers for Composite Polymer Electrolytes. ACS Applied Materials and Interfaces, accepted.

5. Y. Zhu, L. Cheng, B. Ma, S. Gao, W. Feng, Y. Liu, & L. Zhang (2015). Calculation and synthesis of ZrC by CVD from $ZrCl_4$–C_3H_6–H_2–Ar system with high H_2 percentage. Applied Surface Science, 332, 591-598.

6. Y. Zhu, L. Cheng, S. Gao, J. Li, J. Deng, & L. Zhang (2014). Thermodynamic analysis on the co-deposition of ZrC–SiC by chemical vapor deposition using the $ZrCl_4$–C_3H_6–MTS–H_2–Ar system. Ceramics International, 40(5), 6427-6433.

7. C. Xie, Q. Zeng, D. Dong, S. Gao, Y. Cai, & A. R. Oganov, (2014). First-principles calculations of the dielectric and vibrational properties of ferroelectric and paraelectric $BaAl_2O_4$. Physics Letters A, 378 (26-27), 1867-1870.

Presentation

1. S. Gao, X. Zhan, & Y. Cheng, Zirconium-Doped Layered $LiNi_{0.8}Co_{0.1}Mn_{0.1}O_2$ as A High-Rate and Durable Lithium Ion Battery Positive Electrode Material. Talk. Materials Research Society, Apr. 2018. Phoenix, AZ.

2. S. Gao, Y. Cheng, & M. Shirpour, Role of Cation Deficiency in Tuning the Electrochemical Performance of Nickel-Rich Layered Transition-Metal Oxides. Poster. Materials Research Society, Nov. 2017. Boston, MA.